BOLETIN DE LA SOCIEDAD ESPAÑOLA DE
Cerámica y Vidrio
www.elsevier.es/bsecv

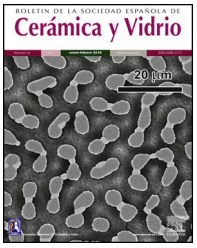

A review of the properties of hybrid ceramic nanocomposites

Nouari Saheb[a,b,*], *Umer Hayat*[c], *Hassan Syed Fida*[a,b]

[a] *Department of Mechanical Engineering, King Fahd University of Petroleum and Minerals, Dhahran 31261, Saudi Arabia*
[b] *Interdisciplinary Research Center for Advanced Materials, King Fahd University of Petroleum and Minerals, Dhahran 31261, Saudi Arabia*
[c] *Khalifa University of Science and Technology, United Arab Emirates*

ARTICLE INFO

Article history:
Received 24 November 2024
Accepted 1 March 2025
Available online 11 April 2025

Keywords:
Hybrid ceramic nanocomposites
Mechanical properties
Thermal properties
Electrical properties
Structural applications
Functional applications

ABSTRACT

Although monolithic ceramics have many desirable properties, such as high-temperature resistance, excellent hardness, and chemical inertness, they also have limitations that can restrict their use in various applications. The limitations include, but are not limited to, low fracture toughness, low ductility, high electrical resistance, and low thermal conductivity. Researchers have been able to address some of these limitations by developing ceramic composites, nanocomposites, and hybrid nanocomposites. The later are ceramic matrices that incorporate two or more reinforcements. They represent an advanced class of materials that combine the excellent characteristics of monolithic ceramics and the outstanding properties of the reinforcements, offering exceptional mechanical, thermal, and functional properties for advanced applications. There are many comprehensive review papers on ceramic composites and nanocomposites, however, only one review paper on hybrid ceramic nanocomposites has been published, and it was dedicated solely to alumina-based nanocomposites prepared by spark plasma sintering. The aim of this work is to review the properties of hybrid ceramic nanocomposites, highlight their potential applications in various industries, and formulate directions for future research endeavors.

Abbreviations: BN_{nf}, boron nitride nanofiber; BNNP, boron nitride nanoplateles; BNNT, boron nitride nanotubes; C_f, carbon fibers; C_{np}, carbon nanoparticles; CNTs, carbon nanotubes; CTE, coefficient of thermal expansion; EDS, energy dispersive spectroscopy; GN, graphene; GNPs, graphene nanoplatelets; GNSs, graphene nanosheets; GPLs, graphene platelets; GO, graphene oxide; HFIHS, high frequency induction heat sintering; HP, hot pressing; MLG, multilayer graphene; MWCNTs, multi-walled carbon nanotubes; G_{nf}, nano-graphite flakes; C_{nb}, nano-sized carbon black; SiC_{np}, SiC nanoparticles; SiC_{nw}, SiC nanowire; SiC_w, SiC whiskers; SLG, single-layer graphene; SPS, spark plasma sintering; SWCNTs, single walled carbon nanotubes; TGA, thermogravemetric analysis; UHTC, ultrahigh temperature ceramics; XRD, X-ray diffraction; ZTA, zirconia-toughened-alumina.

* *Corresponding author.*
E-mail address: nouari@kfupm.edu.sa (N. Saheb).

https://doi.org/10.1016/j.bsecv.2025.03.001

Una revisión de las propiedades de los nanocompuestos cerámicos híbridos

Palabras clave:
Nanocompuestos cerámicos híbridos
Propiedades mecánicas
Propiedades térmicas
Propiedades eléctricas
Aplicaciones estructurales
Aplicaciones funcionales

RESUMEN

Aunque las cerámicas monolíticas tienen muchas propiedades deseables, como resistencia a altas temperaturas, excelente dureza e inercia química, también tienen limitaciones que pueden restringir su uso en diversas aplicaciones. Las limitaciones incluyen, pero no se limitan a, baja tenacidad a la fractura, baja ductilidad, alta resistencia eléctrica y baja conductividad térmica. Los investigadores han podido abordar algunas de estas limitaciones desarrollando compuestos cerámicos, nanocompuestos y nanocompuestos híbridos. Estos últimos son matrices cerámicas que incorporan dos o más refuerzos. Representan una clase avanzada de materiales que combinan las excelentes características de las cerámicas monolíticas y las propiedades sobresalientes de los refuerzos, ofreciendo propiedades mecánicas, térmicas y funcionales excepcionales para aplicaciones avanzadas. Hay muchos artículos de revisión exhaustivos sobre compuestos cerámicos y nanocompuestos; sin embargo, solo se ha publicado un artículo de revisión sobre nanocompuestos cerámicos híbridos, y este se dedicó exclusivamente a nanocompuestos a base de alúmina preparados por sinterización por plasma de chispa. El objetivo de este trabajo es revisar las propiedades de los nanocompuestos cerámicos híbridos, resaltar sus aplicaciones potenciales en diversas industrias y formular direcciones para futuros esfuerzos de investigación.

Introduction

Ceramics are materials used in various engineering applications because of their unique properties. Some of their important characteristics include: (i) the ability to withstand high temperatures, (ii) excellent wear and abrasion, (iii) chemical resistance, (iv) electrical insulation, (v) biocompatibility, and (vi) lightweight and low density [1–4]. These properties make ceramics suitable for: (i) use in harsh environments, (ii) manufacturing of cutting tools, bearings, and wear-resistant coatings, (iii) applications where corrosion resistance is critical, such as in the chemical industry, semiconductor manufacturing, and healthcare, (iv) electrical and electronic applications where high levels of insulation are required to prevent electrical leakage or short circuits, (v) medical implants and dental prosthetics, and (vi) applications where weight reduction is important, such as in the transportation, automotive, and aerospace industries [1–4]. Nevertheless, the utilization of ceramics in some applications has been restricted because of their low resistance to fracture, insufficient strength, high electrical resistance, and low thermal conductivity. As a result, composites [5], nanocomposites [6], and hybrid nanocomposites [7] were developed to overcome the limitations of unreinforced ceramic materials. Composites are materials made up of a matrix that incorporates particles, whiskers, fibers, or sheets, resulting in enhanced properties when compared to ceramics that are not reinforced. Additional enhancements to the properties have been achieved through the development of nanocomposites and hybrid nanocomposites. In the former, the matrix is reinforced with a single phase, while in the latter, the matrix is reinforced with two or more phases that have different dimensionalities, morphologies, and properties. Fig. 1 [14] shows typical reinforcements and structures for ceramic nanocomposites while Fig. 2 [33] displays the structure of Al_2O_3–SiC–CNTs nanocomposites. In the later, CNTs are present within the grain boundaries of Al_2O_3 while SiC particles are present within grains and at the grain boundaries. The properties of hybrid ceramic nanocomposites are influenced by: (i) the inherent characteristics, type, size, dimensionality (0D, 1D, 2D), and distribution of the reinforcements, (ii) nature and composition of the matrix, and (iii) process parameters. The matrix offers high strength, high hardness, and thermal stability, while the reinforcements further improve these properties and adds functionalities such as enhanced toughness, wear resistance, and electrical, magnetic, or optical properties. This enables the development of materials with tailored properties that are well-suited for a wide range of applications [8–13]. Review papers on ceramic composites and nanocomposites can be found in the literature [14–20]. However, only one review paper on spark plasma sintered hybrid ceramic nanocomposites [7] has been published so far. The objective of this work is to review the properties of hybrid ceramic nanocomposites, highlight their potential applications in various industries, and formulate directions for future research endeavors.

Properties of some reinforcements

Carbonaceous reinforcements, such as carbon nanotubes (CNTs), graphite, and graphene, along with other reinforcements like SiC, exhibit outstanding mechanical and physical properties that make them highly suitable for enhancing the performance of ceramic composite materials. For example, CNTs have a high stiffness of around 1 TPa [21,22] and a tensile strength of up to 60 GPa [23]. As for thermal properties, at 300 K, CNTs have an electrical conductivity of around 10^6 S/m for

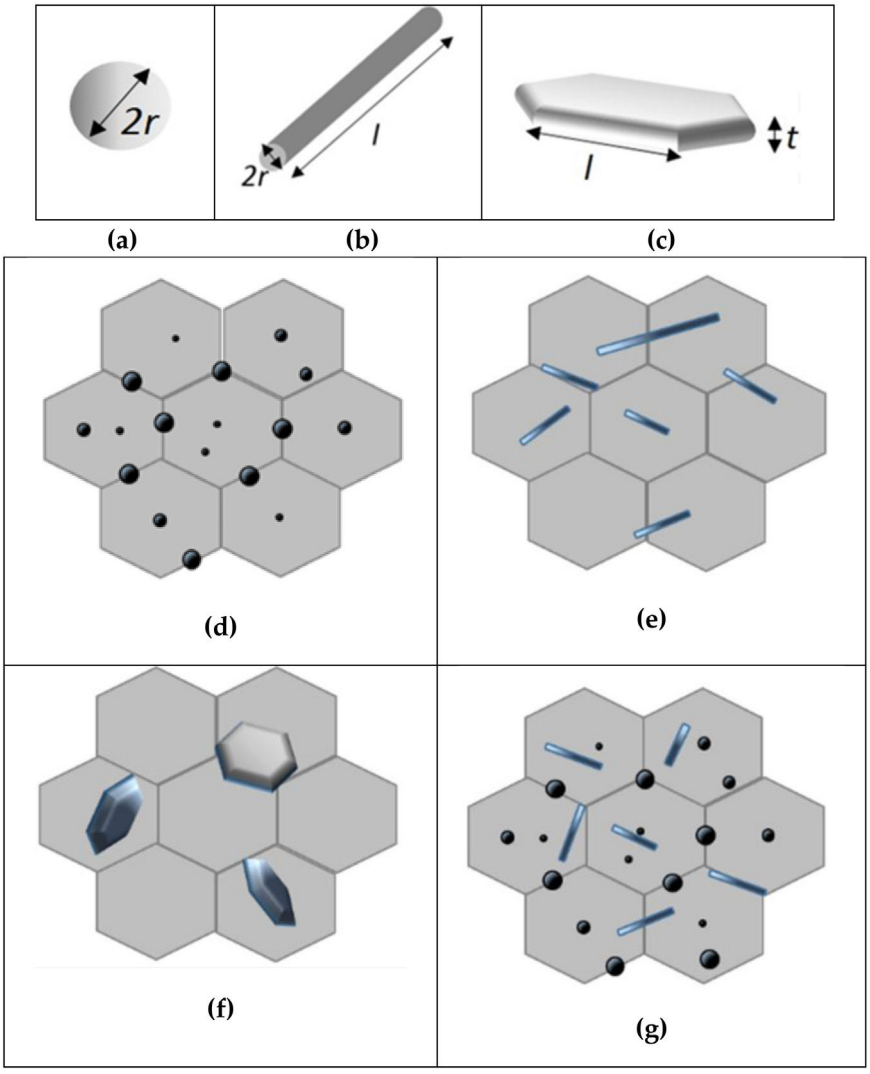

Fig. 1 – Some common nanoreinforcements and nanocomposite structures for ceramics. (a) zero-dimensional (0-D) round nanomaterials, (b) one-dimensional (1-D) needlelike-shaped nanomaterials, (c) two-dimensional (2-D) platelike shaped nanomaterials, (d) 0D nanomaterials embedded in the matrix grains, located at the grain boundaries or occupy both inter- and intra-granular positions, (e) 1D nanomaterials embedded in a micronic matrix, (f) 2D nanomaterials embedded in a micronic matrix, and (g) mixture of 0D and 1D nanoscale phases that are embedded in a micron-sized matrix [14].

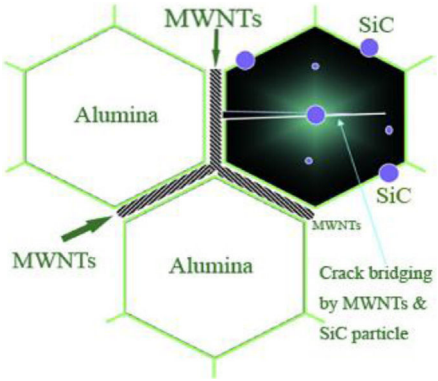

Fig. 2 – A schematic of hybrid microstructure design [53].

single walled carbon nanotubes (SWCNTs) and greater than 10^5 S/m for multi-walled carbon nanotubes (MWCNTs) [24,25]. Moreover, they have very high thermal conductivity [26,27], with room temperature measured values of 3000 W/m K for MWCNTs [28] and 3500 W/m K for SWCNTs [29]. Graphene is a two-dimensional material consisting of sp2-hybridized carbon atoms and has exceptional mechanical properties. A perfect single-layer graphene has a stiffness of 1.0 TPa and a fracture strength of 130 GPa [30]. In contrast to monolayer graphene, graphene nanosheets (GNSs) or graphene nanoplatelets (GNPs) possess outstanding mechanical properties [31–33]. The stiffness of GNPs with a thickness of 2–8 nm is reported to be around 0.5 TPa [34]. The fracture toughness of graphene was found to be equal to 4 MPa $m^{1/2}$ [35]. Graphene possesses outstanding in-plane thermal conductivity in the range of 1000–5300 W/m K and through-plane thermal conductivity in the range of 5–20 W/m K. The room temperature

thermal conductivity of single-layer graphene was reported to be around 5300 W/m K [36]. Moreover, graphene has a negative coefficient of thermal expansion (CTE) of -1.28×10^{-6} to $-8 \times 10^{-6}\,K^{-1}$ [37,38]. SiC is known to have a hardness of approximately 30 GPa [39], and it possesses a thermal conductivity and CTE of 200–300 W/m K and $4.5 \times 10^{-6}\,K^{-1}$, respectively [40].

Hybrid ceramic nanocomposites

Al_2O_3 nanocomposites

Alumina is the most widely applied and investigated ceramic material because of its exceptional mechanical properties and excellent thermal stability. However, its inherent brittleness limits its use in a wider range of structural applications [41]. Improvements in alumina toughness were made possible through the addition of a second phase such as CNTs [41–44], SiC [41,45–48], graphene [49,50], TiC [51], WC [51], and Si_3N_4 [52]. Additionally, it was found that reinforcing alumina with two phases, resulting in hybrid nanocomposites, can further improve its properties through the synergistic toughening mechanisms of reinforcements [53]. Below is a summary of published work on alumina-based hybrid nanocomposites.

Al_2O_3–SiC–CNTs nanocomposites

Hybrid microstructure design for Al_2O_3–SiC–CNTs nanocomposite materials was first introduced by Ahmad and Pan [53]. The authors prepared alumina and Al_2O_3–1 vol.%SiC–(5, 7, 10) vol.% CNTs hybrid nanocomposites through spark plasma sintering (SPS) at 1550 °C. The relative density of alumina was found to be 100%, but decreases with the increase in the reinforcement content and reached 95.1% for Al_2O_3–1 vol.%SiC–10 vol.%CNTs nanocomposite. Although no significant reduction in hardness was observed, the fracture toughness and bending strength of the nanocomposites increased by 117 and 44%, respectively, compared to alumina. In another study, Ahmad et al. [54] reported the effect of SiC on the microstructure of spark plasma sintered Al_2O_3–(1–3) vol.%SiC–5 vol.% CNTs nanocomposites as presented in Figs. 3 and 4, and on the mechanical properties

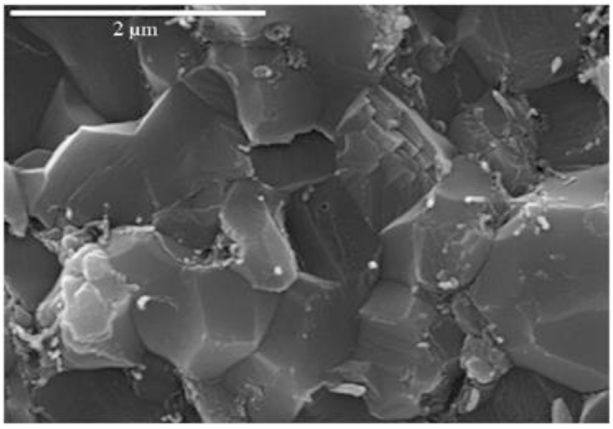

Fig. 3 – Microstructure of Al_2O_3–SiC–CNT hybrid nanocomposites [54].

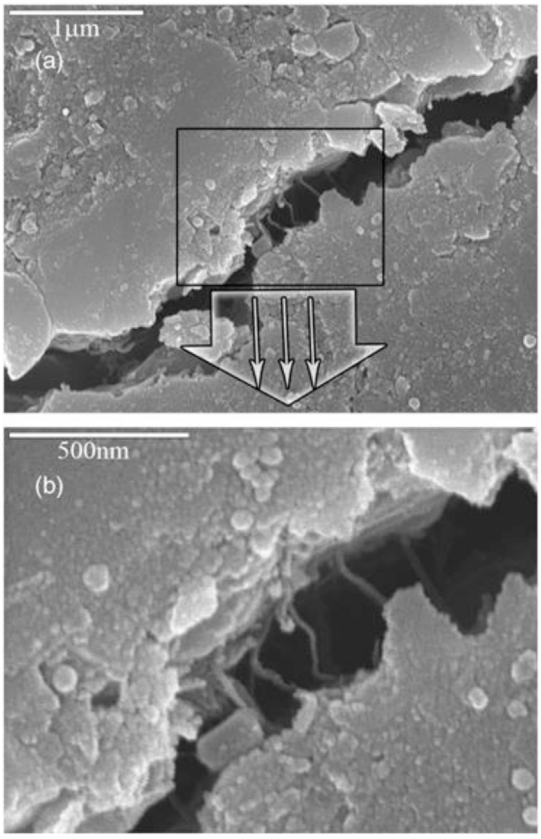

Fig. 4 – Toughening in Al_2O_3–SiC–CNT hybrid nanocomposites [14].

as shown in Fig. 5 [54]. A 104% increase in fracture toughness and 46% increase in bending strength were reported for the Al_2O_3–1 vol.% SiC–5 vol.%CNTs nanocomposite, compared to alumina. Al_2O_3 thermal conductivity decreased from 29.5 to 23 W/m K at 1 vol.% SiC and 5 vol.% CNTs and further decreased with an increase in reinforcement content. A very high electrical conductivity of 9 S/m was reported for the

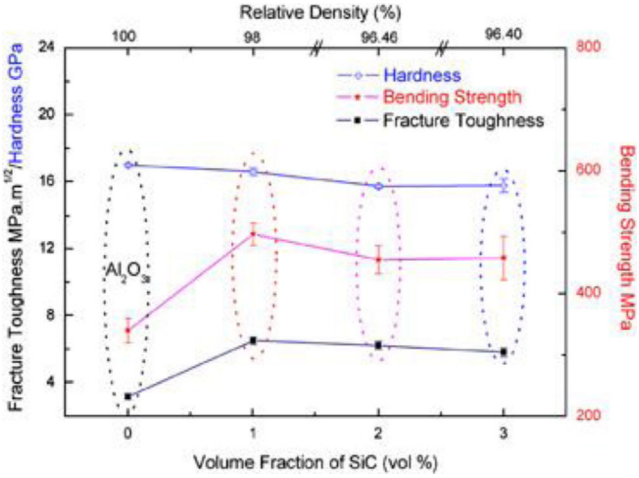

Fig. 5 – Properties Al_2O_3–(1–3) vol.% SiC–5 vol.% CNT hybrid nanocomposites [54].

Al_2O_3–3 vol.% SiC–5 vol.%CNTs nanocomposite, compared to 10^{-12} S/m for alumina.

Mohammad and Saheb [55] used molecular level mixing to prepare homogeneous Al_2O_3–5 wt.%SiC–1 wt.%CNTs nanocomposite powder with uniform distribution of SiC and CNTs, and sintered it using SPS at 1500 °C. They obtained full density alumina (100%), but the relative density of the nanocomposite decreased to 91.65%. The fracture toughness of the nanocomposite increased by 33% compared to alumina, while a slight decrease in hardness (4%) was observed. In another work, Saheb and Mohammad [56] investigated the influence of SiC and CNTs on mechanical and microstructural properties of Al_2O_3–SiC–CNTs hybrid nanocomposites as shown in Fig. 6 [36]. Al_2O_3–(5, 10) wt.%SiC–(1, 2) wt.%CNTs nanocomposite powders were prepared using sonication and ball milling. Spark plasma sintering at 1500 °C resulted in densification higher than 98% for all samples. All nanocomposites showed improved hardness than alumina (18.56 HV) except Al_2O_3–10 wt.%SiC–2 wt.%CNTs nanocomposite (17.5 HV), which was attributed to low densification. An increase of a maximum of 12.12% in hardness was reported for Al_2O_3–10 wt.%SiC–1 wt.%CNTs nanocomposite. Similarly, all nanocomposites displayed enhanced fracture toughness values, with maximum increase of 93.95% for Al_2O_3–10 wt.%SiC–2 wt.%CNTs, compared. The effect of varying sintering temperature on microstructural and mechanical properties of Al_2O_3–5 wt.%SiC–1 wt.%CNTs nanocomposite was investigated by Saheb and Mohammad [57]. Nanocomposite powder, produced by molecular level mixing, was spark plasma sintered at 1500 °C, 1550 °C and 1600 °C. The relative density, hardness, and fracture toughness were found to increase with the increase in temperature, and reached maximum values of 98.91%, 23.32 GPa, and 7.10 MPa $m^{1/2}$, respectively, at 1600 °C. The increase in hardness (25.65%) and fracture toughness (96.67%) compared to monolithic alumina was attributed to higher densification, finer microstructure, change of fracture mode to transgranular along with other toughening mechanisms such as CNTs pull-out, CNTs breaking, crack deflection and crack bridging. In another work, Saheb and Hayat [58] reported thermal and electrical properties of spark plasma sintered Al_2O_3–SiC–CNT hybrid nanocomposites as shown in Fig. 7 [58]. Thermal conductivity, thermal diffusivity, and specific heat capacity values of 34.44 W/m K, 7.62 mm^2/s and 1.24 J/g K for alumina decreased to 21.2 W/m K, 6.64 mm^2/s and 0.87 J/g K, respectively, for the Al_2O_3–5 wt.%SiC–1 wt.%CNTs nanocomposite. These properties continued to decrease with further addition of reinforcements. However, a drastic increase in electrical conductivity was observed with the addition of SiC and CNTs reinforcements, where the electrical conductivity of alumina increased from 6.87×10^{-10} S/m to 8.87 S/m for the Al_2O_3–5 wt.%SiC–2 wt.%CNTs nanocomposite. Siddique et al. [59] presented a model for the estimation of thermal conductivity of spark plasma sintered Al_2O_3–SiC–CNTs hybrid nanocomposites. In the proposed model, thermal conductivity was taken as a function of average matrix crystallite size compared to conventional approach of using constant thermal conductivity for the matrix. They found good agreement between the predicted and experimentally measured values, as shown in Fig. 8 [59].

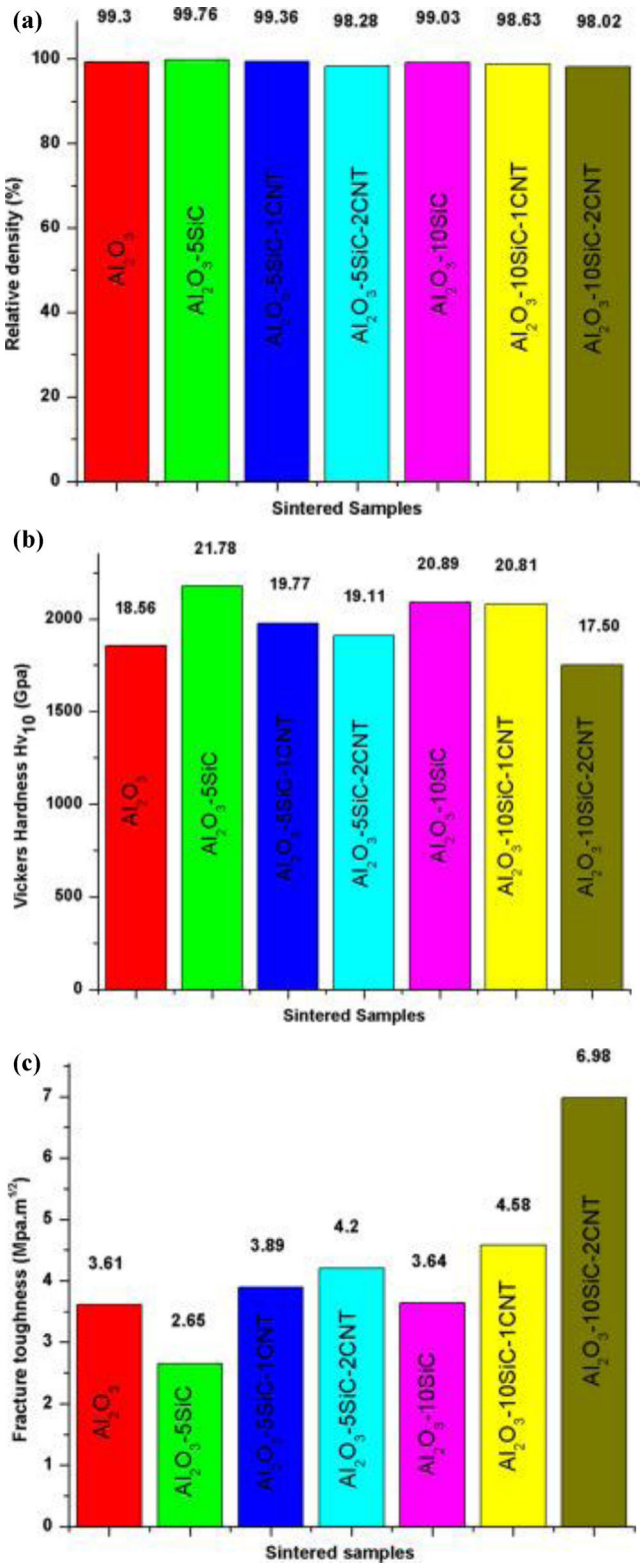

Fig. 6 – Properties of Al_2O_3–SiC–CNTs hybrid nanocomposites prepared by spark plasma sintering (a) density, (b) hardness, and (c) fracture toughness [56].

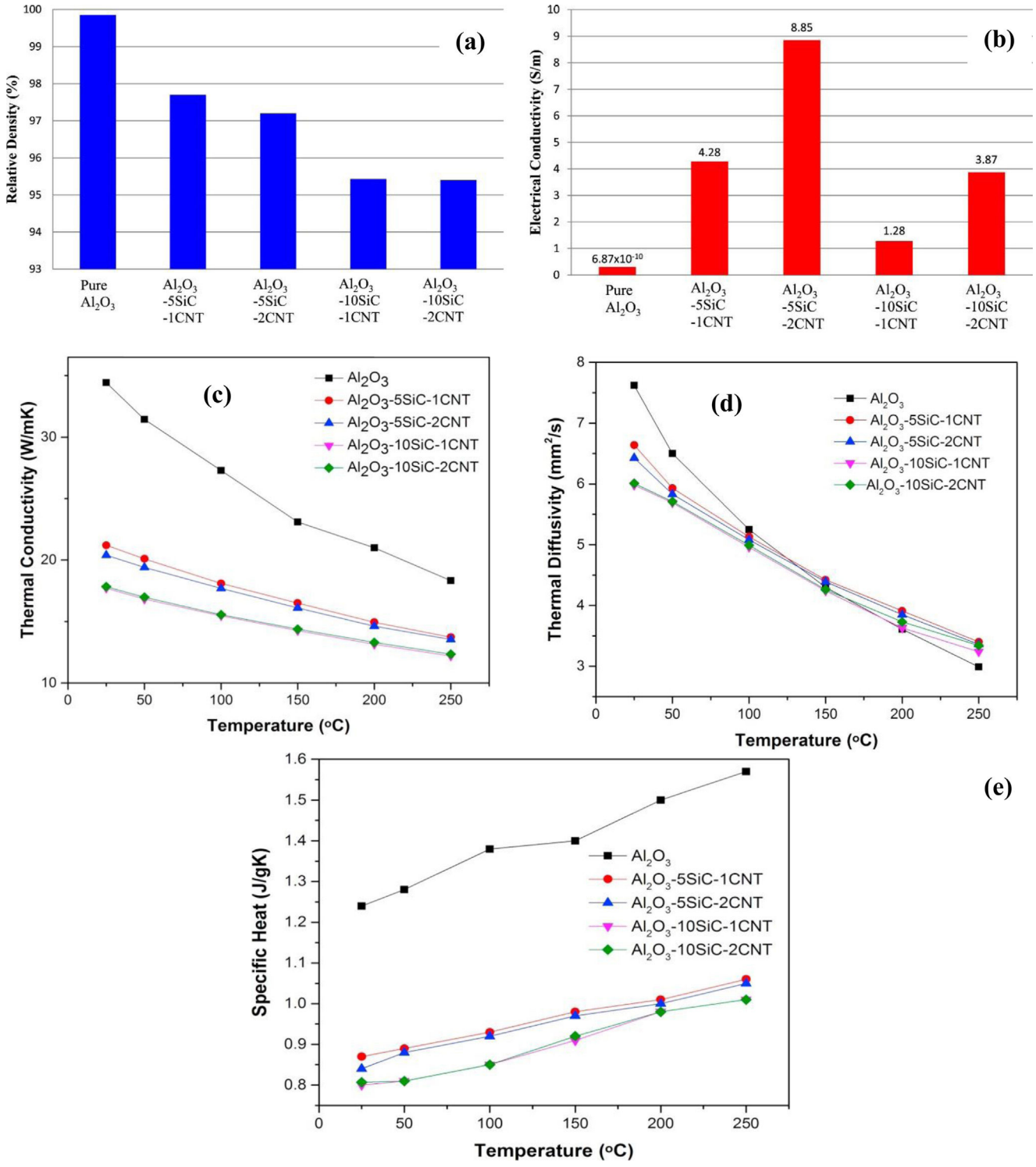

Fig. 7 – Physical properties of spark plasma sintered Al_2O_3–SiC–CNT hybrid nanocomposites (a) relative density, (b) electrical conductivity, (c) thermal conductivity, (d) thermal diffusivity, and (e) specific heat capacity [58].

Ahmad and Islam [60] investigated the effect of SiC nanoparticles and CNTs on mechanical properties, bonding characteristics, and thermal stability of Al_2O_3–SiC–CNTs hybrid nanocomposites. The relative density of inductive hot-pressed Al_2O_3–6 wt.%SiC_{np}–4 wt.%CNTs nanocomposite, sintered at 1500 °C, was found to be 97.2% while that of alumina was 99.2%. Moreover, a 160% refinement in microstructure, a 81% increase in fracture toughness, and a 25% increase in hardness were reported for the Al_2O_3–SiC–CNTs nanocomposite, compared to alumina. However, 11% decrease in elastic modulus was recorded for the Al_2O_3–SiC–CNTs nanocomposite. Interfacial and

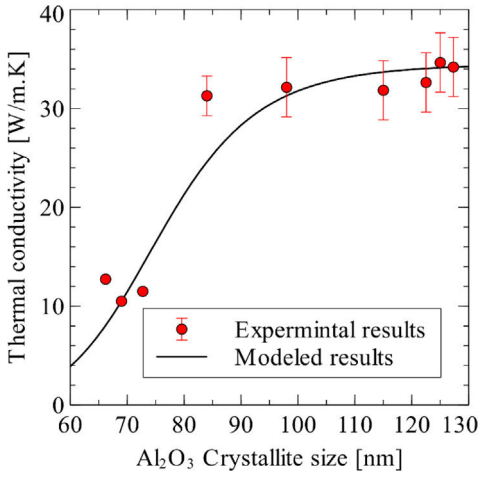

Fig. 8 – Predicted and measured thermal conductivity of alumina as a function of its average crystallite size [59].

thermal analysis suggested the formation of intermediate phase (Al_2OC) at Al_2O_3/CNTs interface in the nanocomposite. The Al_2O_3–SiC–CNT nanocomposite showed good thermal stability up to 760 °C in inert atmosphere and up to 425 °C in oxygen-rich environment. In another study, Ahmad et al. [61] used high frequency induction heat sintering (HFIHS) method to consolidate alumina nanocomposite reinforced with SiC nanoparticles (SiC_{np}) and CNTs (Al_2O_3–5 wt.%SiC_{np}–2 wt.%CNTs) at 1600 °C. Fourfold reduction in grain size along with 110% increase in fracture toughness and 30% increase in hardness were reported for the nanocomposite, compared to alumina. However, the elastic modulus of alumina decreased from 418 MPa to 350 MPa for the Al_2O_3–5SiC_{np}–2CNTs nanocomposite. Enhancements in mechanical properties and cutting performance of alumina–matrix nanocomposite reinforced with silicon carbide whiskers (SiC_w) and CNTs were reported by Lee and Yoon [62]. They prepared Al_2O_3–25 wt.%SiC_w–(0.1–1) wt.%CNTs nanocomposites using hot pressing at 1750 °C. All the Al_2O_3–SiC_w–CNTs nanocomposites showed relative density higher than 99%. Improvements in fracture toughness and flexural strength of more than 60% were reported for all Al_2O_3–SiC_w–CNTs nanocomposites, compared to Al_2O_3–CNTs. The cutting performance of Al_2O_3–SiC_w–CNTs nanocomposites was evaluated by finish turning of Inconel 718 super alloy. Fig. 9 [62] shows the crater wear and flank wear performance of various Al_2O_3–SiC_w–CNTs nanocomposites. All Al_2O_3–SiC_w–CNTs nanocomposites showed lower wear rate compared to Al_2O_3–25 wt.%SiC_w, with Al_2O_3–25 wt.%SiC_w–0.5 wt.%CNTs nanocomposite showing the lowest wear rate.

Al_2O_3–ZrO_2–MWCNTs nanocomposites

Al_2O_3 ZrO_2 MWCNTs nanocomposites were prepared through colloidal processing and freeze drying, followed by hot pressing at 1500 °C [44]. Increase in fracture toughness was observed for all nanocomposites, with a maximum of 35% for Al_2O_3–5 vol.%ZrO_2–1 vol.%MWCNTs. However, around 21% decrease in hardness was reported for all Al_2O_3–5 vol.%ZrO_2–(0.5–2) vol.%MWCNTs nanocomposites. The electrical conductivity increased for all composites with a maximum value of 0.22 S/m for Al_2O_3–5%ZrO_2–2%MWCNTs as compared to 10^{-12} S/m for alumina. In another work, a slight increase in thermal conductivity, from 29 W/m K for Al_2O_3 to 30 W/m K for Al_2O_3–5%ZrO_2–0.5%MWCNTs nanocomposite, was observed [63]. Further increase in CNTs content caused a decrease in thermal conductivity. Mechanical properties of Al_2O_3 hybrid nanocomposite were enhanced by addition of 8 vol.% ZrO_2 nanoparticles and 4 vol.% MWCNTs [64]. The materials were prepared using hot-pressing at 1600 °C for 60 min. High relative density values of 99.7% and 98.3% were obtained for Al_2O_3 and the nanocomposite, respectively, and the microstructure was refined by 10 folds. The fracture toughness and hardness of monolithic alumina were increased by 116% and 12%, respectively, as a result of the addition of reinforcements. The improvements in mechanical properties were attributed to the synergistic role of nano-ZrO_2 and CNTs reinforcements through grain refining and the introduction of various toughening mechanisms. Duntu et al. [65] studied the mechanical and wear properties of CNTs

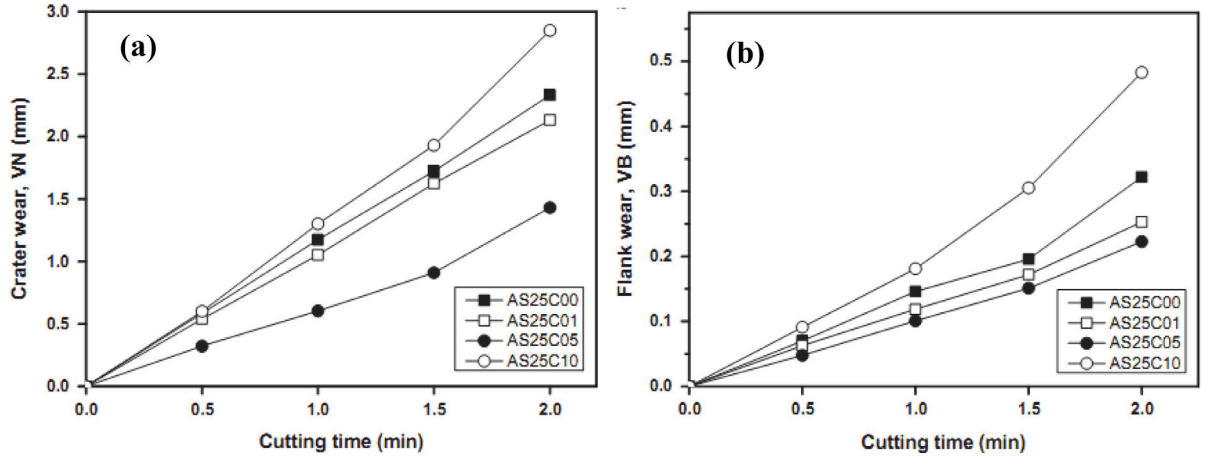

Fig. 9 – (a) Crater wear and (b) flank wear performance for various Al_2O_3–SiC_w–CNT nanocomposites as a function of time [62]. (AS25C00 represents Al_2O_3–25 wt.%SiC_w, AS25C01:Al_2O_3–25 wt.%SiC_w–0.1 wt.%CNT, AS25C05: Al_2O_3–25 wt.%SiC_w–0.5 wt.%CNT, AS25C10: Al_2O_3–25 wt.%SiC_w–1 wt.%CNT nanocomposite).

and graphene (GN) reinforced Al_2O_3–ZrO_2 hybrid nanocomposites. They prepared Al_2O_3–4 wt.%ZrO_2–2 wt.%CNTs and Al_2O_3–4 wt.%ZrO_2–0.5 wt.%GN nanocomposite powders and hot pressed them at 1600 °C and 60 MPa for 1 h. All samples showed a relative density of at least 99%. Grain size refinements of 77% and 37% were observed for the CNTs and GN reinforced hybrid nanocomposites. As a result, hardness and flexural strength were found to increase by 26 and 44% for CNTs-reinforced composites and by 14 and 23% for graphene-reinforced Al_2O_3–ZrO_2 nanocomposites. Moreover, 118 and 97% increases in fracture toughness were reported for Al_2O_3–4 wt.%ZrO_2–2 wt.%CNTs and Al_2O_3–4 wt.%ZrO_2–0.5 wt.%GN nanocomposites, respectively. The enhancements in mechanical properties were attributed to grain refinement, crack bridging, crack deflection, and strong interfacial bonding of reinforcements. Enhanced wear performance with a decrease in wear rate of up to 90% and 98% was also reported in CNTs and GN reinforced nanocomposites, respectively, compared to alumina. The effect of MWCNTs on zirconia-toughened-alumina (ZTA) reinforced with MgO composite was investigated by Biswas et al. [66]. The authors fabricated ZTA–0.6 wt.%MgO and ZTA–0.6 wt.%MgO–(0.05, 0.1 wt.%)MWCNTs nanocomposites by hot-pressing at 1500 °C for 30 min. All nanocomposites showed relative density of 99%. XRD analysis revealed the formation of $MgAl_2O_4$ secondary phase during sintering in all nanocomposites. The addition of MWCNTs resulted in grain refinement. Hardness and elastic modulus increased with increase in MWCNTs content, reaching values of 31.25 and 341.15 GPa for ZTA–MgO–0.1 wt.%MWCNTs compared to 24.57 and 302.88 GPa for ZTA–MgO. The fracture toughness was found to be 22% higher in the ZTA–MgO–0.05 wt.%MWCNTs nanocomposite. The ZTA–MgO–0.05 wt.%MWCNTs nanocomposite also showed superior wear properties, with 42% and 81% reduction in specific wear rate at room temperature and high-temperature, respectively. Moreover, 23% and 29% decrease in coefficient of friction was reported for the ZTA–MgO–0.05 wt.%MWCNTs nanocomposite at room temperature and high-temperature, respectively.

Al_2O_3–SiC–Graphene nanocomposites

Ahmad et al. [67] studied the mechanical, interfacial, and thermal performance of Al_2O_3 reinforced with SiC_{np} and GN hybrid reinforcements. The alumina and Al_2O_3–3 wt.%SiC–0.5 wt.%GN nanocomposite were inductively hot-pressed at 1300–1600 °C. Relative density values of 99% were obtained for all samples. Compared to alumina, the nanocomposite displayed 70% reduction in grain size, 97% increase in fracture toughness, 15% increase in hardness, and 78% higher ballistic performance. The superior ballistic performance was attributed to higher densification, finer microstructure, high hardness, and high fracture toughness. The authors performed an interfacial investigation and concluded that a carbo-thermal reduction reaction between Al_2O_3 and GN resulted in the formation of Al_2OC phase during sintering. In another investigation, Ahmad et al. [68] reported a 160% increase in fracture toughness and a 27% increase in hardness, when alumina was reinforced with 0.5 wt.%GN and 5 wt.%SiC to form a hybrid nanocomposite. Both Al_2O_3 and Al_2O_3–5 wt.%SiC–0.5 wt.%GN nanocomposite, were prepared through inductive sintering at 1300–1600 °C, and showed relative density values greater than 99%.

Improvements in mechanical and electrical properties of Al_2O_3–SiC_w reinforced with graphene oxide (GO) have been reported by Grigoriev et al. [69]. They prepared Al_2O_3–17 vol.%SiC_w–(0.2–5) vol.%GO nanocomposites using colloidal processing, followed by SPS at 1780 °C. Compared to Al_2O_3–SiC_w composite, the Al_2O_3–SiC_w–0.5 wt.%GO displayed increases of 4%, 29%, and 10% in hardness, strength, and fracture toughness, respectively. The electrical resistivity was found to decrease with the increase in GO content and reached 2.2 Ω cm for Al_2O_3–17 vol.%SiC_w–5 vol.%GO nanocomposite. In other work, spark plasma sintered Al_2O_3–(1–5) vol.%SiC–0.38 vol.%GPLs nanocomposites showed increased hardness, flexural strength, and fracture toughness by 36%, 40%, and 50%, compared to alumina [70]. Zhang et al. [71] prepared Al_2O_3–5 vol.%SiC–(0.5–1) vol.%GNS nanocomposites by SPS at 1450 °C. All nanocomposites had relative density values higher than 99%. The electrical conductivity of Al_2O_3–5 vol.%SiC–1 vol.%GNS nanocomposite was found to be 13 orders higher than that of alumina. The Nanocomposites showed moderate improvements in hardness and fracture toughness. The Al_2O_3–5 vol.%SiC–1 vol.%GNS nanocomposite displayed 29.4% decrease in coefficient of friction and 90.1% decrease in wear rate. The enhanced tribological properties of the hybrid nanocomposites were attributed to the formation of graphene tribofilm as sketched in Fig. 10 [71], refined microstructure, and enhanced mechanical properties. Smirnov et al. [72] investigated the wear behavior of Al_2O_3–SiC_w–GO nanocomposites. They prepared nanocomposite powder of Al_2O_3, 17 vol.% SiC_w and 0.5 vol.% GO using colloidal processing and sintered it by SPS at 1780 °C. The authors also prepared Al_2O_3–17 vol.% SiC composite at same conditions for comparison. The Al_2O_3–SiC_w–GO nanocomposite displayed better tribological performance than Al_2O_3–SiC_w. At 10 N load, Al_2O_3–SiC_w–GO nanocomposite showed 20 and 45% decrease in the coefficient of friction and wear rate, respectively, compared to Al_2O_3–SiC_w. And at 40 N load, the coefficient of friction and wear rate further decreased to 30 and 55%, respectively. The decrease in the wear rate and coefficient of friction was attributed to the formation of a tribofilm in Al_2O_3–SiC_w–GO nanocomposite. Shah et al. [73] produced alumina reinforced with multilayer graphene (MLG) and SiC composites. Al_2O_3–0.4 wt.%MLG–(5, 10, 15 wt.%)SiC nanocomposites were prepared by SPS at 1500 °C and 21 MPa for 3 min. The authors investigated the effect of SiC content on the mechanical and thermal properties of the nanocomposites. They found that the densification decreased with the increase in the SiC content, however, all samples showed relative density values higher than 97%. The Al_2O_3–0.4 wt.%MLG–5 wt.%SiC nanocomposite displayed the highest mechanical properties where the bending strength and hardness increased by 57% and 19.22% compared to Al_2O_3. The enhancements were attributed to matrix grain refinement, homogeneous microstructure, toughening effects of the reinforcements, and change in fracture mode. The thermal conductivity and diffusivity of alumina were found to be 25.5 W/m K and 8.1 mm^2/s at 50 °C, respectively, which decreased with increase in the SiC content as well as with the increase in temperature, as shown in Fig. 11 [73].

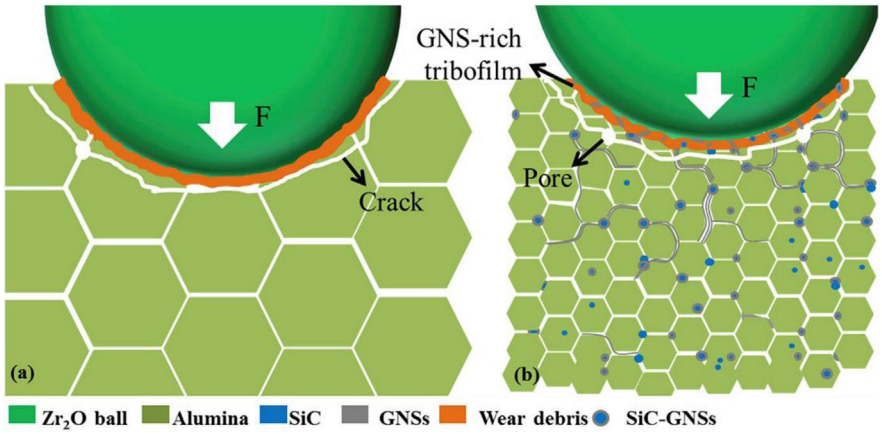

Fig. 10 – Schematic of the wear behaviour of alumina (a), and alumina–SiC–GNSs composites [71].

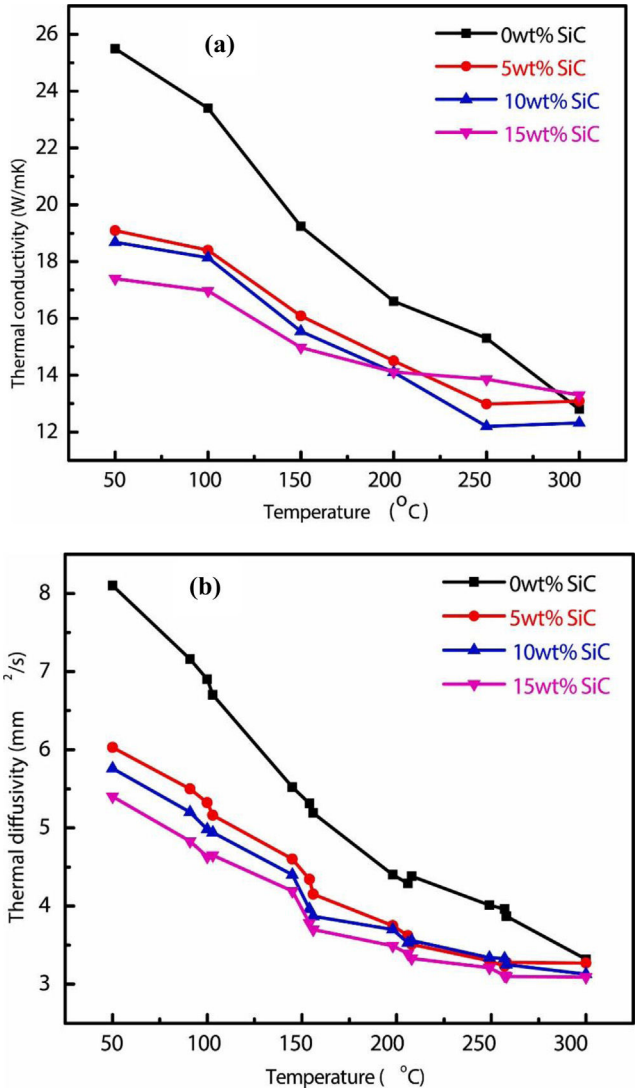

Fig. 11 – (a) Thermal conductivity and (b) thermal diffusivity of Al_2O_3–0.4 wt.%graphene–(0, 5, 10, 15 wt.%)SiC hybrid nanocomposites [73].

Al_2O_3–ZrO_2–graphene nanocomposites

Microstructural, mechanical, and ballistic properties of GNPs and ZrO_2 reinforced-alumina hybrid nanocomposites were investigated by Ahmad et al. [74]. The authors produced Al_2O_3 and Al_2O_3–4 wt.%ZrO_2–0.5 wt.%GNPs nanocomposite by hot-pressing at 1600 °C. Compared with alumina, the nanocomposite displayed: (i) slight decrease in relative density from 99.7 to 98.5%, (ii) 68% decrease in grain size, (iii) 155% increase in fracture toughness, (iv) 17% increase in hardness, and (v) 88% increase in ballistic properties. These enhancements were attributed to grain refinement as well as toughening mechanisms induced by the reinforcements. Microstructural analysis showed wrapping and anchoring of graphene around alumina grains, resulting in very good interfacial strength. Petrus et al. [75] reported mechanical and tribological properties of GML and GO reinforced Al_2O_3–ZrO_2 nanocomposites where 0, 0.2, 0.5, 0.7 and 1 wt.%MLG and nikel-coated-graphene were added to Al_2O_3–ZrO_2. The samples were consolidated by SPS at 1550 °C for 4 min. All nanocomposites had relative density values larger than 98%. The Al_2O_3–ZrO_2–0.2 wt.%GO nanocomposite displayed highest hardness and fracture toughness values of 1940 HV and 5.5 MPa $m^{1/2}$, compared to 1840 HV and 5.2 MPa $m^{1/2}$ for Al_2O_3–ZrO_2. Also, all graphene-reinforced nanocomposites showed higher coefficient of friction and higher wear rate (at a load of 10 N), compared to Al_2O_3–ZrO_2.

Al_2O_3–WC–TiC–graphene nanocomposite

Wang et al. [76] reported improvements in fracture toughness of Al_2O_3–WC–TiC ceramic tool material due to the addition of single layer graphene (SLG). Al_2O_3–18 vol.%WC–6 vol.%TiC was reinforced with 0.5–2 vol.%SLG and hot pressed at 1700 °C. Increase in densification and enhancements in mechanical properties were observed with the addition of 0.5 vol.% SLG, beyond which properties began to decrease. Densification, flexural strength, hardness, and fracture toughness values of 99.58%, 646 MPa, 24.64 GPa, and 9.42 MPa $m^{1/2}$, respectively, were obtained for Al_2O_3–WC–TiC–0.25 vol.%SLG nanocomposite, compared to values of 98.94%, 550 MPa, 23.54 GPa, and 8.76 MPa $m^{1/2}$ for Al_2O_3–WC–TiC. The enhancements in properties were attributed to rugged graphene surface, grain refinement during densification, and crack bridging and deflection.

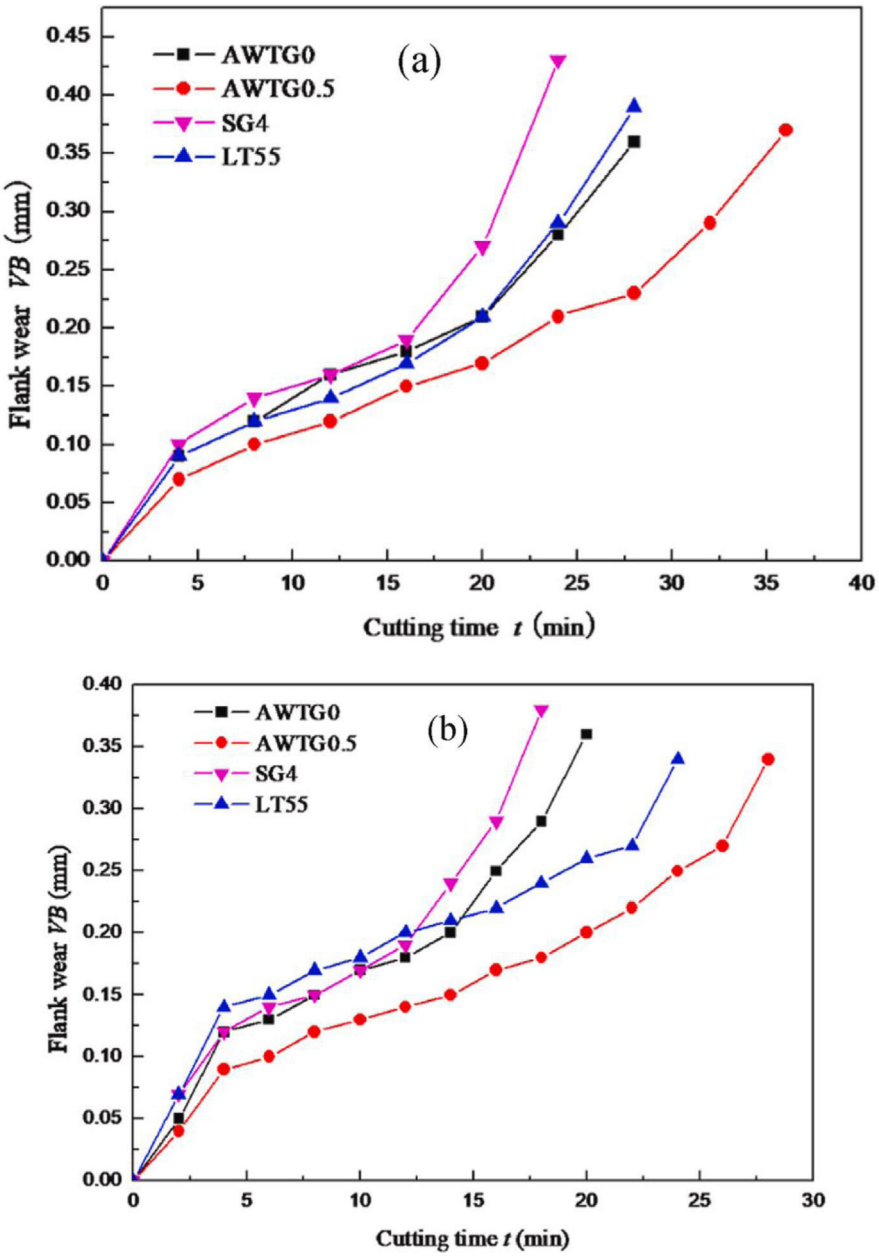

Fig. 12 – Wear behavior of different tool materials Al_2O_3–WC–TiC (AWTG0), Al_2O_3–WC–TiC–0.5 vol.%Graphene (AWTG0.5), Al_2O_3–(W, Ti)C (SG4) and Al_2O_3–TiC (LT55) in machining hardened 40Cr steel at; (a) 100m/min. (b) 150m/min [77].

In another work, Wang et al. [77] reported superior cutting and wear performance of Al_2O_3–WC–TiC–0.5 vol.%Graphene nanocomposite while machining hardened 40Cr steel, in comparison with Al_2O_3–WC–TiC and other commercial tool materials including Al_2O_3–(W, Ti)C and Al_2O_3–TiC, as shown in Fig. 12 [77]. Cutting force and cutting temperature were found to be lower in graphene reinforced Al_2O_3–WC–TiC tool. Moreover, reinforcement with graphene (thickness: ~0.8 nm, lateral size: 0.5–5 μm) resulted in reduction in coefficient of friction from 0.33 for Al_2O_3–WC–TiC to 0.1 for Al_2O_3–WC–TiC–0.5 vol.% Graphene nanocomposite. The superior properties of graphene-reinforced nanocomposite were attributed to; increased mechanical properties due to graphene reinforcement, good lubrication properties and higher thermal conductivity which resulted in friction reduction and decrease in cutting temperatures. Wang et al. [78], in another work, studied the mechanical properties and interfacial structure of Al_2O_3–WC–TiC–Graphene nanocomposite. They used graphene with a thickness of ~0.8 nm and lateral size of 0.5–5 μm. Al_2O_3–WC–TiC composite and Al_2O_3–WC–TiC–0.5 vol.% Graphene nanocomposite, with constant 18 vol.% WC and 6 vol.% TiC, were hot-pressed in two steps, first heated to 1750 °C and without dwell time cooled to 1600 °C for dwell period of 15 min. Apart from parent phases, (W, Ti)C solid solution was formed in sintered samples. Al_2O_3–WC–TiC composite and Al_2O_3–WC–TiC–0.5 vol.% Graphene showed relative density values of 98.41% and 99.52%, respectively. Hardness, flexural strength and frac-

ture toughness were found to be 22.5 GPa, 860 MPa, and 9 MPa $m^{1/2}$ for Al_2O_3–WC–TiC–Graphene nanocomposite; compared to 19 GPa, 500 MPa, and 6 MPa $m^{1/2}$ for Al_2O_3–WC–TiC, respectively. A TEM analysis showed three type of interfaces; Al_2O_3–graphene, graphene–Al_2OC, and graphene–WC interface. On basis of calculated adhesion energy and interfacial strengths, the authors ranked the interfaces; Al_2O_3–graphene > graphene–WC > graphene–Al_2OC. Effects of different thickness and lateral sizes of graphene reinforcement on Al_2O_3–WC–TiC nanocomposites were reported by Wang et al. [79]. Al_2O_3–18 vol.%WC–6 vol.%TiC composite and Al_2O_3–18 vol.%WC–6 vol.%TiC–0.5 vol.%graphene nanocomposites, with different types of graphene, were hot-pressed at 1700 °C for 10 min. A relative density of 98.4% was reported for Al_2O_3–WC–TiC while other nanocomposites showed values greater than 99%. Compared to Al_2O_3–WC–TiC, the Al_2O_3–WC–TiC–graphene nanocomposite with SLG displayed increased hardness, flexural strength, and fracture toughness by 14.80%, 67.59%, and 54.10%, respectively. Moreover, the authors concluded that graphene thickness and lateral size has no effect on matrix grain size and hardness. However, thinner graphene with larger lateral area was found beneficial to improve densification, flexural strength, and fracture toughness. Cheng et al. [80] investigated the effect of varying GNPs content on mechanical and microstructural properties of Al_2O_3–TiC–GNPs nanocomposite ceramic tool material. 60 wt.%Al_2O_3, 30 wt.%TiC, 0.2–0.8 wt.%GNPs along with 10 wt.%sintering aids (Mo, Ni, MgO, Y_2O_3) were used for composite preparation. The samples were consolidated by microwave sintering at 1700 °C for 10 min. The densification of sintered samples decreased with the increase in GNPs content. As compared to Al_2O_3–TiC composite, the fracture toughness of Al_2O_3–30 wt.%TiC–0.2 wt.%GNPs increased by 67.3% while the hardness decreased by 12.7%. Similar investigation was made by Cui et al. [81], where (0.2–0.8 wt.%) GNP was used for toughness enhancement in Al_2O_3–(W, Ti)C ceramic tool material. Maximum improvements were reported for 0.2 wt.%GNP reinforced Al_2O_3–(W, Ti)C nanocomposite, with 35.3% increase in fracture strength and 49% increase in flexural strength, as compared to Al_2O_3–(W, Ti)C without graphene. The enhancements were attributed to break of GNPs and crack guiding along with other conventional toughening mechanisms. Improvements in fracture toughness and flexural strength of multi-layer graphene (MLG) reinforced Al_2O_3–TiC nanocomposite tool material were reported by Li et al. [82]. The authors hot pressed 65.4 wt.%Al_2O_3 and 33.2–33.7 wt.%TiC reinforced with 0.1–0.5 wt.%MLG nanocomposites at 1650 °C. Fracture toughness and flexural strength values of 6.14 MPa $m^{1/2}$ and 981.5 MPa were obtained for Al_2O_3–TiC–0.2 wt.%MLG nanocomposite, which are 23.2% and 30.9% higher, respectively, than those of the Al_2O_3–TiC composite without MLG reinforcement. Zhao et al. [83] investigated the effect of varying the content of WC microparticles and TiC nanoparticles on the properties of Al_2O_3–TiC–WC ceramic tool material. They prepared Al_2O_3–(21–36) vol.%TiC–(14–4) vol.%WC nanocomposites by hot pressing at 1700 °C for 10 min and found that the Al_2O_3–24 vol.%TiC–16 vol.%WC nanocomposite show optimal mechanical properties with flexural strength of 842 MPa, fracture toughness of 6.82 MPa $m^{1/2}$, and hardness of 22.19 GPa.

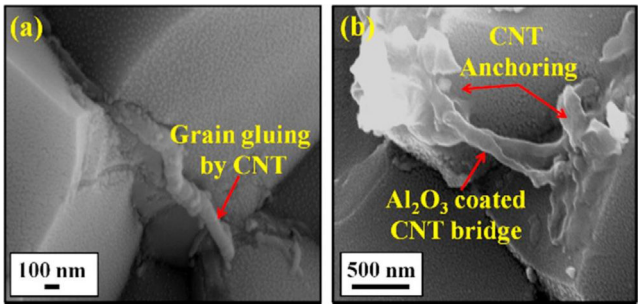

Fig. 13 – (a) CNT-grain gluing and (b) CNT-grain bridging or anchoring in the composite [64].

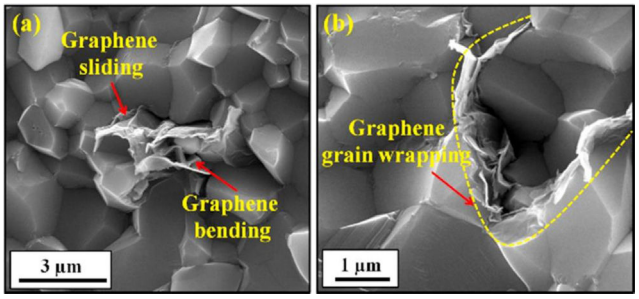

Fig. 14 – (a) graphene sliding and bending between Al_2O_3 grains and (b) graphene-grain wrapping [84].

Al_2O_3–CNTs–graphene nanocomposites

Synergistic effects of 1 wt.%CNTs and 0.5 wt.%graphene nanoplatelets (GNP) on alumina have been investigated by Rahman et al. [84]. The authors used spray drying for powder preparation and sintered the samples by SPS at 1500 °C. They reported an increase in relative density from 91% to 99.9%, a 44% decrease in grain size, and a 20% decrease in hardness for Al_2O_3–1 wt.%CNT–0.5 wt.%GNP nanocomposite compared to alumina. The interfacial shear stress for Al_2O_3–1 wt.%CNT–0.5 wt.%GNP nanocomposite was found to be 28 times higher than that of Al_2O_3–1 wt.%CNT. Improvements by 29% and 250% in the elastic modulus and fracture toughness, respectively, were reported for Al_2O_3–1 wt.%CNT–0.5 wt.%GNP nanocomposite compared to alumina. The significant enhancement in toughness was linked not just to conventional toughening mechanisms like CNT pullout, grain gluing, bridging, graphene pullout, bending, sliding, and grain wrapping, illustrated in Figs. 13 and 14 [84], but also to other toughening mechanisms such as CNT yarning and CNT-embedded graphene, as depicted in Fig. 15 [84]. Furthermore, the high interfacial shear stress could have played a role in the toughness improvement [84]. Damavandi et al. [85] examined the effect of different powder preparation processes and varying content of reduced graphene oxide (rGO) and CNTs on mechanical and microstructural properties of alumina nanocomposites. Al_2O_3–(0.5–2) wt.%rGO–(0.5–4) wt.% CNT nanocomposites were prepared using two different powder mixing techniques i.e. wet mixing and sol–gel mixing, followed by hot pressing at 1650 °C. All the nanocomposites showed relative density values higher than 98%. The nanocomposites prepared using sol–gel process dis-

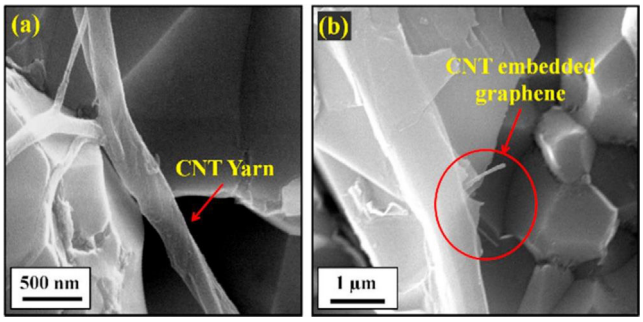

Fig. 15 – (a) CNT yarn in Al_2O_3–1 wt.% CNT and (b) CNT implanted graphene in Al_2O_3–1 wt.% CNT–0.5 wt% GNP sintered nanocomposites [84].

played superior properties i.e. 13, 70, and 14% improvements in hardness, fracture toughness, and flexural strength for Al_2O_3–1 wt.%rGO–1 wt.%CNT compared to alumina. The Al_2O_3–1 wt.%rGO–1 wt.%CNT nanocomposite prepared by sol–gel showed 62% reduction in grain size, 13% increase in hardness, 14% increase in fracture toughness, and 13% increase in flexural strength, compared to the same nanocomposite prepared through wet-mixing. Effect of changing the sintering route on microstructural and mechanical properties of Al_2O_3–GNP–CNT nanocomposites was studied by Yazdani et al. et al. [86]. Al_2O_3–(0.5–1) wt.%GNP–(0.5–2) wt.%CNT nanocomposites were prepared at 1650 °C using hot pressing for 1 hour and SPSfor 10 min. All nanocomposites had relative density values greater than 98%. Samples prepared using HP showed finer microstructure with homogenous grain distribution, than those prepared through SPS. Consequently, hardness and flexural strength of hot-pressed samples were larger than those of samples prepared by SPS. Highest values of flexural strength and hardness, in both cases, were reported to be >400 MPa and 5.5 MPa $m^{1/2}$, respectively. The Al_2O_3–0.5 wt.%GNP–0.5 wt.%CNT nanocomposite, prepared by SPS, showed highest mechanical properties. While for the hot-pressed samples, the Al_2O_3–0.5 wt.%GNP–1 wt.%CNT nanocomposite displayed highest mechanical properties. A 63% increase in fracture toughness and a 12% increase in flexural strength were observed [87], compared to alumina. In another investigation, Yazdani et al. [88] reported tribological properties of hot pressed Al_2O_3–GNP–CNT hybrid nanocomposites, under various loading conditions, using ball-on-disk wear test configuration. The Al_2O_3–0.3 wt.%GNP–1 wt.%CNT nanocomposite showed 20% reduction in coefficient of friction and 74% reduction in wear rate, compared to alumina. The enhanced tribological properties of the nanocomposite were attributed to the formation of a tribofilm as well as superior mechanical properties due to CNT and GNP reinforcements.

Shah et al. [89] prepared Al_2O_3 and Al_2O_3–1 wt.%CNT–(0.4, 0.8 wt.%) graphene nanocomposites by SPSat 1500 °C and 21 MPa for 3 min. All sintered samples had relative density values greater than 99%. The authors reported 49.5% increase in the fracture toughness of Al_2O_3–1 wt.%CNT–0.4 wt.%graphene nanocomposite, compared to alumina. The Al_2O_3–1 wt.%CNT–0.4 wt.%graphene nanocomposite and alumina had flexural strength values of 494 and 415 MPa, respectively. The thermal properties decreased with the increase in reinforcement content. At 50 °C, thermal conductivity and thermal diffusivity of Al_2O_3 were found to be 23.25 W/m K and 7.56 mm^2/s, respectively, which decreased to values of 16 W/m K and 5.5 mm^2/s for Al_2O_3–1 wt.%CNT–0.8 wt.%graphene nanocomposite. Duntu et al. [90] investigated the fracture behavior of graphene and/or CNT reinforced Al_2O_3–ZrO_2 hybrid nanocomposites. Al_2O_3–10 wt.%ZrO_2 was reinforced with 0.5 wt.%graphene and 2 wt.%CNTs, and the nanocomposite powders were hot pressed at 1600 °C for 1 h. Addition of 10 wt.%ZrO_2 and 0.5 wt.%graphene to Al_2O_3 resulted in 56% increase in fracture toughness. Similarly, Al_2O_3–10wt.%ZrO_2–2wt.%CNTs nanocomposite showed fracture toughness and bending strength values of 7.55 MPa $m^{1/2}$ and 460 MPa, compared to 3.4 MPa $m^{1/2}$ and 259 MPa for Al_2O_3. Highest increases of 159% in fracture toughness and 86% in bending strength were observed when 2 wt.%CNTs and 0.5 wt.%graphene were added to Al_2O_3–10wt.%ZrO_2. In another work, Duntu et al. [91] studied the wear behavior of Al_2O_3–ZrO_2–graphene/CNT hybrid nanocomposites. Al_2O_3–ZrO_2–0.5wt.%GN showed 2% increase in hardness and 91% increase in wear resistance compared to alumina. Similarly, the hardness and fracture toughness of Al_2O_3–ZrO_2–2wt.%CNT increased by 11 and 92%, while those of Al_2O_3–ZrO_2–0.5wt.%GN–2wt.%CNT increased by 48 and 93%.

Other Al_2O_3 nanocomposites

The effect TiC and Ni on alumina was investigated by Rodrigues Suarez et al. [92]. They produced Al_2O_3–25 vol.%TiC–1.9 vol.%Ni nanocomposite by SPS at 1375 °C. Improvements of 30% and 75% in hardness and flexural strength, respectively, were reported for Al_2O_3–TiC–Ni nanocomposite, compared to alumina, while no significant change in fracture toughness was observed. A very low value of electrical resistivity (very high electrical conductivity) of 3.15×10^{-5} Ωm was reported for the Al_2O_3–TiC–Ni nanocomposite. Moreover, the wear rate of Al_2O_3–TiC–Ni nanocomposite was found to be 25 times lower than alumina. In other work [73], no significant change in fracture toughness was observed when Al_2O_3 was reinforced with 10 vol.% niobium and 5 vol.% single wall carbon nanotubes (SWCNT) [93]. SPS sintering at 1200 °C resulted in 98.4% densification, fracture toughness of 3.3 MPa $m^{1/2}$, and hardness of 19.3 GPa for Al_2O_3–5 vol.%SWCNT–10 vol.%Nb nanocomposite. The authors proposed that the damage to SWCNTs during sintering and the non-optimal interfacial bond at the SWCNT–alumina interface were reasons for not observing improvements in fracture toughness. Effects of varying TiC content (2–6 vol.%) and particle size (40–500 nm) on mechanical and microstructural properties of Al_2O_3–20 vol.%SiC–TiC nanocomposites were investigated by Zhao and co-authors [94]. Increase in hardness, fracture toughness, and flexural strength were observed with the increase in TiC content up to 4 vol.%, beyond which the properties decreased. Varying particle size was found to affect only flexural strength, while hardness and fracture toughness remained unaffected. Optimized properties were obtained at 40 nm particle size and 4 vol.% TiC content for the Al_2O_3–20 vol.%SiC–4 vol.%TiC nanocomposite. In another

work, Zhao and co-authors [95] used the same optimized Al_2O_3–20 vol.%SiC–4 vol.%TiC nanocomposite and studied its mechanical properties at elevated temperatures up to 1200 °C in comparison with Al_2O_3–20 vol.%SiC composite. Hardness and fracture toughness of the Al_2O_3–SiC–TiC nanocomposite at all temperatures were higher than those of the Al_2O_3–SiC composite. The Al_2O_3–SiC–TiC nanocomposite showed low high temperature flexural strength, in contrast with high flexural strength at room temperature, compared to Al_2O_3–SiC composite. The low high-temperature flexural strength was attributed to change in fracture mode to intergranular at elevated temperatures. Both hardness and flexural strength decreased with the increase in temperature. At 1000 °C, the Al_2O_3–SiC–TiC nanocomposite maintained 68.4% of its room temperature hardness. At 1100 °C, the flexural strength of the Al_2O_3–SiC–TiC nanocomposite was maintained at 60% of the room temperature value. The elastic modulus of both Al_2O_3–SiC and Al_2O_3–SiC–TiC nanocomposites remain unchanged up to 1000 °C and begin to decrease at 1100 °C. Sun et al. [96] studied the properties of Al_2O_3-based tool materials reinforced with nano-TiC and graphene. They prepared Al_2O_3–(0–30 vol.%)TiC–(0–0.75 vol.%)Graphene nanocomposites using hot pressing at 1650 °C for 10 min. They used 10 vol.% nano-Al_2O_3, 0.5 vol.% MgO, and Y_2O_3 as sintering aid and 0.5 vol.% Ni and Mo as metal binders. The optimum composition was found to be Al_2O_3–10 vol.%TiC–0.5 vol.%Graphene giving flexural strength of 705 MPa, fracture toughness of 7.4 MPa $m^{1/2}$, and hardness of 20.5 GPa. The enhancement in toughness was attributed to the toughening mechanisms induced by both reinforcements. Mechanical and tribological properties of graphene-reinforced Al_2O_3–Ti(C,N) nanocomposites have been reported by Petrus et al. [75]. They used 0, 0.2, 0.5, 0.7 and 1 wt.%graphene in form of multilayer graphene (MLG), graphene oxide (GO), and nikel-coated-graphene to produce Al_2O_3–Ti(C,N) hybrid nanocomposites by SPSat 1550 °C for 4 min. All nanocomposites showed relative density values between 95 and 98%. The Al_2O_3–Ti(C,N)–0.2 wt.%GO nanocomposite showed slightly higher hardness value of 2025 HV compared to 1950 HV for Al_2O_3–Ti(C,N) composite. A decrease in fracture toughness was reported for the graphene-reinforced Al_2O_3–Ti(C,N) nanocomposites. However, the Al_2O_3–Ti(C,N)–0.2 wt.%GO nanocomposite showed 800% lower wear rate, compared to Al_2O_3–Ti(C,N) composite. Sun et al. [97] reported the properties of Al_2O_3–TiC–GNP–MWCNTs prepared by addition of 0.2–0.8 wt.%MWCNT and 0.2–0.7 wt.%GNP to Al_2O_3–TiC. The composites were spark plasma sintered at 1600 °C for 5 min. The Al_2O_3–TiC reinforced with 0.8 wt.%MWCNTs and 0.2 wt.%GNP nanocomposite showed the best properties with relative density of 97.3%, hardness of 18.38%, and fracture toughness of 9.40 MPa $m^{1/2}$. Toughening mechanisms like crack bridging and branching, crack deflection and drawing by CNT and GNP reinforcements were mainly responsible for the enhanced toughness. Chen et al. [98] investigated the effect of sintering parameter and graphene content on mechanical properties of Al_2O_3–TiB_2 nanocomposites. Al_2O_3 was reinforced with 20 wt.%TiB_2 and varying GNP content (0.1–0.6 wt.%), and 0.5 wt.%MgO and 0.5 wt.%Y_2O_3 were used as sintering aids. The authors sintered Al_2O_3–TiB_2 samples by SPS at varying temperatures and times to find the optimum conditions. They found that 1525 °C and 5 min give the optimum mechanical properties and sintered the graphene-reinforced nanocomposites at the same conditions. All nanocomposites showed relative density greater than 98%. The Al_2O_3–TiB_2 reinforced with 0.3 wt.%GNP showed optimum mechanical properties with 6.4% increase in flexural strength and 46.1% increase in fracture toughness compared to Al_2O_3–TiB_2 composite. Nevertheless, a 5.2% decrease in hardness was observed.

ZrB_2 nanocomposites

Zirconium diboride (ZrB_2) belongs to the class of advanced materials known as ultrahigh temperature ceramics (UHTC) [99], which are applied in extreme environments as electrodes for electric discharge machining, crucibles in the metal industry, and structural and functional parts in the aerospace industry [99,100]. Among various UHTC materials, ZrB_2 is the most widely investigated and applied ceramic material because of its very high melting temperature, relatively low density and cost, chemical inertness, high temperature stability and strength, acceptable thermal and electrical conductivity [99]. Typical properties of ZrB_2 are listed in Table 1. However, despite such an excellent combination of properties, there are certain challenges that limit the use of ZrB_2 ceramic such as brittleness and difficulty to sinter. While the use of hot pressing (HP) and SPS improved the sinterability of ZrB_2, the improvement of its fracture toughness was possible by introducing a single reinforcement such as SiC [101–103], CNTs [104,105], and graphene [105,106], resulting in the formation of nanocomposites [99]. It was also reported that introducing reinforcements in ZrB_2 ceramic facilitated densification, and contributed to the improvement of fracture toughness and resistance to oxidation [107,108]. Moreover, it was found that further enhancements in fracture toughness were possible through the incorporation of two distinct reinforcements in the ZrB_2 matrix [109,110], forming hybrid nanocomposites.

Graphite/graphene reinforced ZrB_2–SiC nanocomposites

Asl and co-authors [119] investigated the effect of SPS parameters and nano-graphite flakes (G_{nf}) content on the densification of ZrB_2–25 vol.%SiC–(5, 10 wt.%)G_{nf} nanocomposites. The authors used Taguchi design of experiments approach to set the experimental conditions. They observed that, among all parameters, sintering temperature and G_{nf} content had the most influential effect on the relative density. The ZrB_2–25 vol.%SiC–5 wt.%G_{nf} nanocomposite sintered at 1900 °C and 40 MPa for 4 min had a relative density of 99.5%. Microstructural analysis of the fully dense sample showed the formation of ZrC/B_4C clusters at ZrB_2/G_{nf} interface. The addition of G_{nf} helped in the removal of oxide film from ZrB_2 surface as well as formation of ZrC/B_4C within the grain boundaries, both of which have contributed toward increased sinterability of the nanocomposite. In another work, Asl et al. [120] investigated the interfacial behavior of spark plasma sintered ZrB_2–20 vol.%SiC–10 vol.%GNPs nanocomposite. Full densification was achieved using SPS conditions of 1800 °C and 6 min. Analysis of TEM nanographs of ZrB_2/SiC and ZrB_2/ZrB_2 interfaces did not reveal the presence of ZrC or B_4C compounds. Because of these clean interfaces, it was

Table 1 – Properties of some ultrahigh temperature ceramics.

	ZrB_2 [99,100]	ZrC [111–113]	TiN [113–115]	TiC [113,116]	TaC [113,117]	HfC [113,118]
Melting Point (°C)	3245	3420	2950	3160	3950	3900
Density (g/cm^3)	6.1	6.64	5.40	4.93	14.5	12.2
Fracture toughness (MPa m$^{1/2}$)	1.8–3.5	3.1	2.5	3.1–3.7	3.1	1.73
Hardness (GPa)	>20	25.5	20	>24	16.7	22–25
Elastic modulus (GPa)	489	350–440	251	320	285–560	300–500
Thermal conductivity (W/m K)	60–80	20.5	19.2	21	22.1	20
Coefficient of thermal expansion ($\times10^{-6}$/°C)	6.6	6.6	9.3	7.4	6.3	6.6
Electrical conductivity ($\times10^6$ S/m)	10	1.28	4	1.5	4	2.7

concluded that GNPs acted as sintering aids, by facilitating diffusion-induced joining of particles. Other researchers [107] reported the densification and mechanical behavior of GNSs reinforced ZrB_2–SiC nanocomposites, prepared by in situ thermal reduction of graphene oxide during hot-pressing. Formation of GNSs was confirmed by Raman spectroscopy. The relative density of the ZrB_2–SiC composite (98.2%) increased to 98.9% and 99.2% for the ZrB_2–20 vol.%SiC–2 vol.%GNSs and ZrB_2–20 vol.%SiC–5 vol.%GNSs nanocomposites, respectively. The fracture toughness and flexural strength increased with the increase in the content of GNSs, and reached 7.32 MPa m$^{1/2}$ and 1055 MPa for the ZrB_2–20 vol.%SiC–5 vol.%GNSs nanocomposite, which are 73.8% and 100% higher than those of ZrB_2–SiC. However, slight decrease in hardness was observed, from 23.07 GPa for ZrB_2–20 vol.%SiC composite to 22.76 GPa for ZrB_2–20 vol.%SiC–5 vol.%GNSs. Asl et al. [110] investigated the effect of the addition of G_{nf} (0–10 wt.%) on the properties of spark plasma sintered ZrB_2–25 vol.%SiC composites. A relative densification more than 98% was reported for all samples. The ZrB_2–25 vol.%SiC–5 wt.%G_{nf} nanocomposite showed uncommon relative density of 100.7% which was attributed to the in-situ formation of ZrC phase. The hardness of ZrB_2–25 vol.%SiC composite decreased from 19.5 to 12.1 GPa for ZrB_2–25 vol.%SiC–10 wt.%G_{nf}. However, fracture toughness increased with the increase in graphite content and reached a value of 8.2 MPa m$^{1/2}$ for ZrB_2–25 vol.%SiC–7.5 wt.%G_{nf}, which is twice the value of ZrB_2–25 vol.%SiC. The increase in fracture toughness was attributed to toughening effect of the reinforcements, microstructure refinement, and in-situ formation of ZrC and B_4C compounds. In another work, Asl et al. [121] reported an increase in relative density from 90.1% to 99.6%, with the addition of 20 vol.%SiC and 10 vol.% G_{nf} to ZrB_2. Also, the hardness and fracture toughness of ZrB_2–20 vol.%SiC–10 vol.%G_{nf} nanocomposite increased by 38 and 294%, respectively, compared to ZrB_2. In a similar work, Asl et al. [122] reported 30% increase in hardness and more than 250% increase in fracture toughness of hot-pressed ZrB_2–25 vol.%SiC–5 wt.%GNPs nanocomposite, compared to ZrB_2. The effect of varying the content of G_{nf} on microstructural and mechanical properties of ZrB_2–SiC_w–G_{nf} nanocomposites has been investigated by Asl et al. [123]. ZrB_2–SiC_w–G_{nf} nanocomposites were prepared by reinforcing ZrB_2 with 25 vol.%SiC_w and 0–7.5 wt.% G_{nf}. The samples were sintered using SPS at 1900 °C for 7 min. A relative densification of more than 99.9% was observed for all samples significant grain refinement was observed with the increase in graphite content. The obtained hardness and fracture toughness of ZrB_2–SiC_w–G_{nf} nanocomposites are shown in Fig. 16.

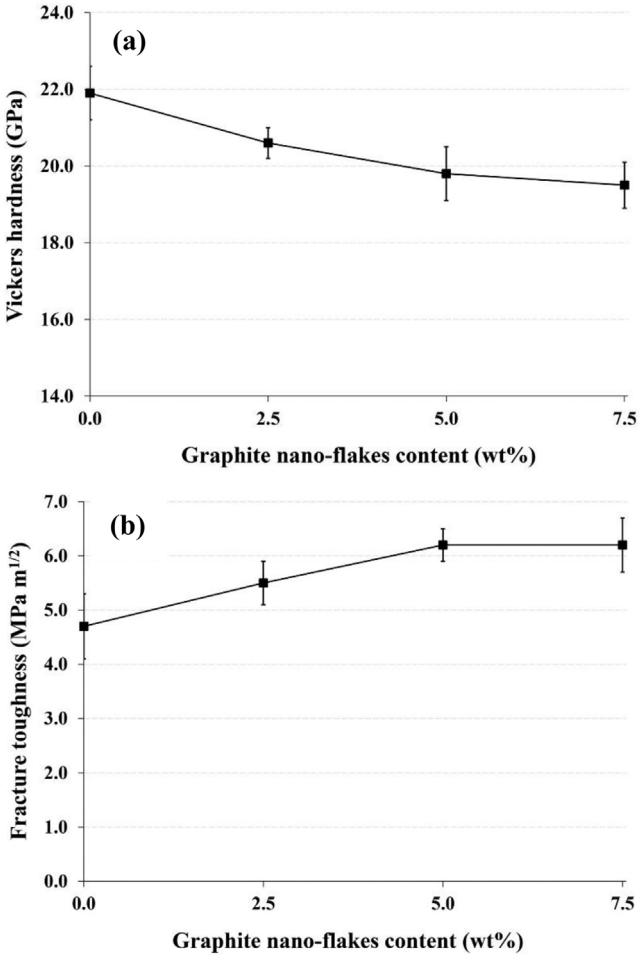

Fig. 16 – (a) Hardness and (b) fracture toughness of ZrB_2–25 vol.%SiC_w–G_{nf} nanocomposites as a function of G_{nf} [123].

A 10% decrease in hardness and 32% increase in fracture toughness were reported for ZrB_2–25 vol.%SiC_w–7.5 wt.%G_{nf} and ZrB_2–25 vol.%SiC_w–5 wt.%G_{nf} nanocomposites, respectively, compared to ZrB_2–25 vol.%SiC_w. Enhancements in fracture toughness of ZrB_2 because of the addition of 0–7.5 wt.% GNPs and 25 vol.% SiC_w were reported by Xia et al. [124]. The ZrB_2–GNPs–SiC_w hybrid nanocomposites were sintered by SPS at 1900 °C for 7 min. All nanocomposites showed relative density values higher than 99.75%. Microstructural analysis showed grain growth inhibition in the hybrid nanocomposites by GNPs. The average grain size

of ZrB_2 in ZrB_2–25 vol.%SiC_w composite decreased from 5.2 to 3.1 μm for ZrB_2–25 vol.%SiCw–7.5 wt.%GNPs nanocomposite. A slight increase in hardness, from 22 to 22.2 GPa was observed because of the inclusion of 2.5 wt.%GNPs in ZrB_2–25 vol.%SiC_w nanocomposite. However, 30% increase in fracture toughness was reported for ZrB_2–25 vol.%SiC_w–7.5 wt.%GNPs nanocomposite. A ZrB_2–20 vol.%SiC–Graphite nanocomposite was prepared by sol gel process and spark plasma sintered at 1950 °C for 10 min [125]. Microstructural analysis of the sintered sample showed uniform distribution of SiC, along with the presence of graphite nanosheets. Flexural strength and fracture toughness of the ZrB_2–20 vol.%SiC–Graphite nanosheets composite was found to be 318 MPa and 3.09 MPa $m^{1/2}$, respectively. Parvizi et al. [126] studied the synergistic effect of graphite nano-flakes (G_{nf}) and SiC reinforcements on properties of spark plasma sintered ZrB_2. The relative density of ZrB_2 increased from 96.1 to 100.7% for ZrB_2–25 vol.%SiC–5 wt.%G_{nf}. Hardness, fracture toughness, and flexural strength of 13.1 GPa, 3.2 MPa $m^{1/2}$, and of 445 MPa for ZrB_2 increased to 16.6 GPa, 6.7 MPa $m^{1/2}$, and 631 MPa for ZrB_2–25 vol.%SiC–5 wt.%G_{nf} nanocomposite, respectively. The effect of varying diameter of graphite reinforcement on mechanical and thermal shock properties of ZrB_2–20 vol.%nano-SiC–20 vol.%Graphite nanocomposites was investigated by Hou et al. [127]. ZrB_2–20 vol.%SiC–20 vol.%Graphite nanocomposites, with different graphite diameters of 5, 10 and 20 μm, were hot pressed at 1900 °C. Relative density of more than 98% was observed for all samples. ZrB_2–20 vol.%SiC–20 vol.%Graphite nanocomposites with 10 μm diameter graphite showed the highest flexural strength of 523 MPa, fracture toughness of 4.54 MPa $m^{1/2}$, and Young's modulus of 356 GPa. The nanocomposite with smallest graphite diameter showed better thermal shock resistance. Nguyen et al. [128] investigated sintering behavior and microstructure of ZrB_2 reinforced with 25 vol.%SiC_w whiskers and 5 wt.%GNPs. Fully dense ZrB_2–SiC_w–GNPs nanocomposite was prepared using SPS at 1900 °C. XRD analysis showed no new phase formation during sintering. Microstructural analysis revealed ultra-thin amorphous layer at ZrB_2–GNPs interface and dislocation in ZrB_2.

CNT reinforced ZrB_2–SiC nanocomposites

Tian and co-authors investigated the effect of CNTs on densification, mechanical and thermal properties of hot-pressed ZrB_2–SiC [129]. Slight decrease in densification, hardness (6%) and thermal conductivity (4%) were observed for ZrB_2–20 vol.%SiC–2 wt.%CNTs nanocomposite compared to ZrB_2–20 vol.%SiC. But, the same composite showed 15% increase in fracture toughness and 6% increase in flexural strength. In other work [130], hot-pressed ZrB_2 reinforced with 20 vol.%SiC and 10 vol.%MWCNTs displayed better properties compared to ZrB_2. The relative density of ZrB_2 increased from 90.1% to 93.9% for ZrB_2–20 vol.%SiC–10 vol.%CNTs nanocomposite. The reinforcements also contributed to inhibiting the grain growth during sintering. A 180% increase in fracture toughness while 30% decrease in hardness were reported for the ZrB_2–20 vol.%SiC–10 vol.%CNTs nanocomposite compared to ZrB_2. Nisar et al. [131] reported enhancements in the properties of ZrB_2 ceramic composite, produced by SPS, through the synergistic reinforcement of SiC and CNTs. The relative density increased from 93.1 (ZrB_2) to 99.7 (ZrB_2–20 vol.% SiC–10 vol.% CNTs), while the fracture toughness and flexural strength were 3 and 1.6 times higher, respectively. In other work, Nisar et al. [132] observed significant improvements in densification, mechanical properties and thermal performance of spark plasma sintered ZrB_2–20 vol.%SiC–10 vol.%CNTs nanocomposite. The relative density of ZrB_2 increased from 93.1 to 99.7% for ZrB_2–20 vol.%SiC–10 vol.%CNTs. To study the oxidation behavior, samples were exposed to plasma arc-jet with heat flux of 2.5 MW/m^2 for 30 seconds. After the oxidation test, 42% ZrB_2 phase retention along with lower oxidation rate of 0.44 μm/s were observed for ZrB_2–20 vol.%SiC–10 vol.%CNTs, compared to 30% and 0.77 μm/s for ZrB_2, respectively. The thickness of oxide layer was 10 μm for ZrB_2–20 vol.%SiC–10 vol.%CNTs, showing more oxidation resistance, compared to 23 μm for ZrB_2. Compared to ZrB_2, higher hardness was reported for ZrB_2–20 vol.%SiC–10 vol.%CNTs nanocomposite in both cases; 1.6 times higher in unexposed samples and 2.1 times higher in exposed samples. The thermal conductivity, thermal diffusivity, and specific heat of ZrB_2 increased from 48.9 W/m K, 0.236 mm^2/s, and 340.4 J/kgK at 50 °C to 61.8 W/m K, 0.24 mm^2/s, and 485.2 J/kgK for ZrB_2–20 vol.%SiC–10 vol.%CNTs, respectively. The TGA results showed that the oxidation temperature shifted from 679.3 °C for ZrB_2 to 406.3 °C for ZrB_2–20 vol.%SiC–10 vol.%CNTs, an indication of enhanced oxidation resistance. Popov and co-authors [133] prepared ZrB_2–31 wt.%SiC and ZrB_2–29 wt.%SiC–8 vol.%CNTs composites by reactive hot pressing ZrC, B_4C, Si, and CNTs powders in the temperature range 1100–1830 °C. The ZrB_2–29 wt.%SiC–8 vol.%CNTs nanocomposite showed 60% improvement in fracture toughness compared to ZrB_2–29 wt.%SiC.

Nano-carbon reinforced ZrB_2–SiC nanocomposites

Nano-sized carbon black (C_{nb}) was used to prepare a ZrB_2–20 vol.%SiC–10 vol.%C_{nb} nanocomposite by HP at 1850 °C for 60 min [134]. The sintered nanocomposite nearly reached fully density (99.8%). A pore-free microstructure and strong interfaces between ZrB_2, SiC and C_{nb} could be observed in the TEM image of ZrB_2–20 vol.%SiC–10 vol.%C_{nb} nanocomposite shown in Fig. 17. XRD analysis revealed partial conversion of carbon-black to crystalline graphite, which was also confirmed by TEM. In other work, Azizian Kalandaragh et al. [109] studied the effect of varying carbon nanoparticles (C_{np}) content on microstructural and mechanical properties of spark plasma sintered ZrB_2–25 vol.%SiC_w–C_{np} nanocomposites. They reported a relative density higher than 99.8% for all sintered samples and observed reduction in grain growth. The hardness was found to decrease linearly from 21.9 to 14.6 GPa for ZrB_2–25 vol.%SiC_w–7.5 wt.%C_{np} nanocomposite. However, the fracture toughness increased from 4.7 MPa $m^{1/2}$ for ZrB_2–25 vol.%SiC_w composites to 7.1 MPa $m^{1/2}$ for ZrB_2–25 vol.%SiC_w–5 wt.%C_{np}. Hu et al. [135] used carbon fibers (C_f) to produce ZrB_2–20 vol.%SiC–30 vol.%C_f by HP at relatively low temperature of 1450 °C. They reported a relative density of 95.8%, flexural strength of 341 MPa, and fracture toughness of 6.12 MPa $m^{1/2}$. The ZrB_2–20 vol.%SiC–30 vol.%C_f nanocomposite displayed high work of fracture compared to other ZrB_2-based composites without C_f. Nasiri et al.

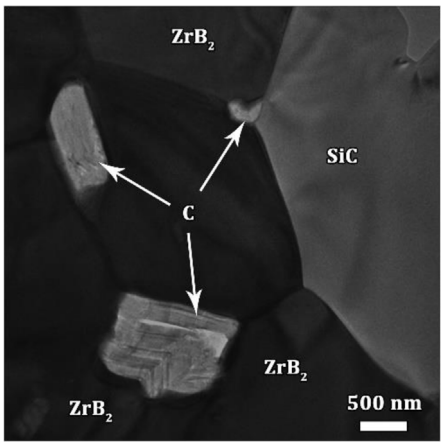

Fig. 17 – TEM image of ZrB_2–20 vol.%SiC–10 vol.%C_{nb} nanocomposite [134].

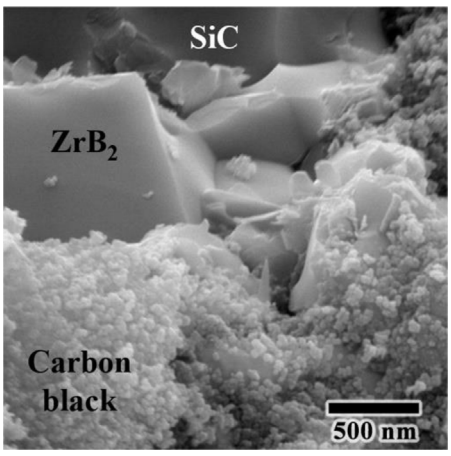

Fig. 18 – FE-SEM image of fractured surface of ZrB_2–20 vol.%SiC–10 vol.%C_{nb} nanocomposite showing unreacted nano-carbon black [137].

[136] studied the effect of varying the content of C_f (2.5–15 wt.%) and SiC nanoparticles (2.5–10 wt.%) on densification and mechanical properties of pressure-less sintered ZrB_2–SiC–C_f nanocomposites. The relative density, hardness, and fracture toughness increased with the increase in SiC content up to 10 wt.%, beyond which the properties began to decrease. However, the increase in C_f reinforcement content caused the density, hardness, and fracture toughness to decrease in ZrB_2–SiC–C_f nanocomposites. The ZrB_2–10 vol.%SiC–2.5 vol.%C_f had optimum properties with a relative density of 93%, hardness of 14.5 GPa, and fracture toughness of 5.9 MPa $m^{1/2}$. The effect of C_{nb} addition on microstructural and mechanical properties of ZrB_2–SiC composites were reported by Farahbakhs and co-authors [137]. They hot pressed ZrB_2, and ZrB_2–20 vol.%SiC and ZrB_2–20 vol.%SiC–10 vol.%C_{nb} composites at 1850 °C. Relative density values of 90 and 93% were reported for ZrB_2 and ZrB_2–20 vol.%SiC samples, which increased to 99.8% for ZrB_2–20 vol.%SiC–10 vol.%C_{nb} sample. The authors observed refinement of the microstructure and concluded that C_{nb} acted as a sintering aid. The SEM analysis of the ZrB_2–20 vol.% SiC–10 vol.% C_{nb} nanocomposite, presented in Fig. 18, showed the presence of some unreacted C_{nb} along with SiC and ZrB_2, while some carbon was believed to react with the surface oxides of ZrB_2, resulting in enhanced densification. Hardness and flexural strength values of 11.9 GPa and 355 MPa for ZrB_2 increased to 16.7 GPa and 687 MPa, respectively, for the ZrB_2–20 vol.%SiC–10 vol.%C_{nb} nanocomposite. Moreover, a 180% increase in fracture toughness was observed for ZrB_2–20 vol.%SiC–10 vol.%C_{nb} nanocomposite compared to ZrB_2 (2.1 MPa $m^{1/2}$). Zhou et al. [138] also observed improvements in fracture toughness and thermal properties of hot-pressed ZrB_2–20 vol.%SiC composite because of the addition of 5 vol.% C_{nb}. The ZrB_2–20 vol.%SiC–5 vol.%C_{nb} nanocomposite had a high fracture toughness of 6.6 MPa $m^{1/2}$. Also, the thermal shock resistance parameter of the hybrid nanocomposite was 15% higher than ZrB_2–20 vol.%SiC nanocomposite. Savari and co-authors [139] investigated the densification and toughness of ZrB_2 reinforced with SiC (15 and 30 vol.%) and C_{nb}(10 and 15 vol.%). The nanocomposites were spark plasma sintered at 1850 °C and 35 MPa for 8 min. The ZrB_2 showed low relative density of 81%, however, nearly full density was obtained when ZrB_2 was reinforced with SiC and C_{nb}. Significant improvements in fracture toughness were reported for single reinforcement with C_{nb}, but only a marginal increase of 26% was observed for hybrid reinforcement in ZrB_2–30 vol.%SiC–(10, 15 vol.%)C_{nb} nanocomposites.

Other ZrB_2–SiC nanocomposites

Li et al. [140] reported properties of hot-pressed ZrB_2–15 vol.%SiC_w–(10,15,20) vol.%$MoSi_2$ nanocomposites. A relative density of 99.9% was obtained for all samples at 1750 °C. ZrB_2–15 vol.%SiC_w–15 vol.%$MoSi_2$ nanocomposite showed the highest mechanical properties, with hardness of 17.64 GPa, fracture toughness of 5.52 MPa $m^{1/2}$, and flexural strength of 564 MPa. Yue et al. [141] used SPS to prepare ZrB_2–SiC reinforced with mixture of boron nitride nanotubes (BNNT) and boron nitride nanoplateles (BNNP). While the hardness and elastic modulus remained unchanged, a 24% increase in the fracture toughness was observed in the ZrB_2–20 vol.% SiC–1 wt.% (BNNT–BNNP) nanocomposite compared to ZrB_2–20 vol.% SiC. Fattahi et al. [142] studied the effect of 0–3 wt.% nano-diamond on microstructural and mechanical properties of ZrB_2–25 vol.% SiC nanocomposites. They prepared samples using SPS at 1900 °C for 7 min. All nanocomposites showed relative density higher than 98.8%. The authors analyzed the microstructure of the reinforced nanocomposites and observed the formation of ZrC and B_4C. They reported increased hardness and fracture toughness, and the highest values were 24.6 GPa for ZrB_2–25 vol.% SiC–2 wt.% nano-diamond nanocomposite and 5.8 MPa $m^{1/2}$ for the ZrB_2–25 vol.% SiC–3 wt.% nano-diamond, as compared to 19.5 GPa and 4.3 MPa $m^{1/2}$ for ZrB_2–25 vol.% SiC composite, respectively. They attributed the increase in hardness to the formed hard phases during sintering, while the toughness increase was attributed to the establishment of toughening mechanisms such as crack deflection, branching, and crack bridging due to the presence of nano-diamond.

ZrC nanocomposites

Zirconium carbide (ZrC) belonging to the UHTCs group and has low density, very good mechanical and electrical properties, and good chemical and thermal stability [111]. Typical properties of ZrC are listed in Table 1. Difficulty to sinter and small fracture toughness are some challenges in the application of ZrC. [143]. Using new sintering techniques along with reinforcing ZrC matrix with a second phase have resulted in significant improvements in both fracture toughness and sinterability [112,144–147]. However, limited work is available on ZrC reinforced with hybrid reinforcements.

Acicbe et al. [111] studied the effect of TiC and MWCNTs on densification and mechanical properties of ZrC–TiC and ZrC–TiC–CNTs nanocomposites. ZrC showed relative density of 95.5%, which increased to more than 98% for all ZrC–TiC and ZrC–TiC–CNTs nanocomposites. Microstructural analysis showed homogeneous distribution along with some micro-cracks in ZrC–TiC composite, which disappeared by introducing CNTs in case of ZrC–TiC–CNTs nanocomposite. The hardness of ZrC increased from 17.6 to 22 GPa for ZrC–TiC. However, introduction of CNTs caused the hardness to decrease, reaching a value of 20 GPa for ZrC–20 vol.%TiC–1 wt.%CNTs nanocomposite. Increase in fracture toughness of ZrC (3.30 MPa $m^{1/2}$) was observed with increasing the reinforcement content, reaching a value of 4.27 MPa $m^{1/2}$ for ZrC–20 vol.%TiC–1 wt.%CNTs nanocomposite. Similar enhancements in properties of ZrC, by addition of 20 vol.% Ti and 3 vol.%CNTs, have been reported by Sha et al. [143]. A relative density of 98.27%, a hardness of 18.11 GPa, a flexural modulus of 207 GPa, and a flexural strength of 415 MPa were measured for ZrC–20 vol.%Ti–3 vol.%CNTs nanocomposite. Moreover, a fracture toughness of 5.27 MPa $m^{1/2}$ was obtained for the nanocomposite, which is 32% higher than that of ZrC. Li et al. [147] investigated the effect of 20 vol.%Nb and 3 vol.%CNTs on properties of hot-pressed ZrC as shown in Fig. 19. Improved sinterability was observed for ZrC–20 vol.%Nb–3 vol.%CNTs nanocomposite, reaching 99.28%. Microstructural analysis showed the formation of (Zr, Nb)C solid solution and $Zr_xC_yO_z$ compound during hot-pressing. An 80% increase in fracture toughness was reported for the nanocomposite, compared to ZrC. Furthermore, a hardness of 17.93 GPa, a flexural modulus of 281 GPa, and a flexural strength of 590 MPa were obtained for ZrC–Nb–CNT nanocomposite. The effect of GNPs addition on microstructural and mechanical properties of ZrC–TiC based nanocomposites have been reported by Ocak et al. [148]. ZrC–(20−x) vol.%TiC–x vol.%GNPs (where x = 0–9 vol.%) nanocomposites were spark plasma sintered at 1700 °C. Microstructural analysis showed the formation of (Zr, Ti)C solid solution by substitution of Zr^{+4} ions by Ti^{+4} during sintering. Densification of 99.49% and fracture toughness of 5.17 MPa $m^{1/2}$ for ZrC–17 vol.%TiC–3 vol.%GNPs nanocomposite was found to be highest. Further addition of GNPs beyond 3 vol % resulted in a decrease in densification and fracture toughness. The hardness was found to decrease with an increase in GNPs content in ZrC–TiC–GNPs nanocomposites.

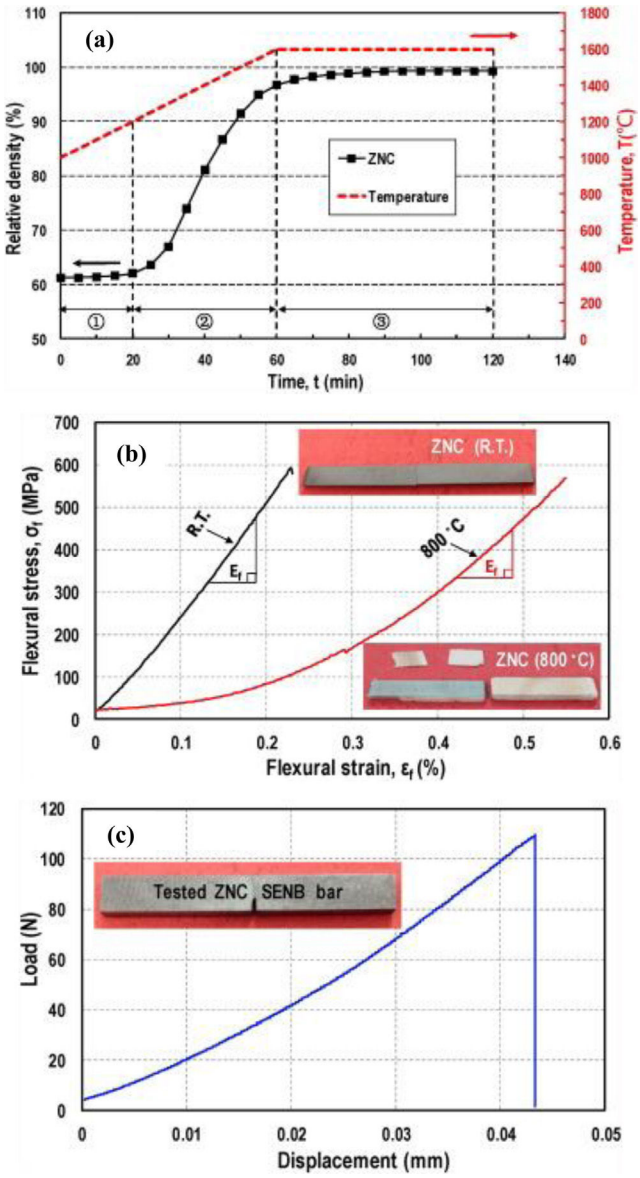

Fig. 19 – Properties of ZrC-based composite doped with Nb and CNT (a) relative density, (b) flexural stress–strain, and (c) load–displacement [147].

TiN nanocomposites

Typical properties of titanium nitride (TiN) are listed in Table 1. TiN has very high melting temperature, high hardness, good thermal and electrical conductivity, and very high corrosion resistance. It is mostly used in fabricating cermets and as coatings on metals and cutting tools [114,115]. Its use in many industries is limited because of its inadequate fracture toughness and poor sinterability [114,149]. Some of these limitations have been countered by the addition of a single reinforcement such as TiC [149], Si_3N_4 [150], AlN [151], HfC [152], and graphene [115]. Due to the fact that TiN is employed as reinforcement for ceramic matrices, very limited work is available on TiN hybrid nanocomposites.

The effect of SiC and MWCNTs on densification and microstructure of TiN was investigated by Delbari and co-authors [114]. TiN and TiN–20 vol.%SiC–5 wt.%MWCNTs nanocomposite were produced by SPS at 1900 °C and 40 MPa

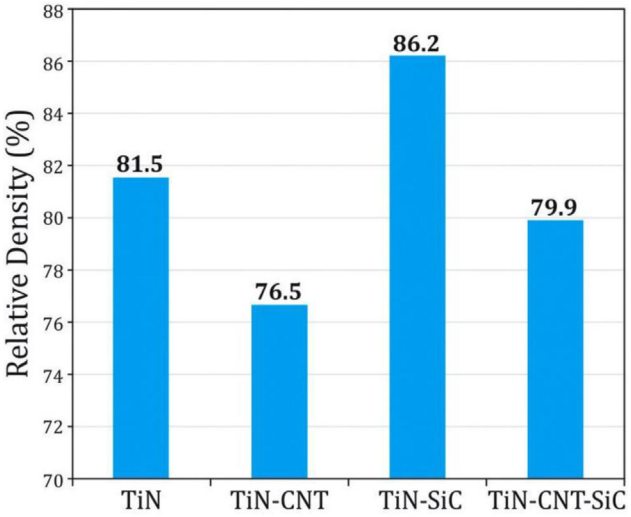

Fig. 20 – Density of TiN-based ceramics [114].

for 7 min. The relative density decreased from 81.5% for TiN to 79.9% for the TiN–20 vol.%SiC–5 wt.%MWCNTs nanocomposite as can be seen in Fig. 20. The authors analyzed the microstructure and observed the presence of SiC and MWCNTs at grain boundaries, which believed to hinder grain growth. They examined the fracture surface of the sintered nanocomposite, which showed several toughening mechanisms such as crack bridging, crack deflection, crack branching, and intergranular fracture mode [114].

TiC nanocomposites

Titanium carbide (TiC) has very high melting temperature, low density, high hardness, high thermal stability and conductivity, and high electrical conductivity as listed in Table 1. It is a suitable material for hypersonic space applications, cutting tools, refractory components, and in the nuclear industry [153–155]. To address issues associated with the sinterability and the inadequate fracture toughness of TiC, researchers developed TiC nanocomposites reinforced with a single phase such as graphene [154], SiC [155,156], ZrC [157], WC [158,159], nano-diamond [160], TiN [161] and CNTs [116], and hybrid nanocomposites that incorporates two phases [116,153,162–168].

TiC and hybrid TiC nanocomposite reinforced with 3.5 wt.% WC and 2 wt.% MWCNTs were prepared by SPS [116]. The relative density of TiC increased from 89 to 99% due to the addition of WC and CNTs. Furthermore, a reduction of 38% in grain size was observed for the TiC–3.5 wt.%WC–2 wt.%CNTs nanocomposite compared to TiC. The hardness, elastic modulus, and fracture toughness of the TiC–3.5 wt.%WC–2 wt.%CNTs nanocomposite increased by 41%, 42%, and 141%, respectively, compared to TiC [116]. In another study, Sribalaji et al. [153] investigated the thermal shock resistance of spark plasma sintered TiC and TiC–3.5 wt.%WC–2 wt.%CNTs nanocomposite. The samples were thermally shocked at 1700 °C in open air for 10 thermal cycles. Microstructural analysis of thermally shocked nanocomposite showed retention of most of CNTs, while some of them collapse to carbon. The nanocomposite showed 63% lower rate of mass change and 89% higher thermal shock resistance parameter (R_{st}), compared to the monolithic ceramic. The significant increase in thermal shock resistance was attributed to higher densification, higher fracture toughness, and homogenous distribution of CNTs. The thermally shocked TiC–3.5 wt.%WC–2 wt.%CNTs nanocomposite showed 74% higher hardness and 54% higher elastic modulus, compared to TiC. Fattahi et al. [162] studied the effect of 0–30 vol.% SiC_w whiskers and 3 wt.% nano-WC on properties of TiC nanocomposites. Samples were prepared by SPS at 1900 °C and 40 MPa for 7 min. The sintered nanocomposites showed high relative density and uniform dispersion of the reinforcements, and no significant grain growth was observed. The TiC–3 wt.%WC_n and TiC–3 wt.%WC_n–20 vol.%SiC_w samples had the highest hardness and flexural strength of 28.6 GPa and 694 MPa, respectively. In another work, Fattahi et al. [163] varied the amount of nano-sized WC (0, 1.5 and 3 wt.%) in TiC–10 vol.%SiC_w; and reported an increase in the relative density of the TiC–SiC_w composite from 98.73 to 99.43% with the addition of 1.5 wt.% nano-WC. However, the density decreased with further addition of WC. Non-stoichiometric TiC_x, in-situ TiC, SiC, and WSi_2 were found to form in sintered samples. The hardness and flexural strength decreased, with the increase in the content of nano-WC, and reached 12 GPa and 368 MPa for TiC–10 vol.%SiC_w–3 wt.%WC nanocomposite, compared to 24.54 GPa and 511 MPa for TiC–10 vol.%SiC_w, respectively. The authors attributed the decrease in the properties to the presence of the brittle WSi_2 at grain boundaries. They reported slight increase in thermal conductivity, from 19.8 to 24.3 W/m K when TiC–10 vol.%SiC_w was reinforced with 1.5 wt.% nano-WC. Nguyen et al. [164] reinforced TiC with 0–5 wt.% h-BN and 0–5 wt.% G_{nf} to form hybrid nanocomposites and characterized the microstructure, and mechanical and frictional properties. They sintered the samples using SPS at 1900 °C for 10 min, and found that the hybrid reinforcements had negative impact on densification, where the relative density decreased from 95.5% (TiC) to 93.2% (TiC–5 wt.%h-BN–5 wt.%G_{nf}). Microstructural analysis of sintered samples revealed the formation of TiB_2 and TiB in-situ phases, and the presence of carbon zones shown by dark areas in the scanning electron microscope (SEM) micrograph presented in Fig. 21 and confirmed by energy dispersive spectroscopy (EDS) results. The h-BN reinforcement and the in-situ phases appeared uniformly distributed while the G_{nf} were present in the form of zones. Vickers hardness and flexural strength of TiC decreased from 3128 HV and 504 MPa to 2477 HV and 457 MPa, respectively, with addition of 5 wt.%h-BN and 5 wt.%G_{nf}. However, the coefficient of friction increased from 0.299 for TiC to 0.315 for the TiC–5 wt.%h-BN–5 wt.%G_{nf}. In another work, Nguyen et al. [165] reported the mechanical and thermal properties of TiC reinforced with 5 wt.%TiN and 5 wt.%nano-diamond. The nanocomposite was sintered using SPS at 1900 °C for 10 min. The authors found that the relative density decreased from 95.5 to 87.4% as a result of the addition of TiN and nano-diamond, and attributed this decrease to the formation of N_2 gas due to the reaction between solid solution of Ti (C, N) formed due to TiN addition and graphitized carbon formed from the nano-diamond. The hybrid reinforcements were found to decrease the hardness and flexural strength. Similarly,

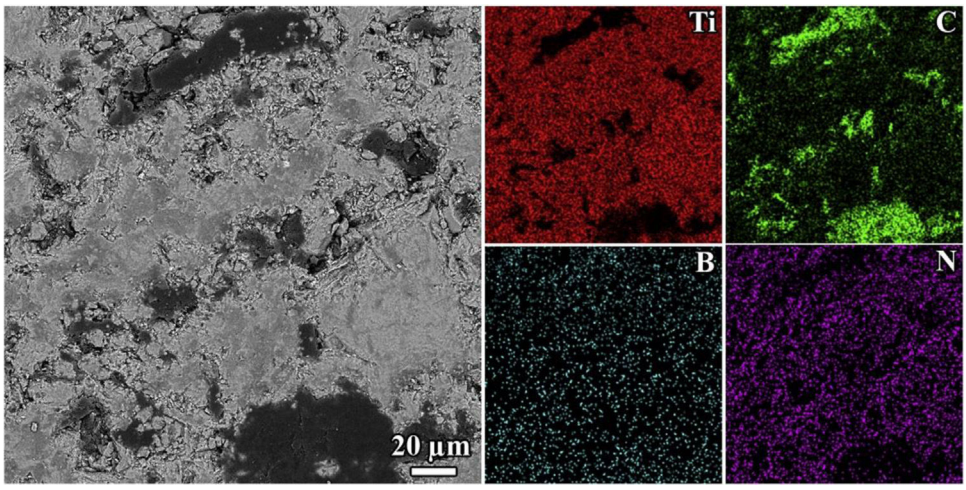

Fig. 21 – SEM image of polished TiC–5 wt.% h-BN–5 wt.% graphite nanocomposite with EDS analysis [184].

the thermal conductivity decreased from 17.7 W/m K (TiC) to 15.4 W/m K (TiC–5 wt.%TiN–5 wt.% diamond). In another work, Nguyen and co-authors [166] reported the strengthening of TiC using 5 wt.%AlN and 5 wt.% GNPs. The nanocomposite samples were sintered using SPS at 1900 °C for 10 min. The relative density increased from 95.5% to 101.2% because of the addition of AlN and GNPs. Moreover, 35% increase in flexural strength was reported for TiC–5 wt.%AlN–5 wt.% GNPs

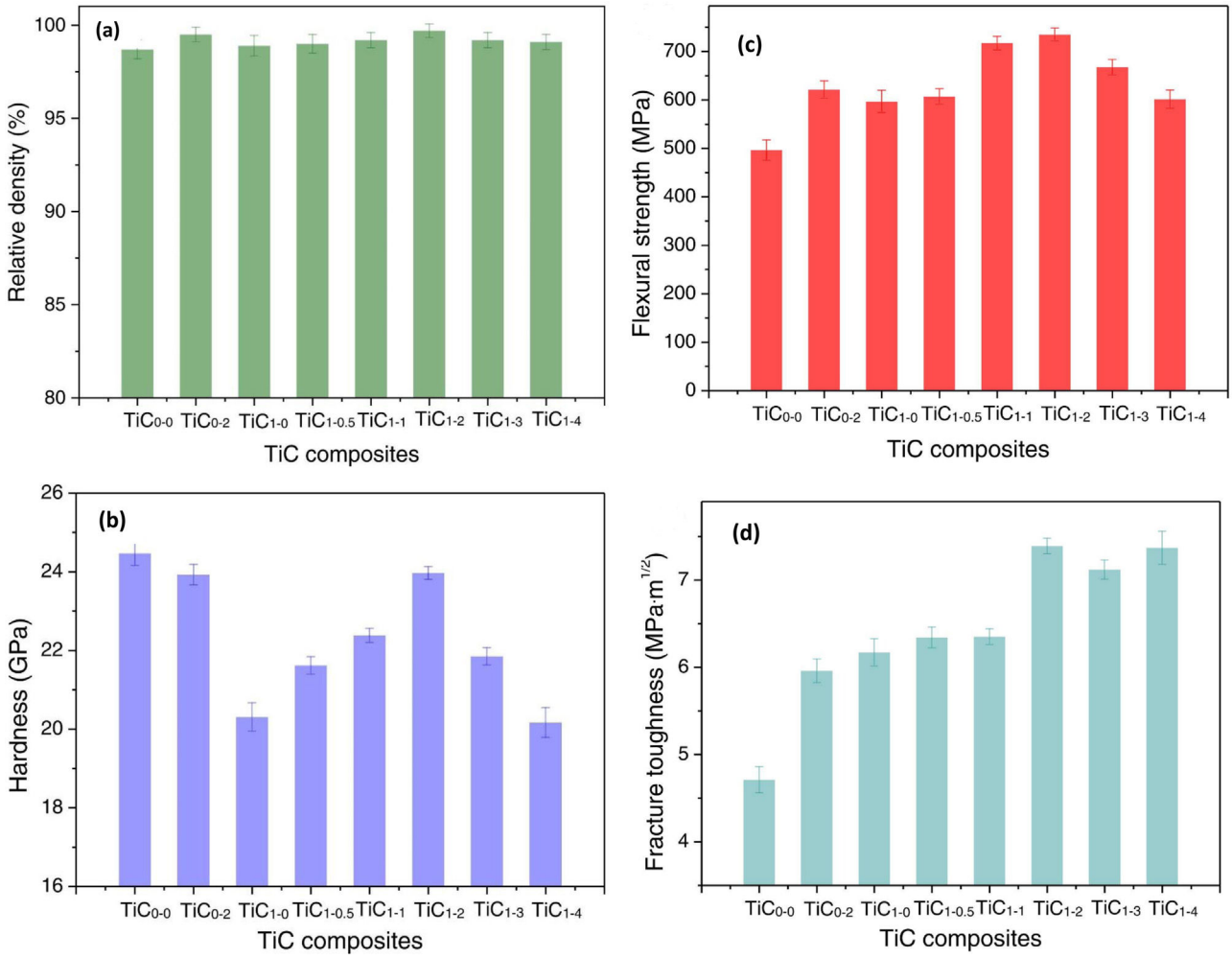

Fig. 22 – Properties of TiC-based nanocomposites with different CNT/SiCnw ratios (a) relative density, (b) hardness, (c) flexural strength, and (d) flexural toughness [168].

nanocomposite, as compared to TiC. The increase in the flexural strength was attributed to grain refinement and uniform distribution of in-situ phases formed during sintering. Properties of MLG reinforced TiC–WC composites, prepared by two step sintering, have been reported by Sun et al. [167]. The authors used micro-TiC, nano-TiC, WC, and MLG powders to prepare TiC–10 wt.%nano–TiC–3 wt.%WC–(0–0.45 wt.%)MLG nanocomposites. They sintered the samples by inductive hot-pressing in two-steps; first step at 1850 °C for 5 min and second step at 1750 °C for 60 min. All nanocomposites showed densification higher than 97%, with TiC–WC reinforced with 0.45 wt.%MLG nanocomposite reaching 99.3%. Hardness and flexural strength were found to increase with the increase in MLG content, and reached 24.2 GPa and 718.6 MPa, respectively, for TiC–WC reinforced with 0.45 wt.%MLG. The enhancements in hardness and flexural strength were attributed to the high densification and grain refinement. A relatively higher fracture toughness of 7.2 MPa $m^{1/2}$ was also reported for TiC–10 wt.%nano-TiC–3 wt.%WC–0.45 wt.%MLG nanocomposite. In other work, Sun et al. [168] reinforced TiC matrix with SiC_{nw} and CNTs. TiC–2 wt.%HfC–3 wt.%ZrO_2 were synergistically reinforced with 1.5 wt.%CNTs and 0–6 wt.%SiC_{nw}. Two-step SPS was employed, 5 min at 1800 °C then cooling to 1650 °C and holding for 30 min. The relative density of all hybrid nanocomposite samples was found to be more than 98.5%. XRD analysis showed formation of solid solution with predominant phases of TiC, ($Ti_{0.8}$, $Hf_{0.2}$)C and ZrO_2 in all samples. The hardness decreased from 24.47 GPa (TiC–HfC–ZrO_2) to 23.97 GPa (TiC–HfC–ZrO_2–1.5 wt.%CNTs–3 wt.SiC_{nw}), but the flexural strength and fracture toughness increased by 48.1 and 56.9, respectively, as can be seen in Fig. 22. CNT/SiC_{nw} bending, pull-out as well as crack deflection and bridging, as shown in Fig. 23, were believed to be the primary toughening mechanisms.

TaC nanocomposites

Besides its extraordinary mechanical properties, corrosion resistance, high thermal conductivity and stability, and high electrical conductivity, tantalum carbide (TaC) has the highest melting point among all the UHTCs [169]. Typical properties of TaC are listed in Table 1. However, like other UHTCs, TaC also has poor sinterability and inadequate fracture toughness [170]. Addition of reinforcements such as graphene [171], CNTs [172], SiC [173], B_4C [174], $TaSi_2$ [175], $MoSi_2$ [175] have resulted in improvements in sinterability and fracture toughness. Similarly, incorporating hybrid reinforcements in TaC have shown promising results [117,176–178].

Nisar et al. [117] studied the toughening of TaC by SiC and MWCNTs. They prepared TaC and TaC–15 vol.%SiC–15 vol.%CNTs nanocomposite by SPS (three-stage sintering) at 1850 °C. The authors analyzed the microstructure of the sintered nanocomposite and did not observe new phases, however, they reported partial CNTs transformation to graphite. The relative density of 93%, fracture toughness of 3.1 MPa $m^{1/2}$, and fracture strength of 23.4 MPa for TaC increased to 98%, 11.4 MPa $m^{1/2}$, and 182.6 MPa for the TaC–15 vol.%SiC–15 vol.%CNTs nanocomposite, respectively. However, a decrease in hardness from 15.5 GPa for TaC to 14.1 GPa for the TaC–15 vol.%SiC–15 vol.%CNTs nanocomposite was observed, which was attributed to partial CNTs to graphite transformation during sintering. In another study, Nisar et al. [176] reported enhanced fretting and scratch wear behavior of TaC–15 vol.%SiC–15 vol.%CNTs nanocomposite. For fretting wear, the wear rate of TaC–15 vol.%SiC–15 vol.%CNTs nanocomposite decreased by 61% (4.1×10^{-7} mm^3/Nm) as compared to 10.5×10^{-7} mm^3/Nm for TaC, while for scratch wear the rate decreased from 8 mm^3/Nm to 2.7 mm^3/Nm. In another work, Nisar and co-authors [177] investigated thermal performance of spark plasma sintered TaC and TaC–15 vol.%SiC–15 vol.%CNTs nanocomposite. They exposed the sintered samples to plasma-arc jet under heat-flux of 2.5 MW/m^2 for 30 seconds. After exposure, 25% and 22% retention of TaC phase was observed in TaC and TaC–SiC–CNTs nanocomposite, respectively. Moreover, the thickness of the oxide scale layer, having major phase of Ta_2O_5, was found to be 30.1 μm for TaC; which decreased to 20.1 μm

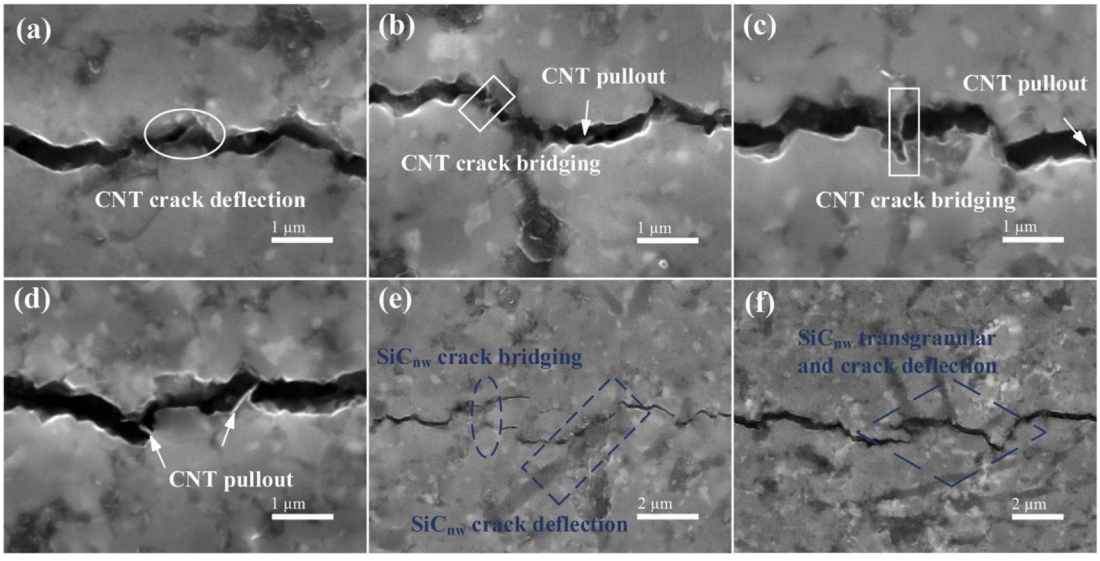

Fig. 23 – Primary toughening mechanism in TiC-based nanocomposites [168].

for TaC–SiC–CNTs nanocomposite. Enhanced thermal conductivity, thermal diffusivity, and specific heat values of 40.8 W/m K, 1731 mm^2/s, and 214.9 J/kg.K were reported for the TaC–SiC–CNTs nanocomposite, compared to 18.5 W/m K, 778 mm^2/s, and 164 J/kgK for TaC at 100 °C, respectively. A shift in the oxide layer formation temperature, from 735 °C for TaC to 901 °C for TaC–SiC–CNTs nanocomposite, was confirmed by thermogravemetric analysis (TGA). TaC was completely oxidized at 800 °C during TGA analysis but not much change was observed in TaC–SiC–CNTs nanocomposite up to 1500 °C. The authors attributed the enhancement in the oxidation resistance of the TaC–SiC–CNTs nanocomposite to the formation of a protective SiO_2 along with grain sealing by CNTs. In other study, Al-Habib et al. [178] investigated the effect of graphene on sintering and mechanical properties of TaC–TiC–SiC composites. They obtained TaC–TiC–25 vol.%SiC composite and TaC–TiC–25 vol.%SiC–5 wt.%graphene nanocomposite using SPS at 2000 °C and 35 MPa for 8 min. Higher densification and hardness values of 95.1% and 19.8 GPa were reported for the graphene–reinforced TaC-based nanocomposite, as compared to 92.4% and 18.5 GPa for the TaC–TiC–SiC composite. Graphene was found to facilitate the densification process and improve hardness. XRD analysis of sintered samples showed the formation of many new phases during sintering such as Ti_5Si_3, $TaC_{0.47}$, Ti_3SiC_2, $Ti_6C_{3.75}$, $TiSi_2$ and Ta_4C_3.

HfC nanocomposites

Hafnium carbide (HfC) is a UHTC ceramic having potential applications in rocket nozzles, nuclear reactors, thermal field emitters, cutting tools, high temperature solar absorbers, and space air-craft components [179–181]. Typical properties of HfC are listed in Table 1. The high hardness, high stiffness, high thermal stability, and corrosion resistance made HfC potential candidate for various applications. Problems such difficulty to sinter and inadequate fracture toughness of HfC were countered using second phase reinforcements including SiCN [179], $MoSi_2$ [182], SiC [173], and CNTs [118]. The properties of HfC-based nanocomposites were not fully explored because of its poor sinterability. Mukherjee et al. [118] prepared HfC–5 wt.%$MoSi_2$ and HfC–5 wt.%$MoSi_2$–2 wt.%CNTs nanocomposites by SPS at 1600 °C. The authors found that CNTs promoted grain refinement, and both $MoSi_2$ and CNTs acted as sintering aid, which enhanced the densification. The relative density increased from 96% for the HfC–5 wt.%$MoSi_2$ composite to 99% for the HfC–5 wt.%$MoSi_2$–2 wt.%CNTs hybrid nanocomposite. The fracture toughness of the HfC–5 wt.%$MoSi_2$–2 wt.%CNTs nanocomposite increased by 91%, while the hardness and stiffness decreased by 12% and 13%, respectively, compared with the HfC–5 wt.%$MoSi_2$.

Si_3N_4 nanocomposites

Silicon nitride (Si_3N_4) has good mechanical characteristics, high wear resistance, good thermal shock resistance, and self-lubricating attributes, which make it a promising candidate material for numerous applications, including high-temperature ball bearings, rollers, and cutting tools [183,184]. Overcoming the poor sinterability and inadequate fracture toughness of Si_3N_4 and improving its mechanical properties were possible through the addition of single-phase reinforcements like TiN [185], SiC [186], CNTs [187], WC [188], and graphene [189] or two phases [190–193].

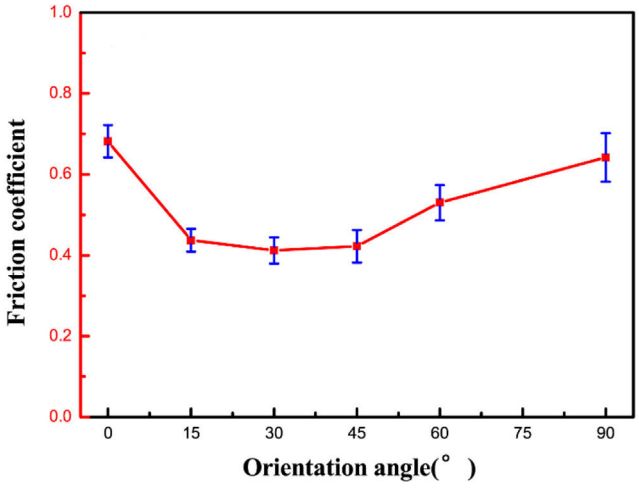

Fig. 24 – Friction coefficient and wear rate of Si_3N_4–15 wt.%TiC–5 wt.%GNP nanocomposites as a function of orientation angle of GNP reinforcement at 40N [192].

The effect of TiN nanoparticles and CNTs on microstructural and mechanical properties of hot-pressed Si_3N_4 has been investigated by Tian et al. [190]. The authors produced Si_3N_4, Si_3N_4–2 wt.%CNTs, Si_3N_4–10 wt.%TiN, and Si_3N_4–2 wt.%CNTs–10 wt.%TiN samples by hot pressing at 1700 °C. They used 5 wt.% Al_2O_3 and Y_2O_3 as sintering aids and obtained a homogenous microstructure with uniform dispersion of reinforcements. They found that the fracture toughness of Si_3N_4–2 wt.%CNTs–10 wt.%TiN nanocomposite increased by 47% compared to Si_3N_4, which was attributed to crack deflection, intergranular fracture mode, crack bridging and CNTs pull-out. Puchy and co-authors [191] prepared Si_3N_4 and Si_3N_4–1.5 wt.%GNPs–(5, 10)wt.%Ag by SPS at 1700 °C for 10 min. The nanocomposites showed higher densification and uniform distribution of the reinforcements. However, a decrease in hardness and fracture toughness was observed for the Si_3N_4–Ag–GNPs nanocomposites compared Si_3N_4. The coefficient of friction slightly decreased for the Si_3N_4–5 wt.%Ag–1.5 wt.%GNPs nanocomposite, but then increased for the Si_3N_4–10 wt.%Ag–1.5 wt.%GNPs nanocomposite. The Si_3N_4–5 wt.%Ag–1.5 wt.%GNPs nanocomposite showed improved wear resistance compared to Si_3N_4. Zhang et al. [192] studied the effect of orientational angle of GNPs on tribological performance of Si_3N_4–TiC–GNPs nanocomposite tool materials. The authors used Si_3N_4, 15 wt.% TiC, and 5 wt.% GNPs for nanocomposite preparation and 2 wt.% Al_2O_3, 5 wt.% Y_2O_3, and 0.5 wt.% MgO as sintering aids. They sintered the samples by hot-pressing at 1700 °C for 60 min. They performed the tribological tests by keeping the angle between GNPs of tool material and rubbing surface at 0°, 15°, 30°, 45°, 60° and 90°. The Si_3N_4–TiC–GNPs nanocomposite with GNPs at 30° angle showed the optimum tribological properties, as shown in Fig. 24. The coefficient of friction of Si_3N_4–TiC–GNPs nanocomposite with GNPs at 30° was found

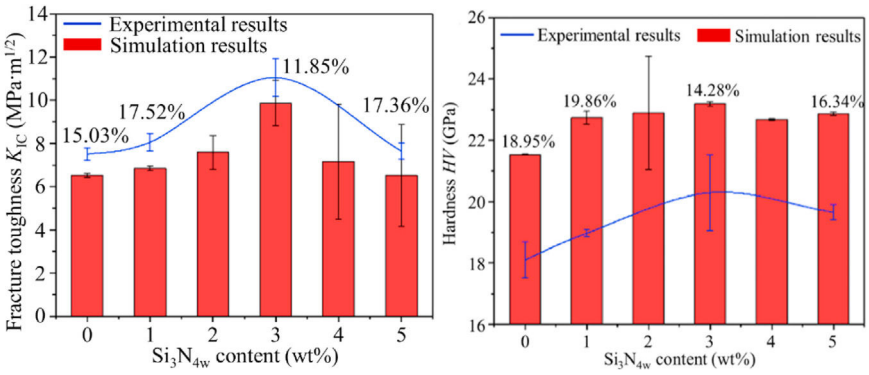

Fig. 25 – Modelling prediction and experimental results of mechanical properties for 1 wt.% MLG–(0–6 wt.%)Si_3N_{4w}–Si_3N_4 hybrid nanocomposites [193].

to be 31.3 and 42.5% lower compared to the nanocomposite with GNPs oriented at 0° and 90°, respectively. The wear rates of the nanocomposite with 30° GNPs orientation were 59.1 and 50.8% lower compared to the nanocomposites with 0° and 90° orientation, respectively. At 30° orientation of GNPs, a continuous tribofilm with a maximum thickness of 2.57 μm was formed. The continuous, relatively thick, defect-free, and tightly bonded tribofilm to the base material was believed to be the cause of the relatively better performance of the nanocomposite with GNPs orientation at 30°. Chen and co-authors [193] predicted the optimum content of the hybrid reinforcements and mechanical properties of MLG and silicon nitride nano-whiskers (Si_3N_{4w}) reinforced Si_3N_4. The predicted results were then verified by testing samples produced by SPS at 1700 °C for 6 min. The simulation results showed the highest hardness of 23.19 GPa and the highest fracture toughness of 9.87 MPa m$^{1/2}$ at an optimum reinforcement content of 1 wt.% MLG and 3 wt.%Si_3N_{4w}. The predicted fracture toughness of the Si_3N_4–1 wt.%MLG–3 wt.%Si_3N_{4w} nanocomposite was found to be 11.85% lower while the predicted hardness was 14.28% higher than the experimental values, as shown in Fig. 25.

TiB_2 nanocomposites

Titanium diboride (TiB_2) has very high melting temperature of 3225 °C, low thermal expansion coefficient of 4.6×10^{-6}/K, hardness of around 25 GPa, and very high elastic modulus of over 500 GPa [174]. TiB_2 also has good chemical stability, high oxidation resistance, and high electrical conductivity, which make it candidate material for many applications including hypersonic re-entry spacecraft, gas turbine blades, advanced rocket motors, wear-resistant coatings, impact-resistant armor, and cutting tools [194–198]. Researchers were able to enhance the properties TiB_2 by the inclusion of a single phase such as SiC [199,200], ZrO_2 [201], boron [202], short-carbon fiber [203], CNT [204] Si_3N_4, graphene, CrB_2, TiC, AlN, TiN [198], or two or more phases [195–197,205–208].

Akin et al. [205] investigated the effect of SiC and GNPs on microstructural, mechanical and thermal properties of TiB_2. The prepared TiB_2 and TiB_2–(10–20)wt.%SiC–(0.5–10)wt.% GNPs nanocomposites by SPS at 1700 °C and 1800 °C, respectively, for 5 min. The nanocomposites showed relative density higher than 98%. Microstructural analysis revealed uniformly distributed reinforcements within TiB_2 matrix, with SiC present at intergranular triple points while GNPs wrapped around the matrix grains. The hardness of TiB_2 was found to decrease from 24.2 GPa with the increase in reinforcement content and reached 17 GPa for TiB_2–10 wt.%SiC–10 wt.% GNPs nanocomposite. TiB_2 and TiB_2–15 wt.%SiC–5 wt.% GNPs nanocomposite had fracture toughness values of 3.9 MPa m$^{1/2}$ and 6.4 MPa m$^{1/2}$, respectively, i.e. an increase of 64.1%. The nanocomposites had lower thermal conductivity than TiB_2, except for TiB_2–19.5 wt.%SiC–0.5 wt.% GNPs nanocomposite, which showed a slight increase in thermal conductivity. Other researchers [196] prepared TiB_2–25 vol.%SiC and TiB_2–25 vol.%SiC–2 wt.%G_{nf} nanocomposites at 1800 °C for 7 min using SPS and reported the effect of 2 wt.% G_{nf} on the microstructural and thermal properties of TiB_2–25 vol.%SiC composite. Microstructural analysis showed the formation of TiC, B_4C, and SiO_2. Relative density values of 95.5% and 96% were obtained for TiB_2–SiC and TiB_2–SiC–graphite, respectively. A slight decrease in the thermal conductivity was observed as a result of reinforcing TiB_2–SiC with G_{nf}. The properties of TiB_2–SiC–CNTs nanocomposites, prepared by reactive sintering, have been reported by Popov et al. [195]. The authors mixed TiB_2, SiC, TiC, B_4C and Si powders, hot-pressed the mixture at 1800 °C for 1 min, and obtained nearly fully dense nanocomposites. They reported slight increase in the hardness from 27.4 GPa (TiB_2–SiC) to 29.3 GPa (TiB_2–SiC–4.5 vol.%CNTs). All other nanocomposites showed a decrease in hardness. The fracture toughness values of all TiB_2–SiC–CNTs nanocomposites were lower than that of the TiB_2–SiC composite (5.9 MPa m$^{1/2}$), except TiB_2–SiC–8.6 vol.%CNTs, which had a fracture toughness value of 6.2 MPa m$^{1/2}$. The nanocomposites showed better thermal shock resistance. Kovalcikova et al. [197] produced TiB_2–20 wt.%SiC–(0–10 wt.%)GNPs nanocomposites by hot-pressing at 2100 °C for 7 min. The GNPs improved the sinterability of TiB_2–20 wt.%SiC composites. However, the hardness was found to decrease with the increase in GNPs content, and reached a value of 13.9 GPa for TiB_2–20 wt.%SiC–10 wt.%GNPs nanocomposite compared to 23.8 GPa for TiB_2–20 wt.%SiC. The fracture toughness slightly increased from 5 MPa m$^{1/2}$ to 6.2 MPa m$^{1/2}$ when TiB_2–20 wt.%SiC was reinforced with 10 wt.%GNPs. The coeffi-

cient of friction and wear rate were found to be less than those of the TiB_2–20 wt.%SiC composite when the content of GNPs exceeded 5 wt.%. The enhanced tribological performance of TiB_2–SiC–GNPs nanocomposites, with GNPs content higher than 5 wt.%, was attributed to the formation of a tribofilm. Asl and co-workers [206] prepared TiB_2–25 vol.%SiC–2 wt.%GNPs hybrid nanocomposite by SPSat 1800 °C for 7 min. The sintered sample had a relative density 96%. XRD and X-ray photoelectron spectroscopy analysis did not reveal the formation of new phases during sintering, while high-resolution transmission electron microscopy analysis showed the presence of dislocations. TiB_2–10 wt.%MgO–6 wt.%TiN hybrid nanocomposites reinforced with SiC whiskers and MLG were developed by Sun et al. [207] and their properties are shown in Fig. 26. TiB_2–10 wt.%MgO–6 wt.%TiN and TiB_2–10 wt.%MgO–6 wt.%TiN–2 wt.%SiC_w–(2,4,6 wt.%)MLG composites were produced by conventional sintering at 1750 °C for 45 min and two-step sintering (1800 °C for 5 min, 1700 °C for 45 min). The samples sintered in two-steps had a relative density of at least 99%. The hardness of TiB_2–MgO–TiN (33 GPa) was found to decrease with the addition of SiC/MLG and its maximum value was 21.2 GPa for TiB_2–MgO–TiN–SiC_w–4 wt.%MLG nanocomposite. In contrast, high flexural strength and fracture toughness values of 1006.3 MPa $m^{1/2}$ and 8.8 MPa $m^{1/2}$, respectively, were reported for TiB_2–MgO–TiN–SiC_w–4 wt.%MLG nanocomposite, compared to values of 700 MPa and 6 MPa $m^{1/2}$ for TiB_2–MgO–TiN. In other work, relative density values of 95.5% and 96% were achieved for TiB_2–SiC and TiB_2–SiC–GNPs samples prepared by SPS at 1800 °C for 7 min. The authors reported 8% decrease in thermal conductivity of TiB_2–25 vol.%SiC–2 wt.%GNPs nanocomposite compared to TiB_2–25 vol.%SiC [208].

WC nanocomposites

Cui and co-authors [209] prepared 47.5 wt.%Al_2O_3–50.2 wt.%Ti(C,N) nanocomposite powders mixed with GNPs. The powders were pre-sintered at 1200 °C for 10 min, then hot-pressed at 1700 °C for 10 min. The authors reported 40.13% increase in fracture toughness and 40.78% increase in flexural strength when 47.5 wt.%Al_2O_3–50.2 wt.%Ti(C,N) was reinforced with 0.4 wt.%GNPs. However, the mechanical properties deteriorated at GNPs content higher than 0.4 wt.%. The nanocomposites did not show significant change in the thermal conductivity. The effect of varying the content of TiO_2 (0–6 wt.%) in WC–30 vol.%Al_2O_3–0.5 wt.%CNTs nanocomposite was investigated by Bai et al. [210]. The authors sintered the samples at 1540 °C for 90 min and found that the relative density increased with the increase in TiO_2 content, reaching a value of 99.5% for the WC–30 vol.%–Al_2O_3–0.5 wt.%CNTs–6 wt.%TiO_2 nanocomposite. A new phase of Al_2TiO_5 was found to form in WC–30 vol.%–Al_2O_3–0.5 wt.%CNTs samples containing more than 2 wt.% TiO_2. A hardness value of 1752 HV was reported for WC–30 vol.%Al_2O_3–0.5 wt.%CNTs–2 wt.%TiO_2 compared to 1623 HV for WC–30 vol.%Al_2O_3–0.5 wt.%CNTs. A slight increase in fracture toughness was observed when the WC–30 vol.%Al_2O_3–0.5 wt.%CNTs nanocomposite was reinforced with 4 wt.% TiO_2. The enhancement

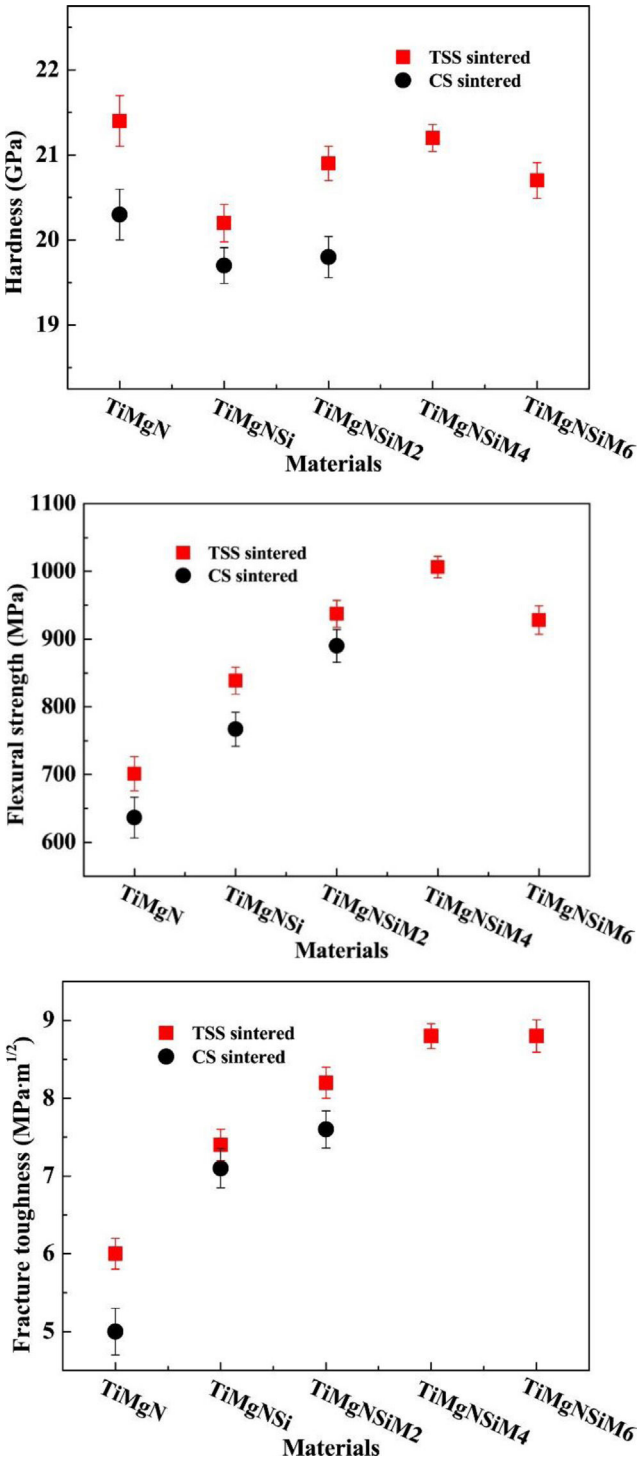

Fig. 26 – Properties of various TiB_2 based nano-composites (a) hardness, (b) flexural strength, and (c) flexural toughness [207].

in mechanical properties, when the content of TiO_2 is equal to or greater than 2 wt.%, was attributed to the formation of Al_2TiO_5. Zhang et al. [211] investigated the effect of varying GPLs content (0–0.9 wt.%) on tribological behavior of WC–Al_2O_3 nanocomposites. The authors hot-pressed 85.4 wt.%WC–(13.7–14.6)wt.%–Al_2O_3–(0–0.9)wt.%GPLs

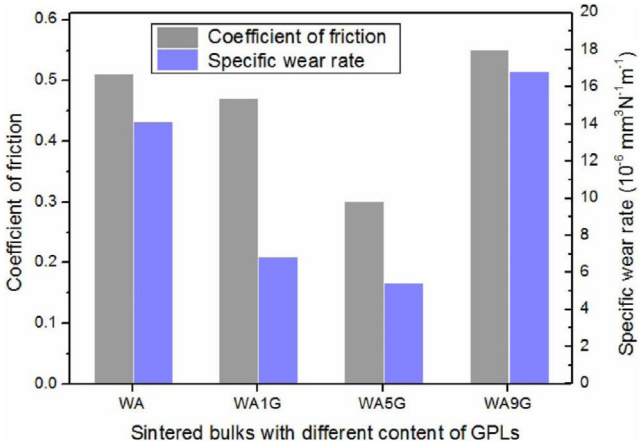

Fig. 27 – Coefficient of friction and wear rates of WC–Al_2O_3–GNP nanocomposites. WA, WA1G, WA2G and WA9G corresponds to WC–Al_2O_3, WC–Al_2O_3–0.1 wt.%GNP, WC–Al_2O_3–0.5 wt.%GNP and WC–Al_2O_3–0.9 wt.%GNP nanocomposites. [111].

nanocomposites at 1540 °C for 90 min. The relative density was found to decrease with the increase in GPLs content, reaching a value of 96.7% for WC–13.7Al_2O_3–0.9 wt.% GPLs nanocomposite. Enhancements in hardness and fracture toughness were reported, reaching values of 17.44 GPa and 9.47 MPa $m^{1/2}$, for WC–Al_2O_3 reinforced with 0.1 and 0.5 wt.% GPLs, respectively. The addition of 0.1 and 0.5 wt.% GPLs to WC–Al_2O_3 nanocomposites resulted in 7.8% and 41.2% decrease in the coefficient of friction, respectively, as well as 52% and 61.8% decrease in wear rate compared to WC–Al_2O_3 composites, as shown in Fig. 27. The superior tribological behavior of the WC–Al_2O_3–GPLs nanocomposites was attributed to GPLs which played lubrication role by forming tribofilms. In another work, Zhang et al. [212] hot-pressing WC–14.3 wt.%Al_2O_3 and WC–14.3 wt.%Al_2O_3–0.3 wt.%GPLs nanocomposites at 1540 °C for 90 min. The found that the addition of GPLs resulted in a decrease in density, from 99.1 to 98.3%, and in grain size from 3.49 to 2.61 μm, however, the hardness and fracture toughness increased from 16.18 GPa and 8.08 MPa $m^{1/2}$ to 18.34 GPa and 11.02 MPa $m^{1/2}$. The increase in hardness was attributed to grain refinement, while the increase in fracture toughness is believed to be due to toughening mechanisms induced by GPLs. Additionally, the coefficient of friction decreased by 40.4% and 33.3% at loads of 40N and 60N, respectively. Similarly, a decrease in the wear rate was observed. The decrease in coefficient of friction and wear rate of the WC–Al_2O_3–GPLs nanocomposite was attributed to the fine microstructure, high hardness, and formation of a tribofilm of graphene. Chen et al. [213] prepared WC–Co, WC–Co–0.06%SWCNTs–0.06%SLG, WC–Co–0.12% SWCNTs, WC–Co–0.12%SLG nanocomposites by SPS at 1200 °C for 10 min. The authors reported 49% and 68% increase in flexural strength for the WC–Co–0.06% SWCNTs–0.06%graphene and WC–Co–0.12%graphene nanocomposites, respectively; and 2.6% and 10% increase in the thermal conductivity for the WC–Co–0.06% SWCNTs–0.06%SLG and WC–Co–0.12%SLG nanocomposites compared to WC–Co. But no change in hardness was observed for WC–Co nanocomposites reinforced with SWCNTs and SLG. Sun et al. [214] reported enhancements in mechanical properties of WC when reinforced with 8 wt.%(ZrO_2–20 wt.%Al_2O_3) and (0–0.4 wt.%)GNPs. WC–ZrO_2–Al_2O_3 composite and WC–ZrO_2–Al_2O_3–GNPs nanocomposites with varying GNPs content were sintered using oscillatory pressure sintering. The 99.1% relative density of WC–ZrO_2–Al_2O_3 increased to 99.8% for WC–ZrO_2–Al_2O_3–0.2 wt.%GNPs. The hardness decreased with the increase in GNPs content. However, 12% increase in fracture toughness and 11% increases in flexural strength were reported for 0.2 wt.%GNPs reinforced WC–ZrO_2–Al_2O_3 nanocomposite as compared to the sample without GNPs. In another work, Sun et al. [215] reported enhanced mechanical and tribological properties of WC matrix reinforced with MLG and SiC_w. Two step sintering SPS (1950 °C for 5 min and then 1850 °C for 20 min) was used for sintering pure WC and WC–3 wt.%SiC_w–(0.1,0.2 wt.%)MLG nanocomposites. The addition of MLG to WC facilitated the densification and the relative density reached 99.5% for the WC–SiC_w–0.1 wt.%MLG nanocomposite. Also, a 81.9% increase in fracture toughness, a 61.2% reduction in friction coefficient, and a 81.3% reduction in wear rate were reported for WC–SiC_w–0.1 wt.%MLG nanocomposite compared to WC. In another study [216], binderless tungsten carbide samples were hot-pressed using two-step sintering; 1700 °C for 4 min and then 1600 °C for 60 min. The relative density of WC–Al_2O_3 improved from 97.8% to 99.8% because of the addition of TiC, TiN, SiC_w, and MLG. The improvement was attributed to the formation of solid solutions and minor-liquid phases. Increases up to 4.1%, 23.8%, and 54.9% in hardness, flexural strength, and fracture toughness were reported for WC–9 wt.%Al_2O_3 reinforced with 3 wt.%TiC, 3 wt.%TiN, 0.15 wt.%SiC_w, and 0.05 wt.%MLG [216]. The effect of ultrafine porous boron nitride nanofiber (BN_{nf}) on mechanical properties of WC–Si_3N_4 was investigated by Cao et al. [217]. The authors sintered WC–10 wt.%Si_3N_4 composites and WC–10 wt.%Si_3N_4–(0–0.15 wt.%)BN_{nf} hybrid composites at 1750 °C and found that all the BN_{nf} reinforced nanocomposites showed higher values of hardness, elastic modulus, and fracture toughness compared to WC–Si_3N_4. The WC–Si_3N_4–0.01 wt.%BN_{nf} nanocomposite showed the highest elastic modulus of 793 GPa and fracture toughness 10.99 MPa $m^{1/2}$ compared to 521 GPa and 7.70 MPa $m^{1/2}$ for WC–10 wt.% Si_3N_4. In other work, WC ceramic nanocomposites reinforced with graphene (G) and SiC nanowire (SiC_{nw}) were prepared through SPS [218]. The WC–0.15 wt.%–G–0.45 wt.%SiC_{nw} nanocomposite sintered at 1900 °C for 15 min under 60 MPa, had a hardness of 25.6 GPa, a flexural strength of 1499 MPa, and a fracture toughness of 11.6 MPa $m^{1/2}$. The high toughness value was mainly attributed to the combination of G and SiC_{nw} induced crack deflection, bridging and pullout.

Mullite nanocomposites

A hybrid nanocomposite powder of mullite–TiB_2–CNTs was prepared by mixing 1 wt.%CNTs and 10 wt.% TiB_2 with nano-mullite powder using high-energy milling and, then, sintered by SPS at 1350 °C [219]. A relative density of 99.1% was reported for the mullite–TiB_2–CNTs nanocomposite. The

authors performed XRD analysis and observed tiny peak of alumina, along with mullite and TiB_2, which might have been formed as in-situ phase during sintering. Uniform dispersion of TiB_2 and CNTs reinforcements was confirmed by EDS analysis. Vickers hardness, flexural strength, and fracture toughness of mullite–TiB_2–CNTs nanocomposite were found to be 18.31 GPa, 531 MPa and 5.46 MPa $m^{1/2}$, respectively. In another work, similar sintering conditions were used to sinter mullite reinforced with 10 wt.% ZrB_2 and 1 wt.% CNTs [220]. Hardness of 16.24 GPa, flexural strength of 488 MPa, and fracture toughness of 4.18 MPa $m^{1/2}$ were reported for the mullite–10 wt.%ZrB_2–1 wt.%CNTs nanocomposite. The influence of reinforcing mullite–TiN–CNTs nanocomposite with ZrB_2 and TiB_2, on the microstructure and mechanical properties, were investigated by Orooji et al. [221]. The authors prepared mullite–TiN–CNTs, mullite–TiN–TiB_2–CNTs, and mullite–TiN–TiB_2–ZrB_2–CNTs nanocomposites by SPS at 1350 °C for 5 min. The content of TiN, TiB_2 and ZrB_2 was 10 wt.% for each compound and the content of CNTs was 1 wt.% for the composites. All samples achieved a relative density higher than 97%. Microstructural analysis showed uniform distribution of the reinforcements with no new in-situ phase formation during sintering. The mullite-TiN–TiB_2–ZrB_2–CNTs nanocomposite showed the highest hardness and fracture toughness values of 17.15 GPa and 4.86 MPa $m^{1/2}$, as compared to 15.84 GPa and 3.98 MPa $m^{1/2}$ for the mullite–TiN–CNTs nanocomposite.

B_4C nanocomposites

Pure B_4C, B_4C–18 wt.%TiB_2 and B_4C–18 wt.%TiB_2–4 wt.%GNPs were hot-pressed at 1900 °C for 1 h at 30 MPa [222] and their mechanical properties were reported as shown in Fig. 28 [222]. All samples had a relative density of more than 97%. B_4C–TiB_2–GNPs nanocomposite showed 169% and 68% increases in fracture toughness and flexural strength, respectively, compared to B_4C. However, marginal increase in hardness from 29.8 for B_4C to 31.8 was observed for B_4C–TiB_2–GNPs nanocomposite. The electrical conductivity of B_4C increased by three folds, from 1.6×10^2 S/m to 9.65×10^5 S/m for B_4C–TiB_2–GNPs nanocomposite.

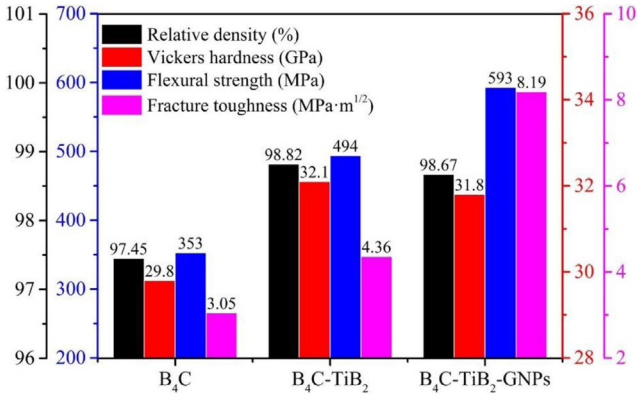

Fig. 28 – Densification and mechanical properties of hot-pressed B_4C ceramic, B_4C–TiB_2 composite and B_4C–TiB_2–GNP nanocomposite [222].

SiC nanocomposites

The effect of CNTs on mechanical properties of SiC–B_4C–Ni hybrid composites was investigated by Bahamirian and co-authors [223]. SiC–45 vol.%B_4C–10 vol.%Ni and SiC–45 vol.%B_4C–10 vol.%Ni–5 vol.%CNT samples were prepared by SPS at 1650 °C for 5 min. The relative density was found to be 98.3% and 97.8% for SiC–B_4C–Ni and SiC–B_4C–Ni–CNTs nanocomposite, respectively. XRD anal-

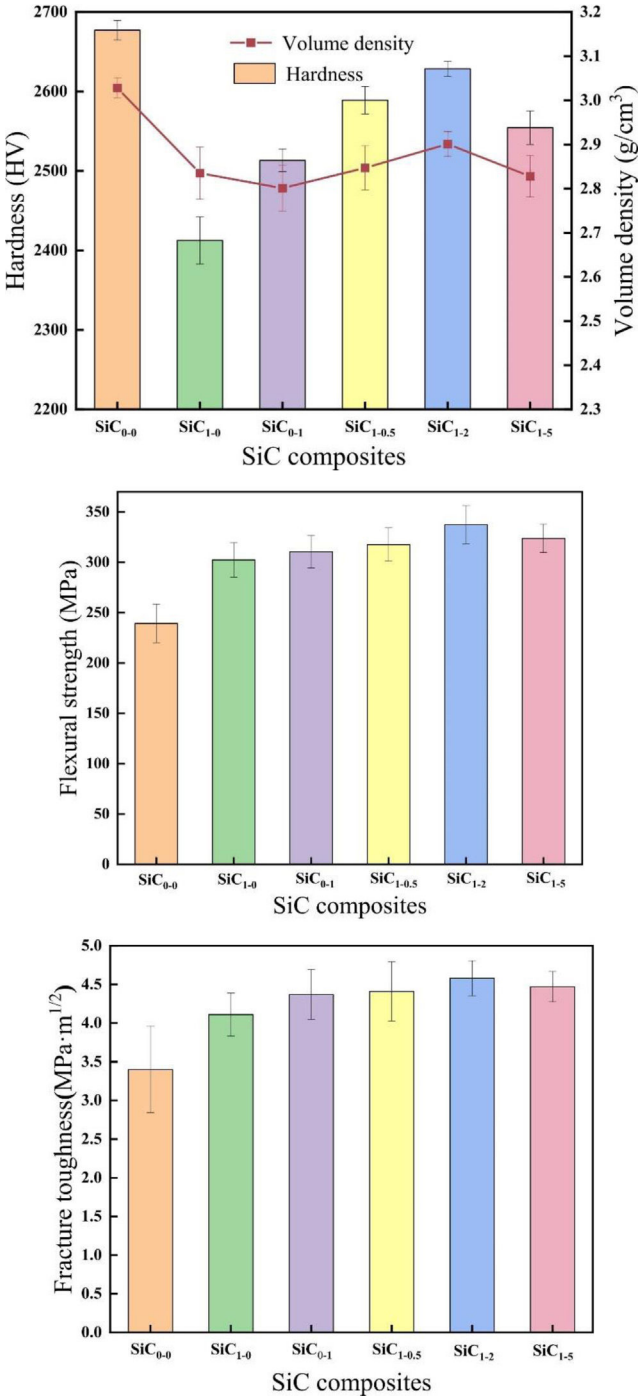

Fig. 29 – Properties of SiC composites with different GO/CNT ratios (a) hardness and density, flexural strength (b), and (c) fracture toughness [8].

ysis confirmed the presence of Ni_2Si phase formed during sintering. FE-SEM analysis showed presence of cracks in the SiC matrix, which were attributed to the migration of Si from SiC to Ni to from Ni_2Si. Slight decrease in hardness from 16.7 to 15.63 GPa was observed when SiC–B_4C–Ni was reinforced with CNTs. Marginal increase in bending strength and fracture toughness from 362 MPa and 3.32 MPa $m^{1/2}$ to 369 MPa and 5.82 MPa $m^{1/2}$ was reported for SiC–B_4C–Ni and SiC–B_4C–Ni–CNTs composites, respectively. In other work, optimal flexural strength of 337.4 MPa and fracture toughness of 4.58 MPa $m^{1/2}$ were obtained for SiC hybrid nanocomposite reinforced with three–dimensional graphene oxide–carbon nanotubes (3D GO-CNTs) at a ratio of 1:2, i.e. enhancement by 40.9% and 34.7%, respectively, compared to that of SiC. The composites were prepared using direct ink writing and liquid silicon infiltration processes. The authors attributed the improvement in densification, hardness, strength, and toughness, as shown in Fig. 29 [8], to the uniform distribution of GO and CNTs in the SiC matrix and the various toughening mechanisms including GO/CNTs pull-out, multiple microcracks, crack bridging, deflection, and branching [8]. In another study, SiC–TiB_2–Al_2O_3 nanocomposites, prepared using the powder metallurgy technique, followed by hot press sintering at a high temperature of 1400 °C, showed impressive reduction in linear ablation rate and in mass ablation rates [9].

Yttria-stabilized zirconia nanocomposites

Yttria-stabilized zirconia hybrid nanocomposites reinforced with CNTs and BN were developed by Buyakov and co-authors [10]. Different compositions, with dual reinforcement content of 0.25–5 wt.%, were sintered using SPS between 1300–1400 °C for 30 min. The authors reported a relative density higher than 98.5% for all samples except YSZ–5 wt.%CNTs–5 wt.%BN, whose relative density was 97.3%. The samples displayed a homogenous microstructure and uniform distribution of the reinforcements. Analysis of sintered samples showed the presence of monoclinic and tetragonal zirconia phases. The elastic modulus of monolithic YSZ was reported to be 197 GPa and remained in the range of 190–198 GPa for all hybrid nanocomposites. The hardness of monolithic YSZ (12.2 GPa) decreased with the increase in reinforcement content and reached a value of 9.6 GPa for YSZ–5 wt.%CNTs–5 wt.%BN nanocomposite. However, the fracture toughness increased with the increase in reinforcement content and reached a value of 7.9 MPa $m^{1/2}$ for YSZ–5CNTs–5BN nanocomposite compared to 6.1 MPa $m^{1/2}$ for YSZ. The fracture toughness enhancement was attributed to zirconia phase transformation, CNTs toughening effects, and crack bifurcation due to BN [10].

A summary of composition, sintering methods and parameters, relative density, hardness, and fracture toughness of various hybrid ceramic nanocomposites is presented in Table 2.

Potential applications

The process of developing quality materials still largely relies on extensive trial and error. It may take years, sometimes even decades, to find an appropriate material for a specific technological use, and even more time is needed to refine that material for commercial viability [11]. The enhancement in mechanical, wear, and tribological properties of ceramic materials brought about by reinforcing them with two or more phases is believed to improve their performance in structural applications. Moreover, hybrid ceramic nanocomposites that demonstrated enhanced physical properties will be candidate materials for many functional and novel applications. Enhancements in the properties of alumina hybrid nanocomposites may significantly improve their performance in a range of applications, including cutting tools, electrical insulators, igniters, heating elements, chemical insulators, and dental implants. Similarly, the improvement in sinterability, densification, and both mechanical and thermal properties of ZrB_2 hybrid nanocomposite materials could extend their use in extreme conditions and harsh environments, enhancing their performance as electrodes for electric discharge machining, crucibles in the metal industry, and structural and functional components in aerospace applications. Hybrid TiC nanocomposites are anticipated to outperform their conventional counterparts due to their high density, exceptional mechanical properties [96], and resistance to thermal shock [153], making them suitable for use in hypersonic space applications, cutting tools, refractory components, and the nuclear industry [133–155]. Despite limited research on HfC hybrid nanocomposites [118], their potential applications remain promising in fields such as rocket nozzles, nuclear reactors, thermal field emitters, cutting tools, high-temperature solar absorbers, and space structures [179–181]. Additionally, the advanced properties of Si_3N_4 hybrid nanocomposites are expected to expand their usage in high-temperature ball bearings, rollers, and cutting tools [183], while TiB_2 hybrid nanocomposites may find applicability in hypersonic reentry spacecraft, gas turbine blades, advanced rocket motors, wear-resistant coatings, impact-resistant armor, and cutting tools. WC hybrid nanocomposites exhibit outstanding mechanical properties, making them highly suitable for use as tool materials in cutting tools, drills, and inserts for the machining and metal fabrication industries. The substantial enhancements in the properties of SiC hybrid nanocomposites obtained through 3D printing could facilitate their future applications in the aerospace industry [8]. SiC–TiB_2–Al_2O_3 hybrid nanocomposites, demonstrating impressive properties [9], are also promising candidates for thermal barrier coatings in both gas turbines and the nuclear industry. Lastly, the high fracture toughness of the YSZ–5CNT–5BN nanocomposite, combined with its acceptable physical properties and thermal stability, paves the way for its application in membranes, oxygen sensors, solid oxide fuel cells, surgical instruments, and medical implants.

Future research directions

The ongoing research in hybrid ceramic nanocomposites is likely to continue capturing the attention of researchers, who aim to enhance their properties, optimize their performance, and expand their applications across different industries. As of today, the reported augmentation in the physical, mechan-

Table 2 – Summary of properties of various hybrid ceramic nanocomposites.

Nanocomposite	Sintering method/parameters	Relative density (%)	Hardness (GPa)	Fracture toughness (MPa $m^{1/2}$)	Ref.
Al_2O_3	SPS. 1550 °C, 50 MPa	100	17	3.3	[53]
Al_2O_3–1 vol.%SiC–5 vol.%CNT		98.2	16.5	6.5	
Al_2O_3–1 vol.%SiC–7 vol.%CNT		97.2	16	7	
Al_2O_3–1 vol.%SiC–10 vol.%CNT		95.1	15	5.5	
Al_2O_3–1 vol.%SiC–5 vol.%CNT	SPS. 1550 °C, 50 MPa	98	16.5	6.5	[54]
Al_2O_3–3 vol.%SiC–5 vol.%CNT		96.46	16	6.2	
Al_2O_3–5 vol.%SiC–5 vol.%CNT		96.40	16	6	
Al_2O_3–5 wt.%SiC–1 wt.%CNT	SPS. 1500 °C, 10 min, 50 MPa	91.65	17.81	5.38	[155]
Al_2O_3		99.3	18.56	3.61	[56]
Al_2O_3–5 wt.%SiC–1 wt.%CNT		99.36	19.77	3.89	
Al_2O_3–5 wt.%SiC–2 wt.%CNT		98.28	19.11	4.2	
Al_2O_3–10 wt.%SiC–1 wt.%CNT		98.63	20.81	4.58	
Al_2O_3–10 wt.%SiC–2 wt.%CNT		98.02	17.50	6.98	
Al_2O_3–5 wt.%SiC–1 wt.%CNT	SPS. 1600 °C	98.9	23.32	7.1	[57]
Al_2O_3	IHP. 1500 °C, 3 min, 50 MPa	99.2	16	3.2	[60]
Al_2O_3–6 wt.%SiC_{np}–4 wt.%CNT		97.2	20	5.9	
Al_2O_3–5 wt.%SiC_{np}–2 wt.%CNT	HFIHS, 1600 °C, 3 min, 60 MPa	97.2	20.9	6.5	[61]
Al_2O_3–25 wt.%SiC_w–0.1 wt.%CNT	HP. 1750 °C, 1 h	>99.5	20.4	4.5	[62]
Al_2O_3	HP. 1500 °C, 2 h, 30 MPa	99.8	17.5	5.5	[44]
Al_2O_3–5 vol.%ZrO_2–0.5%MWCNT		99.4	14.5	6.9	
Al_2O_3–5 vol.%ZrO_2–1 vol.%MWCNT		99.1	14.5	7.5	
Al_2O_3–5 vol.%ZrO_2–2 vol.%MWCNT		99	14.5	6.9	
Al_2O_3	HP. 1600 °C, 50 MPa, 60 min	99.7	17.4	3.1	[64]
Al_2O_3–8 vol.%ZrO_2–4 vol.%MWCNT		98.3	23.2	6.7	
Al_2O_3	HP. 1600 °C, 60 MPa, 1 h	99.5	19	3.3	[65]
Al_2O_3–4 wt.%ZrO_2–2 wt.%CNT		99.8	24	7.2	
Al_2O_3–4 wt.%ZrO_2–0.5 wt.%G		98.5	21.6	6.2	
ZTA–0.6 wt.%MgO	HP. 1500 °C, 30 min, 100 MPa	99	24.57	5.74	[66]
ZTA–0.6 wt.%MgO–0.05 wt.%CNT		99	30.70	7.02	
ZTA–0.6 wt.%MgO–0.1 wt.%CNT		99	31.25	6.28	
Al_2O_3	IHP. 1300–1600 °C, 30–50 MPa, 3 min	99	16.5	3.5	[67]
Al_2O_3–3 wt.%SiC_{np}–0.5 wt.%G		99	19.3	6.9	
Al_2O_3–5 wt.%SiC_{np}–0.5 wt.%GNP		99.5	21	8.3	[68]
Al_2O_3–17 vol.%SiC_w–0.5 vol.%GO	SPS. 1780 °C, 3 min	–	22	10.6	[69]
Al_2O_3	SPS. 1500 °C, 3 min, 50 MPa	100	18.04	3.41	[70]
Al_2O_3–1 vol.%SiC–0.38 vol.%GPL		99.03	21.34	4.77	
Al_2O_3–3 vol.%SiC–0.38 vol.%GPL		98.85	24.65	5.03	
Al_2O_3–5 vol.%SiC–0.38 vol.%GPL		97.35	21.58	4.94	
Al_2O_3–5 vol.%SiC–0.5 vol.%GNS	SPS, 1450 °C, 5 min	>99	18.07	3.51	[71]
Al_2O_3–5 vol.%SiC–1 vol.%GNS		>99	17.07	3.92	

Table 2 – (*Continued*)

Nanocomposite	Sintering method/parameters	Relative density (%)	Hardness (GPa)	Fracture toughness (MPa $m^{1/2}$)	Ref.
Al_2O_3	SPS, 1500 °C, 3 min,	99.7	16.44	–	[73]
Al_2O_3–5 wt.%SiC–0.4 wt.%G	21 MPa	99.6	19.6		
Al_2O_3–10 wt.%SiC–0.4 wt.%G		98.7	18.2		
Al_2O_3–15 wt.%SiC–0.4 wt.%G		97.4	17.2		
Al_2O_3	HP. 1600 °C, 50 MPa	99.7	16.4	3.1	[74]
Al_2O_3–4 wt.%ZrO_2–0.5 wt.%GNP		98.5	19.3	7.9	
Al_2O_3–18 vol.%WC–6%TiC	HP. 1700 °C, 10 min, 35 MPa	98.94	23.54	8.76	[76]
Al_2O_3–18 vol.%WC–6%TiC–0.5%G		99.58	24.64	9.42	
Al_2O_3–18 vol.%WC–6%TiC–0.75%G		98.88	23.2	10.35	
Al_2O_3–18 vol.%WC–6 vol.%TiC	HP two-step.	98.41	19	6	[78]
Al_2O_3–18 vol.%WC–6 vol.%TiC–0.5 vol.%Graphene	1600–1750 °C 15 min, 32 MPa	99.52	22.5	9	
Al_2O_3–18 vol.%WC–6 vol.%TiC	HP. 1700 °C for 10 min	98.41	18.65	5.73	[79]
Al_2O_3–18 vol.%WC–6 vol.%TiC–0.5 vol.%graphene		99.68	21.48	8.83	
Al_2O_3–30 wt.%TiC	MS. 1700 °C, 10 min	99.2	21.2	5.2	[80]
Al_2O_3–30 wt.%TiC–0.1 wt.%GNP		97.9	19.1	7.2	
Al_2O_3–30 wt.%TiC–0.2 wt.%GNP		97.7	18.5	8.7	
Al_2O_3–30 wt.%TiC–0.4 wt.%GNP		96.8	18	8.6	
Al_2O_3–69.2 wt.% (W, Ti)C–0.2%GNP	HP. 1700 °C, 15 min	99	24.22	7.78	[81]
Al_2O_3–33.7 wt.%TiC	HP. 1650 °C	–	19.5	4.98	[82]
Al_2O_3–33.5 wt.%TiC–0.2 wt.%MLG		–	20	6.14	
Al_2O_3–24 vol.%TiC–16 vol.%WC	HP. 1700 °C, 10 min	98.9	22.19	6.82	[83]
Al_2O_3–21 vol.%TiC–14 vol.%WC		98.01	19.02	5.55	
Al_2O_3–1 wt.%CNT–0.5 wt.%GNP	SPS. 1500 °C	99.9	16.66	8.33	[84]
Al_2O_3	HP. 1650 °C, 1 h	99	16.5	3.6	[85]
Al_2O_3–1 wt.%rGO–1 wt.%CNT		99.8	18.61	6.12	
Al_2O_3–0.5 wt.%GNP–1 wt.%CNT	HP. 1650 °C, 1 h	99.9	17	5.7	[87]
Al_2O_3–0.3 wt.%GNP–1 wt.%CNT		99	16	5.8	[88]
Al_2O_3–1 wt.%GNP–1 wt.%CNT		99	11.2	3.5	
Al_2O_3	SPS. 1500 °C, 3 min,	99.7	16.44	4.9	[89]
Al_2O_3–1 wt.%CNT–0.4 wt.%G	21 MPa	99.2	15.8	7.325	
Al_2O_3–1 wt.%CNT–0.8 wt.%G		99.5	11.6	5.96	
Al_2O_3	HP. 1600 °C, 1 h, 60 MPa	18.39	19	3.39	[90,91]
Al_2O_3–10 wt.%ZrO_2		13.8	14	7.27	
Al_2O_3–10 wt.%ZrO_2–0.5 wt.%G		18.79	19	6.69	
Al_2O_3–10 wt.%ZrO2–2 wt.%CNT		20.31	20	7.55	
Al_2O_3–10 wt.%ZrO_2–0.5 wt.%G–2 wt.%CNT		27.21	27.5	8.78	
Al_2O_3–25 vol.%TiC–1.9 vol.%Ni	SPS. 1375 °C	>98	25.6	3.7	[92]
Al_2O_3–5 vol.%SWCNT–10 vol.%Nb	SPS. 1200 °C	98.4	19.3	3.3	[93]
Al_2O_3–20 vol.%SiC–4 vol.%TiC	HP. 1700 °C, 30 min	>99	21.18	6.04	[94]
Al_2O_3–5 vol.%TiC_n–0.5 vol.%G	HP. 1650 °C, 30 MPa,	–	19.9	7.1	[96]
Al_2O_3–10 vol.%TiC_n–0.5 vol.%G	10 min		20.5	7.4	

Table 2 – (*Continued*)

Nanocomposite	Sintering method/parameters	Relative density (%)	Hardness (GPa)	Fracture toughness (MPa $m^{1/2}$)	Ref.
Al_2O_3–20 wt.%TiB_2	SPS. 1520 °C, 30 MPa,	98.6	19.20	5.19	[98]
Al_2O_3–20 wt.%TiB_2–0.1 wt.%GNP	5 min	98.8	18.7	6.74	
Al_2O_3–20 wt.%TiB_2–0.2 wt.%GNP		99	18.55	7.15	
Al_2O_3–20 wt.%TiB_2–0.3 wt.%GNP		99.3	18.20	7.35	
Al_2O_3–20 wt.%TiB_2–0.4 wt.%GNP		98.5	17.70	6.75	
Al_2O_3–20 wt.%TiB_2–0.6 wt.%GNP		98.3	16.56	6.10	
ZrB_2–25vol.SiC	SPS. 1900 °C, 40 MPa, 7 min	99.9	19.5	4.3	[110]
ZrB_2–25vol.SiC–2.5 wt.%G_{nf}		100	18	4.9	
ZrB_2–25vol.SiC–5 wt.%G_{nf}		100.7	16	6.8	
ZrB_2–25vol.SiC–7.5 wt.%G_{nf}		99.7	14	8.2	
ZrB_2–25vol.SiC–10 wt.%G_{nf}		98.3	12.1	–	
ZrB_2	SPS. 1900 °C, 40 MPa, 7 min	96.1	13.1	3.2	[126]
ZrB_2–25 vol.%SiC–5 wt.%G_{nf}		100.7	16.6	6.7	
ZrB_2	HP. 1850 °C, 60 min, 20 MPa	90.1	11.9	1.8	[121]
ZrB_2–20 vol.%SiC–10 vol.%G_{nf}		99.6	16.5	7.1	
ZrB_2–25 vol.%SiC–5 wt.%GNP		99	15.7	6.4	[122]
ZrB_2–25 vol.%SiC_w	SPS. 1900 °C, 40 MPa,	99.9	22	4.7	[123]
ZrB_2–25 vol.%SiC_w–2.5 wt.%G_{nf}	7 min	99.9	20.6	5.5	
ZrB_2–25 vol.%SiC_w–5 wt.%G_{nf}		100	19.8	6.2	
ZrB_2–25 vol.%SiC_w–7.5 wt.%G_{nf}		99.9	19.5	6.2	
ZrB_2–25vol.SiC_w	SPS. 1900 °C, 40 MPa,	100	22	5	[124]
ZrB_2–25vol.SiC_w–2.5 wt.%GNP	7 min	99.95	22.2	5.2	
ZrB_2–25vol.SiC_w–5 wt.%GNP		99.95	19.1	5.7	
ZrB_2–25vol.SiC_w–7.5 wt.%GNP		99.75	16.6	6	
ZrB_2–20 vol.%SiC–10 vol.%CNT	HP. 1850 °C, 60 min, 20 MPa	93.9	8.6	5.1	[130]
ZrB_2–20 vol.%SiC–2 vol.%GNS	HP. 1950 °C, 1 h, 30 MPa	98.9	22.93	6.07	[107]
ZrB_2–20 vol.%SiC–5 vol.%GNS		99.2	22.76	7.32	
ZrB_2–20 vol.%SiC–2 wt.%CNT	HP. 1900 °C, 1 h	–	15.5	4.6	[129]
ZrB_2–20 vol.%SiC–10 vol.%CNT	SPS. 1650 °C	99.7	–	9.5	[131]
ZrB_2–25vol.SiC_w	SPS. 1900 °C, 40 MPa, 7 min	99.9	21.9	4.7	[109]
ZrB_2–25vol.SiC_w–2.5 wt.%C_{np}		100.1	18	5.9	
ZrB_2–25vol.SiC_w–5 wt.%C_{np}		100.2	17	7.1	
ZrB_2–25vol.SiC_w–7.5 wt.%C_{np}		99.8	14.6	7.2	
ZrB_2	HP. 1850 °C, 60 min, 20 MPa	90.1	11.9	2.1	[137]
ZrB_2–20vol.SiC–10 vol.%C_{nb}		99.8	16.7	5.8	
ZrB_2–20vol.SiC–5 vol.%C_{nb}	HP. 1900 °C	99.2	12.3	6.6	[138]

Table 2 – (*Continued*)

Nanocomposite	Sintering method/parameters	Relative density (%)	Hardness (GPa)	Fracture toughness (MPa $m^{1/2}$)	Ref.
ZrB_2–20 vol.%SiC_{np}–20 vol.%Graphite	HP. 1900 °C, 1 h	100	–	4.54	[127]
ZrB_2–20 vol.%SiC–30 vol.%C_f	HP. 1450 °C, 1 h	95.8	–	6.12	[135]
ZrB_2–10 vol.%SiC–2.5 vol.%C_f	CS. 2150 °C	93	14.5	5.9	[136]
ZrB_2	SPS. 1850 °C, 8 min,	81	–	2.9	[139]
ZrB_2–30 vol.%SiC–10 vol.%C_{nb}	35 MPa	100		3.6	
ZrB_2–30 vol.%SiC–15 vol.%C_{nb}		100		3.6	
ZrB_2–15 vol.%SiC_w–10 vol.%$MoSi_2$	HP. 1750 °C, 30 min, 30 MPa	99.9	–	4.3	[140]
ZrB_2–15 vol.%SiC_w–15 vol.%$MoSi_2$		99.9	17.64	5.52	
ZrB_2–15 vol.%SiC_w–20 vol.%$MoSi_2$		99.9	–	5.3	
ZrB_2–20 vol.%SiC–1 wt.% (BNNT–BNNP)	SPS. 1550 °C, 8 min	98.75	16.50	4.64	[141]
ZrB_2–25 vol.% SiC	SPS, 1900 °C, 40 MPa,	99.9	19.5	4.3	[142]
ZrB_2–25 vol.% SiC–1 wt.% D_n	7 min	100	23.4	4.9	
ZrB_2–25 vol.% SiC–2 wt.% D_n		99.9	24.6	5.5	
ZrB_2–25 vol.% SiC–3 wt.% D_n		98.8	22.2	5.8	
ZrC	SPS. 1750–1850 °C, 40 MPa, 300sec, 1.7 °C/s	95.5	17.60	3.30	[101]
ZrC–20 vol.%TiC–0.25 wt.%CNT		98.7	21.09	4.23	
ZrC–20 vol.%TiC–0.5 wt.%CNT		98.5	20.86	4.99	
ZrC–20 vol.%TiC–0.75 wt.%CNT		98.5	20.05	4.37	
ZrC–20 vol.%TiC–1 wt.%CNT		98.5	20	4.27	
ZrC–20 vol.%Ti–3 vol.%CNT	HP. 1600 °C	98.27	18.11	5.27	[143]
ZrC–20 vol.%Nb–3 vol.%CNT		99.28	17.93	7.23	[147]
ZrC–18 vol.%TiC–2 vol.%GNP	SPS. 1700 °C, 300s, 40 MPa	98.43	15.58	4.71	[148]
ZrC–17 vol.%TiC–3 vol.%GNP		99.49	15.16	5.17	
TiC	SPS. 1600 °C, 5 min, 50 MPa	89	23.67	3.24	[116]
TiC–3.5 wt.%WC–2 wt.%CNT		99	33.56	7.81	
TiC–3 wt.% WC	SPS, 1900 °C, 40 MPa,	100	28.6	–	[162]
TiC–3 wt.% WC–10 vol.%SiC_w	7 min	94	12		
TiC–3 wt.% WC–20 vol.%SiC_w		>100	16		
TiC–3 wt.% WC–30 vol.%SiC_w		>100	27.3		
TiC–10 vol.%SiC_w	SPS, 1900 °C, 40 MPa,	98.73	24.54	–	[163]
TiC–10 vol.%SiC_w–1.5 wt.%WC	7 min	99.43	22.54		
TiC–10 vol.%SiC_w–3 wt.%WC		94.13	12		
TiC	SPS. 1900 °C, 40 MPa,	95.5	30.68	–	[164]
TiC–5 wt.% h-BN–5 wt.% G_{nf}	10 min	93.2	24.29		
TiC	SPS. 1900 °C, 40 MPa,	95.5	30.68	–	[165]
TiC–5 wt.%TiN–5 wt.%D_n	10 min	87.4	24.93		
TiC–5 wt.%AlN–5 wt.% GNP		>100	27.38	–	[166]
TiC–10 wt.%nano-TiC–3 wt.%WC–0.45 wt.%MLG	HP (Two-step sintering)	99.3	24.2	7.2	[167]

Table 2 – (*Continued*)

Nanocomposite	Sintering method/parameters	Relative density (%)	Hardness (GPa)	Fracture toughness (MPa $m^{1/2}$)	Ref.
TiC–2 wt.%HfC–3 wt.%ZrO_2	Two-step SPS. 1800 °C	>98.5	24.47	4.6	[168]
TiC–HfC–ZrO_2–1.5 wt.%CNT–3 wt.%SiC_{nw}	for 5 min. 1650 °C for	>98.5	23.97	7.39	
TiC–HfC–ZrO_2–1.5 wt.%CNT–6 wt.%SiC_{nw}	30 min				
		>98.5	20	7.39	
TaC	SPS. 1850 °C, 5 min	93	15.5	3.1	[117]
TaC–15 vol.%SiC–15 vol.%CNT		98	14.1	11.4	
TaC–TiC–25 vol.%SiC	SPS. 2000 °C, 8 min,	92.4	18.5	–	[178]
TaC–TiC–25 vol.%SiC–5 wt.%G	35 MPa	95.1	19.8		
HfC–5 wt.%$MoSi_2$	SPS. 1600 °C, 5 min,	96	24.1	3.08	[118]
	50 MPa				
HfC–5 wt.%$MoSi_2$–2 wt.%CNT		99	21	5.86	
Si_3N_4	HP. 1700 °C, 1 h, 30 MPa	–	15.2	5.6	[190]
Si_3N_4–2 wt.%CNT–10 wt.%TiN		–	15.4	8.26	
Si_3N_4–1.5 wt.%GNP	SPS. 1700 °C, 25/50 MPa,	–	15.16	5.68	[191]
Si_3N_4–5 wt.%Ag–1.5 wt.%GNP	10 min		10.25	3.62	
Si_3N_4–5 wt.%Ag–1.5 wt.%GNP			14.02	5.25	
Si_3N_4–1 wt.% MLG	SPS. 1700 °C, 40 MPa,	–	18	7.4	[193]
Si_3N_4–1 wt.% MLG–1 wt.%Si_3N_{4w}	6 min		18.9	8	
Si_3N_4–1 wt.% MLG–2 wt.%Si_3N_{4w}			19.8	10	
Si_3N_4–1 wt.% MLG–3 wt.%Si_3N_{4w}			20.1	11.04	
Si_3N_4–1 wt.% MLG–4 wt.%Si_3N_{4w}			20	10.2	
Si_3N_4–1 wt.% MLG–5 wt.%Si_3N_{4w}			19.8	7.64	
TiB_2	SPS, 1700/1800 °C,	97	24.2	3.9	[205]
TiB_2–19.5 wt.%SiC–0.5 wt.%GNP	40 MPa, 5 min	98	20.1	5.7	
TiB_2–19 wt.%SiC–1 wt.%GNP		99.4	20.6	5.9	
TiB_2–15 wt.%SiC–5 wt.%GNP		99.9	18.7	6.4	
TiB_2–10 wt.%SiC–10 wt.%GNP		98.6	17	5.4	
TiB2–20 wt.%SiC	HP. 2100 °C, 7 min	98.2	23.8	5	[197]
TiB2–20 wt.%SiC–10 wt.%GNP		99.9	14.5	6.2	
TiB_2–10 wt.%MgO–6 wt.%TiN	Two step sinter.	99.6	33	8.8	[207]
TiB_2–10 wt.%MgO–6 wt.%TiN–2 wt.%SiC_w–4 wt.%MLG	1800 °C, 5 min	100	21.2	6	
	1700 °C, 45 min				
Ti(C.N)–47.7 wt.%Al_2O_3	HP. 1700 °C. 32 MPa,	98	21	6	[209]
Ti(C.N)–47.5 wt.%Al_2O_3–0.4 wt.%GNP	10 min	99.5	24	8.66	
WC–30 vol.%Al_2O_3–0.5 wt.%CNT	HP, 1540 °C, 40 MPa,	97.4	15.9	7.41	[210]
WC–30 vol.%Al_2O_3–0.5 wt.%CNT–2 wt.%TiO_2	90 min	98.9	17.18	7.75	
WC–14.6 wt.%Al_2O_3	HP. 1540 °C, 40 MPa,	99.2	15.82	7.88	[211]
WC–14.5 wt.%Al_2O_3–0.1 wt.%GNP	90 min	98.5	17.44	8.89	
WC–14.1 wt.%Al_2O_3–0.5 wt.%GNP		97.3	14.62	9.47	
WC–13.7 wt.%Al_2O_3–0.9 wt.%GNP		96.7	12.87	8.98	
WC–8 wt.% (ZrO_2–20 wt.%$Al_2O_{3)}$	Oscillatory pressure	99.1	25	7.75	[21]
WC–8 wt.% (ZrO_2–20 wt.%Al_2O_3)–0.2 wt.%GNP	sintering.	99.8	23.72	8.68	

Table 2 – (*Continued*)

Nanocomposite	Sintering method/parameters	Relative density (%)	Hardness (GPa)	Fracture toughness (MPa $m^{1/2}$)	Ref.
WC	Two step SPS.	96.5	26.3	7.2	[215]
WC–3 wt.%SiC_w–0.1 wt.%MLG	1950, 5 min.	99.5	25.6	13.1	
WC–3 wt.%SiC_w–0.2 wt.%MLG	1850, 20 min.	99	23.7	13.2	
WC–9 wt.%Al_2O_3	HP two-step.	97.8	21.9	8.25	[216]
WC–9 wt.%Al_2O_3–3 wt.%TiC–3 wt.%TiN–0.15 wt. %SiC_w–0.05 wt.%MLG	1700 °C, 4 min. 1600 °C, 60 min.	99.8	22.8	12.7	
WC–10 wt.%Si_3N_4	Sintering. 1750 °C	—	17.76	7.70	[217]
WC–10 wt.%Si_3N_4–0.01 wt.%BN_{nf}			18.32	10.99	
WC–10 wt.%Si_3N_4–0.05 wt.%BN_{nf}			20.56	10.57	
WC–10 wt.%Si_3N_4–0.1 wt.%BN_{nf}			19.04	10.50	
WC–10 wt.%Si_3N_4–0.15 wt.%BN_{nf}			19.12	10.09	
Mullite–10 wt.%TiB_2–1 wt.%CNT	SPS. 1350 °C, 30 MPa, 5 min	99.1	18.31	5.46	[219]
Mullite–10 wt.%ZrB_2–1 wt.%CNT		99.13	16.24	4.18	[220]
Mullite–10 wt.%TiN–1 wt.%CNT	SPS. 1350 °C, 30 MPa,	98.9	15.84	3.98	[221]
Mullite–10 wt.%TiN–10 wt.%TiB_2–1 wt.%CNT	5 min	97.7	16.48	4.12	
Mullite–10 wt.%TiN–10 wt.%TiB_2–10 wt.%ZrB_2 –1 wt.%CNT		97.2	17.15	4.86	
B_4C	HP, 1900 °C, 1 h, 30 MPa	97.45	29.8	3.05	[222]
B_4C–18 wt.%TiB_2		98.82	32.1	4.36	
B_4C–18 wt.%TiB_2–4 wt.%GNP		98.67	31.8	8.19	
SiC–45vol.%B_4C–10 vol.%Ni	SPS. 1650 °C, 30 MPa,	98.3	16.7	3.35	[223]
SiC–45 vol.%B_4C–10 vol.%Ni–5 vol.%CNT	5 min	97.8	15.63	5.82	
YSZ	SPS.	99.98	12.2	6.1	[10]
YSZ–1 wt.%CNT–1 wt.%BN	1300–1400 °C, 40 MPa,	98.6	11.2	7	
YSZ–3 wt.%CNT–3 wt.%BN	30 min	98.7	9.4	7.2	
YSZ–5 wt.%CNT–5 wt.%BN		97.3	9.6	7.9	

G_{nf}: graphite nano-flakes, GNP: graphene nano-platelets, GNS: graphene nanosheets, BNNT: boron nitride nanotubes, BNNP: boron nitride nanoplatelets, C_{np}: carbon nano-particles, C_{nb}: nano-sized carbon black, D_n: nano-diamond, YSZ: yttria-stabilized zirconia.
G: graphene, rGO: reduced graphene oxide, MLG: multi-layer graphene, GNS: graphene nano-sheets.
SiC_w: silicon carbide whiskers, SiC_{np}: silicon carbide nano-particles, CS: conventional/pressureless sintering, IHP: inductive hot-pressing, HFIHS: high frequency induction heat sintering.

ical, wear, friction, and lubrications properties of many hybrid ceramic nanocomposite materials is encouraging; however, developing hybrid nanocomposites with optimum properties and enhanced performance is a complex task that involves addressing several key challenges by researchers. Continuous research and advancements in processing methods are essential to obtain hybrid ceramic nanocomposites characterized by fully dense structures, minimal flaws, optimized contents of reinforcements, uniform distribution of reinforcements, and strong interfaces. Ultra-high-temperature ceramics present promising candidates for extreme environments; however, their brittleness and the challenges associated with sintering them limit their applicability in various scenarios. To address these limitations, further exploration of diverse matrices, processing routes, and various combinations of reinforcements, as well as their dimensionalities, morphologies, and inherent properties, is crucial. The layer-by-layer fabrication approach in additive manufacturing shows significant potential for developing hybrid ceramic nanocomposites, offering precise control over material deposition to create tailored structures along with a uniform distribution of nanoscale reinforcements, optimized reinforcement ratios, and improved interfacial bonding. Additionally, machine learning could revolutionize the development of these materials by predicting ideal combinations of ceramic matrices and reinforcements to achieve enhanced mechanical, thermal, or electrical properties without extensive physical trials, thereby reducing both the time and costs associated with material development. It can also optimize various parameters such as pressure, temperature, and sintering time, resulting in improved densification, reduced defects, and enhanced interfacial bonding.

Conclusion

This work presented the properties of hybrid ceramic nanocomposites and highlighted the role of the matrix in providing high strength, hardness, and thermal stability, as well as the role of the reinforcement in enhancing these properties and introducing additional functionalities such as improved toughness, wear resistance, and various physical properties. The combination of the matrix and reinforcement attributes, coupled with the use of innovative sintering methods and optimized process parameters, allows for the processing of hybrid ceramic nanocomposites with tailored properties suitable for a wide range of applications across different industries. Additionally, future research directions were formulated to develop nanocomposites with desired properties and enhanced performance. This requires obtaining dense and homogeneous nanocomposites with optimum composition that are free from defects and have a smooth and strong interface between the reinforcement and matrix.

Authors' contributions

Nouari Saheb contributed to writing and editing the manuscript. Umer Hayat contributed to data collection and writing the manuscript. Syed Fida Hassan contributed to writing and editing the manuscript. All authors reviewed and approved the manuscript.

Funding

"The authors would like to acknowledge the support provided by the Deanship of Scientific Research (DSR) at King Fahd University of Petroleum and Minerals (KFUPM) for funding this work through project No. DF181022."

REFERENCES

[1] L.F. Francis, Materials Processing: A Unified Approach to Processing of Metals, Ceramics and Polymers, second ed., Academic Press, 2024.
[2] K. Nazari, P. Tran, P. Tan, A. Ghazlan, T.D. Ngo, Y.M. Xie, Advanced manufacturing methods for ceramic and bioinspired ceramic composites: a review, Open Ceram. (2023) 100399.
[3] C.B. Carter, M.G. Norton, Ceramic Materials: Science and Engineering, second ed., Springer New York, 2013.
[4] J. Pelleg, Mechanical Properties of Ceramics, Vol. 213, Springer Science & Business, 2014.
[5] A. Kelly, Composites in context, Compos. Sci. Technol. 23 (1985) 171–199.
[6] E.T. Thostenson, C. Li, T.W. Chou, Nanocomposites in context, Compos. Sci. Technol. 65 (2005) 491–516.
[7] N. Saheb, U. Hayat, S.F. Hassan, Recent advances and future prospects in spark plasma sintered alumina hybrid nanocomposites, Nanomaterials 9 (2019) 1607.
[8] Xu Haichao, Yong Liu, Kan Wang, Preparation high-performance SiC ceramic reinforced with 3D hybrid graphene oxide-carbon nanotube by direct ink writing and liquid silicon infiltration, J. Eur. Ceram. Soc. 44 (2024) 5612–5622.
[9] S. Subha, N.S. Raju, K.V.K. Yadav, G.N. Kumar, Investigation of thermomechanical properties of Al_2O_3–TiB_2/silicon carbide ceramic nanocomposites for thermal barrier coatings, J. Inst. Eng. India: Ser. D 105 (2024) 1027–1039.
[10] A.S. Buyakov, Y.A. Mirovoy, A.Y. Smolin, S.P.J.C.I. Buyakova, Increasing fracture toughness of zirconia-based composites as a synergistic effect of the introducing different inclusions, Ceram. Int. 47 (2021) 10582–10589.
[11] A. Jain, S.P. Ong, G. Hautier, W. Chen, W.D. Richards, S. Dacek, S. Cholia, D. Gunter, D. Skinner, G. Ceder, K.A. Persson, Commentary: the materials project: a materials genome approach to accelerating materials innovation, APL Mater. 1 (2013) 011002.
[12] W.A. Shah, X. Luo, B.I. Rabiu, B. Huang, Y.Q. Yang, Toughness enhancement and thermal properties of graphene-CNTs reinforced Al_2O_3 ceramic hybrid nanocomposites, Chem. Phys. Lett. 781 (2021) 138978.
[13] W. Zhao, J. Sun, Z. Huang, Three-dimensional graphene-carbon nanotube reinforced ceramics and computer simulation, Ceram. Int. 47 (2021) 33941–33955.
[14] P. Palmero, Structural ceramic nanocomposites: a review of properties and powders' synthesis methods, Nanomaterials 5 (2015) 656–696.
[15] I. Ahmad, B. Yazdani, Y. Zhu, Recent advances on carbon nanotubes and graphene reinforced ceramics nanocomposites, Nanomaterials 5 (2015) 90–114.
[16] P. Palmero, F. Kern, F. Sommer, M. Lombardi, R. Gadow, L. Montanaro, Issues in nanocomposite ceramic engineering: focus on processing and properties of alumina-based composites, J. Appl. Biomater. Funct. Mater. 12 (2014) 113–128.

[17] D. Galusek, D. Galusková, Alumina matrix composites with non-oxide nanoparticle addition and enhanced functionalities, Nanomaterials 5 (2015) 115–143.
[18] M. Estili, Y. Sakka, Recent advances in understanding the reinforcing ability and mechanism of carbon nanotubes in ceramic matrix composites, Sci. Technol. Adv. Mater. 15 (2014) 064902.
[19] K.F. Chan, M.H.M. Zaid, M.S. Mamat, S. Liza, M. Tanemura, Y. Yaakob, Recent developments in carbon nanotubes-reinforced ceramic matrix composites: a review on dispersion and densification techniques, Crystals 11 (2021) 457.
[20] C. Ramírez, M. Belmonte, P. Miranzo, M.I. Osendi, Applications of ceramic/graphene composites and hybrids, Materials 14 (2021) 2071.
[21] G. Van Lier, C. Van Alsenoy, V. Van Doren, P. Geerlings, Ab initio study of the elastic properties of single-walled carbon nanotubes and grapheme, Chem. Phys. Lett. 326 (2000) 181–185.
[22] M.M.J. Treacy, T.W. Ebbesen, J.M. Gibson, Exceptionally high Young's modulus observed for individual carbon nanotubes, Nature 381 (1996) 678–680.
[23] M.F. Yu, O. Lourie, M.J. Dyer, K. Moloni, T.F. Kelly, R.S. Ruoff, Strength and breaking mechanism of multiwalled carbon nanotubes under tensile load, Science 287 (2000) 637–640.
[24] A. Thess, R. Lee, P. Nikolaev, H. Dai, P. Petit, J. Robert, C. Xu, Y.H. Lee, S.G. Kim, A.G. Rinzler, D.T. Colbert, G.E. Scuseria, D. Tománek, J.E. Fischer, R.E. Smalley, Crystalline ropes of metallic carbon nanotubes, Science 273 (1996) 483–487.
[25] Y. Ando, X. Zhaoa, H. Shimoyama, G. Sakai, K. Kaneto, Physical properties of multiwalled carbon nanotubes, Int. J. Inorg. Mater. 1 (1999) 77–82.
[26] H.Y. Chiu, V.V. Deshpande, H.W.C. Postma, C.N. Lau, C. Miko, L. Forro, M. Bockrath, Ballistic phonon thermal transport in multiwalled carbon nanotubes, Phys. Rev. Lett. 95 (2005) 226101.
[27] C.H. Yu, L. Shi, Z. Yao, D.Y. Li, A. Majumdar, Thermal conductance and thermopower of an individual single-wall carbon nanotube, Nano Lett. 5 (2005) 1842–1846.
[28] P. Kim, L. Shi, A. Majumdar, P.L. McEuen, Thermal transport measurements of individual multiwalled nanotubes, Phys. Rev. Lett. 87 (2001) 215502.
[29] E. Pop, D. Mann, Q. Wang, K. Goodson, H. Dai, Thermal conductance of an individual single-wall carbon nanotube above room temperature, Nano Lett. 6 (2006) 96–100.
[30] C. Lee, X. Wei, J.W. Kysar, J. Hone, Measurement of the elastic properties and intrinsic strength of monolayer graphene, Science 321 (2008) 385–388.
[31] H. Chen, M.B. Müller, K.J. Gilmore, G.G. Wallace, D. Li, Mechanically strong, electrically conductive, and biocompatible graphene paper, Adv. Mater. 20 (2008) 3557–3561.
[32] D. Li, M.B. Mueller, S. Gilje, R.B. Kaner, G.G. Wallace, Processable aqueous dispersions of graphene nanosheets, Nat. Nanotechnol. 3 (2008) 101–105.
[33] M. Fang, K. Wang, H. Lu, Y. Yang, S. Nutt, Covalent polymer functionalization of graphene nanosheets and mechanical properties of composites, J. Mater. Chem. 19 (2009) 7098–7105.
[34] I.W. Frank, D.M. Tanenbaum, A.M. van der Zande, P.L. McEuen, Mechanical properties of suspended graphene sheets, J. Vac. Sci. Technol. B 25 (2007) 2558–2561.
[35] P. Zhang, L. Ma, F. Fan, Z. Zeng, C. Peng, P.E. Loya, Z. Liu, Y. Gong, J. Zhang, X. Zhang, P.M. Ajayan, T. Zhu, J. Lou, Fracture toughness of graphene, Nat. Commun. 5 (2012) 3782.
[36] A.A. Balandin, S. Ghosh, W. Bao, I. Calizo, D. Teweldebrhan, F. Miao, C.N. Lau, Superior thermal conductivity of single-layer graphene, Nano Lett. 8 (2008) 902–907.
[37] K. Chu, X.H. Wang, F. Wang, Y.B. Li, D.J. Huang, H. Liu, W.L. Ma, F.X. Liu, H. Zhang, Largely enhanced thermal conductivity of graphene/copper composites with highly aligned graphene network, Carbon 127 (2018) 102–112.
[38] K. Chu, X.H. Wang, Y.B. Li, D.J. Huang, Z.R. Geng, X.L. Zhao, H. Liu, H. Zhang, Thermal properties of graphene/metal composites with aligned graphene, Mater. Des. 140 (2018) 85–94.
[39] P. Mohanty, S. Mohapatra, J. Mohapatra, S.K. Singh, P. Padhi, D.K. Mishra, Utilization of chemically synthesized fine powders of SiC/Al_2O_3 composites for sintering, Mater. Manuf. Process. 31 (2016) 1311–1317.
[40] M.M.A. Baig, S.F. Hassan, N. Saheb, F. Patel, Metal matrix composite in heat sink application: reinforcement, processing, and properties, Materials 14 (21) (2021) 6257.
[41] I. Momohjimoh, M.A. Hussein, N. Al-Aqeeli, Recent advances in the processing and properties of alumina–CNT/SiC nanocomposites, Nanomaterials 9 (2019) 86.
[42] T. Zhang, L. Kumari, G.H. Du, W.Z. Li, Q.W. Wang, K. Balani, A. Agarwal, Mechanical properties of carbon nanotube–alumina nanocomposites synthesized by chemical vapor deposition and spark plasma sintering, Compos. Part A: Appl. Sci. Manuf. 40 (2009) 86–93.
[43] G.D. Zhan, A.K. Mukherjee, Carbon nanotube reinforced alumina-based ceramics with novel mechanical, electrical, and thermal properties, Int. J. Appl. Ceram. Technol. 1 (2004) 161–171.
[44] M. Michálek, J. Sedláček, M. Parchoviansky, M. Michálková, D. Galusek, Mechanical properties and electrical conductivity of alumina/MWCNT and alumina/zirconia/MWCNT composites, Ceram. Int. 40 (2014) 1289–1295.
[45] I. Levin, W.D. Kaplan, D.G. Brandon, A.A. Layyous, Effect of SiC submicrometer particle size and content on fracture toughness of alumina–SiC nanocomposites, J. Am. Ceram. Soc. 78 (1995) 254–256.
[46] D. Sciti, J. Vicens, A. Bellosi, Microstructure and properties of alumina–SiC nanocomposites prepared from ultrafine powders, J. Mater. Sci. 37 (2002) 3747–3758.
[47] M. Parchovianský, et al., Microstructure and mechanical properties of hot pressed Al_2O_3/SiC nanocomposites, J. Eur. Ceram. Soc. 33 (2013) 2291–2298.
[48] S. Hayun, V. Paris, R. Mitrani, S. Kalabukhov, M.P. Dariel, E. Zaretsky, N. Frage, Microstructure and mechanical properties of silicon carbide processed by Spark Plasma Sintering (SPS), Ceram. Int. 38 (2012) 6335–6340.
[49] A. Centeno, V.G. Rocha, B. Alonso, A. Fernández, C.F. Gutierrez-Gonzalez, R. Torrecillas, A. Zurutuza, Graphene for tough and electroconductive alumina ceramics, J. Eur. Ceram. Soc. 33 (2013) 3201–3210.
[50] I. Ahmad, M. Islam, H.S. Abdo, T. Subhani, K.A. Khalil, A.A. Almajid, B. Yazdani, Y. Zhu, Toughening mechanisms and mechanical properties of graphene nanosheet-reinforced alumina, Mater. Des. 88 (2015) 1234–1243.
[51] W. Acchar, C.R.F. Camara, C.A.A. Cairo, M. Filgueira, Mechanical performance of alumina reinforced with NbC, TiC and WC, Mater. Res. 15 (2012) (2012) 821–824.
[52] T. Ohji, Y.K. Jeong, Y.H. Choa, K. Niihara, Strengthening and toughening mechanisms of ceramic nanocomposites, J. Am. Ceram. Soc. 81 (1998) 1453–1460.
[53] K. Ahmad, W. Pan, Hybrid nanocomposites: a new route towards tougher alumina ceramics, Compos. Sci. Technol. 68 (2008) 1321–1327.
[54] K. Ahmad, W. Pan, Z. Qu, Multifunctional properties of alumina composites reinforced by a hybrid filler, Int. J. Appl. Ceram. Technol. 6 (2009) 80–88.

[55] K. Mohammad, N. Saheb, Molecular level mixing: an approach for synthesis of homogenous hybrid ceramic nanocomposite powders, Powder Technol. 291 (2016) 121–130.
[56] N. Saheb, K. Mohammad, Microstructure and mechanical properties of spark plasma sintered Al_2O_3–SiC–CNTs hybrid nanocomposites, Ceram. Int. 42 (2016) 12330–12340.
[57] N. Saheb, K. Mohammad, Hard and tough Al_2O_3-SiC-CNT hybrid ceramic nanocomposite produced by molecular level mixing and spark plasma sintering, J. Aust. Ceram. Soc. 54 (2018) 401–410.
[58] N. Saheb, U. Hayat, Electrical conductivity and thermal properties of spark plasma sintered Al_2O_3-SiC-CNT hybrid nanocomposites, Ceram. Int. 43 (2017) 5715–5722.
[59] M. Siddiqui, U. Hayat, A.F.M. Arif, N. Saheb, On the thermal conductivity of spark plasma sintered alumina hybrid nanocomposites: estimation modeling and experimental validation, Sci. Sinter. 51 (2019) 101–114.
[60] I. Ahmad, M. Islam, Reinforcing ability and bonding characteristics of multiwall carbon nanotubes and silicon carbide nanoparticles in inductively sintered alumina ceramic hybrid nanocomposites, J. Alloys Compounds 788 (2019) 219–230.
[61] I. Ahmad, S. Ahmed, T. Subhani, K. Saeed, M. Islam, N. Wang, Y. Zhu, Synergic influence of MWCNTs and SiC nanoparticles on the microstructure and properties of Al_2O_3 ceramic hybrid nanocomposites, Curr. Appl. Phys. 16 (2016) 1649–1658.
[62] D.Y. Lee, D.H. Yoon, Properties of alumina matrix composites reinforced with SiC whisker and carbon nanotubes, Ceram. Int. 40 (2014) 14375–14383.
[63] M. Michálek, M. Kašiarová, M. Michálková, D. Galusek, Mechanical and functional properties of Al_2O_3–ZrO_2–MWCNTs nanocomposites, J. Eur. Ceram. Soc. 34 (2014) 3329–3337.
[64] I. Ahmad, M. Islam, S. Parvez, N. AlHabis, A. Umar, K.S. Munir, N. Wang, Y. Zhu, Reinforcing capability of multiwall carbon nanotubes in alumina ceramic hybrid nanocomposites containing zirconium oxide nanoparticles, Int. J. Refract. Met. Hard Mater. 84 (2019) 105018.
[65] S.H. Duntu, J. Agyapong, I. Ahmad, M. Islam, S. Boakye-Yiadom, Combined effect of low ZrO_2 content and carbon nanostructures on mechanical and wear properties of hot-pressed Al_2O_3/ZrO_2 hybrid nanocomposites, Ceram. Int. 48 (2022) 34803–34816.
[66] P. Biswas, P.K. Prajapati, C.O. Bapanapalle, K.K. Sadhu, R. Ghosh, N. Mandal, Effect of MWCNTs on micromechanical and high-temperature tribological behavior of ZTA–MgO ceramic composites, Materials Today 35 (2023) 105869.
[67] I. Ahmad, S. Parvez, K. Saeed, Interfacial investigation, mechanical performance and thermal permanence of the inductively hot-pressed alumina ceramic hybrid nanocomposites reinforced by silicon carbide and multilayer graphene, Int. J. Refract. Met. Hard Mater. 81 (2019) 49–57.
[68] I. Ahmad, M. Islam, T. Subhani, Y. Zhu, Toughness enhancement in graphene nanoplatelet/SiC reinforced Al_2O_3 ceramic hybrid nanocomposites, Nanotechnology 27 (2016) 425704.
[69] S. Grigoriev, P. Peretyagin, A. Smirnov, W. Solis, L.A. Díaz, A. Fernández, R. Torrecillas, Effect of graphene addition on the mechanical and electrical properties of Al_2O_3-SiC_w ceramics, J. Eur. Ceram. Soc. 37 (2017) 2473–2479.
[70] J. Liu, Z. Li, H. Yan, K. Jiang, Spark plasma sintering of alumina composites with graphene platelets and silicon carbide nanoparticles, Adv. Eng. Mater. 16 (2014) 1111–1118.
[71] J. Zhang, S. Yang, Z. Chen, M. Wyszomirska, J. Zhao, Z. Jiang, Microstructure and tribological behaviour of alumina composites reinforced with SiC-graphene core–shell nanoparticles, Tribol. Int. 131 (2019) 94–101.
[72] A. Smirnov, P. Peretyagin, N.W. Solís Pinargote, I. Gershman, J.F. Bartolomé, Wear behavior of graphene-reinforced alumina–silicon carbide whisker nanocomposite, Nanomaterials 9 (2019) 151.
[73] W. Shah, X. Luo, Y.Q. Yang, Mechanical and thermal properties of spark plasma sintered Al_2O_3-graphene-SiC hybrid composites, Ceram. Int. 49 (2023) 7987–7995.
[74] I. Ahmad, M. Islam, N. Al Habis, S. Parvez, Hot-pressed graphene nanoplatelets or/and zirconia reinforced hybrid alumina nanocomposites with improved toughness and mechanical characteristics, J. Mater. Sci. Technol. 40 (2020) 135–145.
[75] M. Petrus, J. Wozniak, T. Cygan, M. Kostecki, S. Cygan, L. Jaworska, D. Teklińska, A. Olszyna, Comprehensive study on graphene-based reinforcements in Al_2O_3–ZrO_2 and Al_2O_3–Ti (C, N) systems and their effect on mechanical and tribological properties, Ceram. Int. 45 (2019) 21742–21750.
[76] X. Wang, J. Zhao, E. Cui, S. Song, H. Liu, W. Song, Microstructure, mechanical properties and toughening mechanisms of graphene reinforced Al_2O_3-WC-TiC composite ceramic tool material, Ceram. Int. 45 (2019) 10321–10329.
[77] X. Wang, J. Zhao, Y. Gan, X. Tang, S. Gai, X. Sun, Cutting performance and wear mechanisms of the graphene-reinforced Al_2O_3-WC-TiC composite ceramic tool in turning hardened 40Cr steel, Ceram. Int. 48 (2022) 13695–13705.
[78] X. Wang, J. Zhao, E. Cui, X. Tian, Z. Sun, Effect of interfacial structure on mechanical properties of graphene reinforced Al_2O_3–WC matrix ceramic composite, Nanomaterials 11 (2021) 1374.
[79] X. Wang, J. Zhao, E. Cui, Z. Sun, H. Yu, Nano/microstructures and mechanical properties of Al_2O_3-WC-TiC ceramic composites incorporating graphene with different sizes, Mater. Sci. Eng. A 812 (2021) 141132.
[80] Y. Cheng, Y. Zhang, T. Wan, Z. Yin, J. Wang, Mechanical properties and toughening mechanisms of graphene platelets reinforced Al_2O_3/TiC composite ceramic tool materials by microwave sintering, Mater. Sci. Eng. A 680 (2017) 190–196.
[81] E. Cui, J. Zhao, X. Wang, J. Sun, X. Huang, C. Wang, Microstructure and toughening mechanisms of Al_2O_3/(W, Ti) C/graphene composite ceramic tool material, Ceram. Int. 44 (2018) 13538–13543.
[82] Z. Li, J. Zhao, J. Sun, F. Gong, X. Ni, Reinforcement of Al_2O_3/TiC ceramic tool material by multi-layer graphene, Ceram. Int. 43 (2017) 11421–11427.
[83] J. Zhao, X. Yuan, Y. Zhou, Processing and characterization of an Al_2O_3/WC/TiC micro-nano-composite ceramic tool material, Mater. Sci. Eng. A 527 (2010) 1844–1849.
[84] O.A. Rahman, M. Sribalaji, B. Mukherjee, T. Laha, A.K. Keshri, Synergistic effect of hybrid carbon nanotube and graphene nanoplatelets reinforcement on processing, microstructure, interfacial stress and mechanical properties of Al_2O_3 nanocomposites, Ceram. Int. 44 (2019) 2109–2122.
[85] B.Y. Damavandi, Y. Xia, I. Ahmad, Y. Zhu, A sol–gel approach to produce highly dispersed graphene oxide–carbon nanotube hybrid reinforcement into alumina matrix, Funct. Nanomater. 1 (2017), BKE2BP.
[86] B. Yazdani, H. Porwal, Y. Xia, H. Yan, M.J. Reece, Y. Zhu, Role of synthesis method on microstructure and mechanical properties of graphene/carbon nanotube toughened Al_2O_3 nanocomposites, Ceram. Int. 41 (2015) 9813–9822.
[87] B. Yazdani, Y. Xia, I. Ahmad, Y. Zhu, Graphene and carbon nanotube (GNT)-reinforced alumina nanocomposites, J. Eur. Ceram. Soc. 35 (2015) 179–186.

[88] B. Yazdani, F. Xu, I. Ahmad, X. Hou, Y. Xia, Y. Zhu, Tribological performance of Graphene/Carbon nanotube hybrid reinforced Al_2O_3 composites, Sci. Rep. 5 (2015) 11579.
[89] W. Shah, X. Luo, Y.Q. Yang, Microstructure, mechanical, and thermal properties of graphene and carbon nanotube-reinforced Al_2O_3 nanocomposites, J. Mater. Sci.: Mater. Electron. 32 (2021) 13656–13672.
[90] S.H. Duntu, K. Hukpati, I. Ahmad, M. Islam, S. Boakye-Yiadom, Deformation and fracture behaviour of alumina-zirconia multi-material nanocomposites reinforced with graphene and carbon nanotubes, Mater. Sci. Eng. A 835 (2022) 142655.
[91] S.H. Duntu, A. Eliasu, I. Ahmad, M. Islam, S. Boakye-Yiadom, Synergistic effect of graphene and carbon nanotubes on wear behaviour of alumina-zirconia nanocomposites, Mater. Charact. 175 (2021) 111056.
[92] T. Rodriguez-Suarez, J.F. Bartolomé, A. Smirnov, S. Lopez-Esteban, L.A. Díaz, R. Torrecillas, J.S. Moya, Electroconductive alumina–TiC–Ni nanocomposites obtained by spark plasma sintering, Ceram. Int. 37 (2011) 1631–1636.
[93] K. Thomson, D. Jiang, W. Yao, R. Ritchie, A. Mukherjee, Characterization and mechanical testing of alumina-based nanocomposites reinforced with niobium and/or carbon nanotubes fabricated by spark plasma sintering, Acta Mater. 60 (2012) 622–632.
[94] B. Zhao, H. Liu, C. Huang, J. Wang, M. Cheng, Fabrication and mechanical properties of Al_2O_3-SiC_w-TiC_{np} ceramic tool material, Ceram. Int. 43 (2017) 10224–10230.
[95] B. Zhao, H. Liu, C. Huang, J. Wang, M. Cheng, Q. Zhan, Evolution mechanisms of high temperature mechanical properties and microstructures of Al_2O_3/SiC_w/TiC_n nanocomposite materials, J. Alloys Compounds 737 (2018) 46–52.
[96] Z. Sun, J. Zhao, X. Wang, E. Cui, H. Yu, Reinforcing mechanisms of graphene and nano-TiC in Al_2O_3-based ceramic-tool materials, Nanomaterials 10 (2020) 1815.
[97] D. Sun, X. Jiang, L. Su, H. Sun, C. Hu, T. Song, Z. Luo, Fabrication and mechanical properties of Al_2O_3–TiC ceramic composites synergistically reinforced with multi-walled carbon nanotubes and graphene nanoplates, Ceram. Int. (2020) 20068–20080.
[98] B. Chen, G. Xiao, M. Yi, J. Zhang, T. Zhou, Z. Chen, C. Xu, Mechanical properties and microstructure of Al_2O_3/TiB_2 and Al_2O_3/TiB_2/GNPs ceramic tool materials prepared by spark plasma sintering, Ceram. Int. 47 (2021) 11748–11755.
[99] M.S. Asl, B. Nayebi, Z. Ahmadi, M.J. Zamharir, M. Shokouhimehr, Effects of carbon additives on the properties of ZrB2–based composites: a review, Ceram. Int. 44 (2018) (2018) 7334–7348.
[100] S. Chakraborty, P. Das, D. Ghosh, Spark plasma sintering and structural properties of ZrB_2 based ceramics: a review, Rev. Adv. Mater. Sci. 44 (2016) 182–193.
[101] Q. Liu, W. Han, P. Hu, Microstructure and mechanical properties of ZrB_2–SiC nanocomposite ceramic, Scripta Mater. 61 (2009) 690–692.
[102] Q. Liu, W. Han, J. Han, Influence of SiC_{np} content on the microstructure and mechanical properties of ZrB_2–SiC nanocomposite, Scripta Mater. 63 (2010) 581–584.
[103] S. Wang, Y. Li, X. Zhang, Influence of the microstructure evolution of ZrO_2 fiber on the fracture toughness of ZrB_2–SiC nanocomposite ceramics, Mater. Des. (2013) 808–813.
[104] J. Lin, Y. Huang, H. Zhang, Y. Yang, Y. Hong, Microstructure and mechanical properties of multiwalled carbon nanotube toughened spark plasma sintered ZrB_2 composites, Adv. Appl. Ceram. 115 (2016) 308–312.
[105] G. Balaraman Yadhukulakrishnan, Spark plasma Sintering of Silicon Carbide Multi-walled Carbon Nanotube and Graphene Reinforced Zirconium Diboride Ceramic Composite, Oklahoma State University, 2012.
[106] G.B. Yadhukulakrishnan, S. Karumuri, A. Rahman, R.P. Singh, A.K. Kalkan, S.P. Harimkar, Spark plasma sintering of graphene reinforced zirconium diboride ultra-high temperature ceramic composites, Ceram. Int. 39 (2013) 6637–6646.
[107] X. Zhang, Y. An, J. Han, W. Han, G. Zhao, X. Jin, Graphene nanosheet reinforced ZrB_2–SiC ceramic composite by thermal reduction of graphene oxide, RSC Adv. 5 (2015) 47060–47065.
[108] M.S. Asl, Microstructure, hardness and fracture toughness of spark plasma sintered ZrB_2–SiC–C_f composites, Ceram. Int. 43 (2017) 15047–15052.
[109] Y. Azizian-Kalandaragh, A.S. Namini, Z. Ahmadi, M.S. Asl, Reinforcing effects of SiC whiskers and carbon nanoparticles in spark plasma sintered ZrB_2 matrix composites, Ceram. Int. 44 (2018) 19932–19938.
[110] M.S. Asl, M.J. Zamharir, Z. Ahmadi, S. Parvizi, Effects of nano-graphite content on the characteristics of spark plasma sintered ZrB_2–SiC composites, Mater. Sci. Eng. A 716 (2018) 99–106.
[111] R.B. Acicbe, G. Goller, Densification behavior and mechanical properties of spark plasma-sintered ZrC–TiC and ZrC–TiC–CNT composites, J. Mater. Sci. 48 (2013) 2388–2393.
[112] D. Sciti, S. Guicciardi, M. Nygren, Spark plasma sintering and mechanical behaviour of ZrC-based composites, Scripta Mater. 59 (2008) 638–641.
[113] H.O. Pierson, Handbook of Refractory Carbides and Nitrides: Properties, Characteristics, Processing and Applications, William Andrew, 1996.
[114] S.A. Delbari, B. Nayebi, E. Ghasali, M. Shokouhimehr, M.S. Asl, Spark plasma sintering of TiN ceramics codoped with SiC and CNT, Ceram. Int. 45 (2019) 3207–3216.
[115] I.J. Shon, Enhanced mechanical properties of TiN-graphene composites rapidly sintered by high-frequency induction heating, Ceram. Int. 43 (2017) 890–896.
[116] M. Sribalaji, B. Mukherjee, A. Islam, A.K. Keshri, Microstructural and mechanical behavior of spark plasma sintered titanium carbide with hybrid reinforcement of tungsten carbide and carbon nanotubes, Mater. Sci. Eng. A 702 (2017) 10–21.
[117] A. Nisar, S. Ariharan, K. Balani, Synergistic reinforcement of carbon nanotubes and silicon carbide for toughening tantalum carbide based ultrahigh temperature ceramic, J. Mater. Res. 31 (2016) 682–692.
[118] B. Mukherjee, O.A. Rahman, M. Sribalaji, S.R. Bakshi, A.K. Keshri, Synergistic effect of carbon nanotube as sintering aid and toughening agent in spark plasma sintered molybdenum disilicide-hafnium carbide composite, Mater. Sci. Eng. A 678 (2016) 299–307.
[119] M.S. Asl, A statistical approach towards processing optimization of ZrB_2–SiC–graphite nanocomposites. Part I: relative density, Ceram. Int. 44 (2018) 6935–6939.
[120] M.S. Asl, B. Nayebi, M. Shokouhimehr, TEM characterization of spark plasma sintered ZrB_2–SiC–graphene nanocomposite, Ceram. Int. 44 (2018) 15269–15273.
[121] M.S. Asl, M.G. Kakroudi, R.A. Kondolaji, H. Nasiri, Influence of graphite nano-flakes on densification and mechanical properties of hot-pressed ZrB_2–SiC composite, Ceram. Int. 41 (2015) 5843–5851.
[122] M.S. Asl, M.G. Kakroudi, Characterization of hot-pressed graphene reinforced ZrB_2–SiC composite, Mater. Sci. Eng. A 625 (2015) 385–392.

[123] M.S. Asl, Y. Pazhouhanfar, A.S. Namini, S. Shaddel, M. Fattahi, M. Mohammadi, Role of graphite nano-flakes on the characteristics of ZrB_2-based composites reinforced with SiC whiskers, Diamond Relat. Mater. (2020) 107786.
[124] C. Xia, M.S. Asl, A.S. Namini, Z. Ahmadi, S.A. Delbari, Q. Van Le, M. Shokouhimehr, M. Mohammadi, Enhanced fracture toughness of ZrB_2–SiC_w ceramics with graphene nano-platelets, Ceram. Int. 46 (2020) 24906–24915.
[125] Y.H. Cheng, Y. Qi, P. Hu, S. Zhou, G. Chen, J. An, K. Jin, W. Han, ZrB_2–SiC–G composite prepared by spark plasma sintering of in-situ synthesized ZrB2–SiC–C composite powders, J. Am. Ceram. Soc. 99 (2016) 2131–2137.
[126] S. Parvizi, Z. Ahmadi, M.J. Zamharir, M.S. Asl, Synergistic effects of graphite nano-flakes and submicron SiC particles on the characteristics of spark plasma sintered ZrB_2 nanocomposites, Int. J. Refract. Met. Hard Mater. 75 (2018) 10–17.
[127] Y. Hou, P. Hu, X. Zhang, K. Gui, Effects of graphite flake diameter on mechanical properties and thermal shock behavior of ZrB_2–nanoSiC–graphite ceramics, Int. J. Refract. Met. Hard Mater. 41 (2013) 133–137.
[128] V.H. Nguyen, S.A. Delbari, M.S. Asl, Q.V. Le, A.S. Namini, Z. Ahmadi, M. Farvizi, M. Mohammadi, M. Shokouhimehr, Combined role of SiC whiskers and graphene nano-platelets on the microstructure of spark plasma sintered ZrB_2 ceramics, Ceram. Int. 47 (2021) 12459–12466.
[129] W.B. Tian, Y.M. Kan, G.J. Zhang, P.L. Wang, Effect of carbon nanotubes on the properties of ZrB_2–SiC ceramics, Mater. Sci. Eng. A 487 (2008) 568–573.
[130] M.S. Asl, I. Farahbakhsh, B. Nayebi, Characteristics of multi-walled carbon nanotube toughened ZrB_2–SiC ceramic composite prepared by hot pressing, Ceram. Int. 42 (2016) 1950–1958.
[131] A. Nisar, S. Ariharan, K. Balani, Establishing microstructure-mechanical property correlation in ZrB_2-based ultra-high temperature ceramic composites, Ceram. Int. vol. 43 (2017) 13483–13492.
[132] A. Nisar, S. Ariharan, T. Venkateswaran, N. Sreenivas, K. Balani, Effect of carbon nanotube on processing, microstructural, mechanical and ablation behavior of ZrB_2-20SiC based ultra-high temperature ceramic composites, Carbon 111 (2017) 269–282.
[133] O. Popov, J. Vleugels, E. Zeynalov, V. Vishnyakov, Reactive hot pressing route for dense ZrB_2-SiC and ZrB_2-SiC-CNT ultra-high temperature ceramics, J. Eur. Ceram. Soc. 40 (2020) 5012–5019.
[134] M.S. Asl, B. Nayebi, M.G. Kakroudi, M. Shokouhimehr, Investigation of hot pressed ZrB_2–SiC–carbon black nanocomposite by scanning and transmission electron microscopy, Ceram. Int. 45 (2019) 16759–16764.
[135] P. Hu, K. Gui, W. Hong, X. Zhang, S. Dong, High-performance ZrB_2-SiC-C_f composite prepared by low-temperature hot pressing using nanosized ZrB_2 powder, J. Eur. Ceram. Soc. 37 (2017) 2317–2324.
[136] Z. Nasiri, M. Mashhadi, A. Abdollahi, Effect of short carbon fiber addition on pressureless densification and mechanical properties of ZrB_2–SiC–C_{sf} nanocomposite, Int. J. Refract. Met. Hard Mater. 51 (2015) 216–223.
[137] I. Farahbakhsh, Z. Ahmadi, M.S. Asl, Densification, microstructure and mechanical properties of hot pressed ZrB_2–SiC ceramic doped with nano-sized carbon black, Ceram. Int. 43 (2017) 8411–8417.
[138] S. Zhou, Z. Wang, X. Sun, J. Han, Microstructure, mechanical properties and thermal shock resistance of zirconium diboride containing silicon carbide ceramic toughened by carbon black, Mater. Chem. Phys. 122 (2010) 470–473.
[139] V. Savari, Z. Balak, V. Shahedifar, Combined and alone addition effect of nano carbon black and SiC on the densification and fracture toughness of SPS-sintered ZrB_2, Diamond Relat. Mater. 128 (2022) 109244.
[140] C.W. Li, Y.M. Lin, M.F. Wang, C.A. Wang, Preparation and mechanical properties of ZrB_2-based ceramics using $MoSi_2$ as sintering aids, Front. Mater. Sci. China 4 (2010) 271–275.
[141] C. Yue, W. Liu, L. Zhang, T. Zhang, Y. Chen, Fracture toughness and toughening mechanisms in a (ZrB_2–SiC) composite reinforced with boron nitride nanotubes and boron nitride nanoplatelets, Scripta Mater. 68 (2013) 579–582.
[142] M. Fattahi, Y. Azizian-Kalandaragh, S.A. Delbari, A.S. Namini, Z. Ahmadi, M.S. Asl, Nano-diamond reinforced ZrB_2–SiC composites, Ceram. Int. 46 (2020) 10172–10179.
[143] J. Sha, J. Li, S. Wang, Z. Zhang, Y. Wang, J. Dai, Microstructure and mechanical properties of hot-pressed ZrC–Ti–CNTs composites, Mater. Des. 107 (2016) 520–528.
[144] X.G. Wang, W.M. Guo, Y.M. Kan, G.J. Zhang, P.L. Wang, Densification behavior and properties of hot-pressed ZrC ceramics with Zr and graphite additives, J. Eur. Ceram. Soc. 31 (2011) 1103–1111.
[145] D.L. Yung, S. Cygan, M. Antonov, L. Jaworska, I. Hussainova, Ultra high-pressure spark plasma sintered ZrC-Mo and ZrC-TiC composites, Int. J. Refract. Met. Hard Mater. 61 (2016) 201–206.
[146] B. Niu, F. Zhang, W. Ji, J. Zhang, Z. Fu, W. Wang, Effect of solid solution formation on densification of spark plasma sintered ZrC ceramics with TiC as sintering aid, Adv. Appl. Ceram. 115 (2016) 55–59.
[147] J. Li, Z. Zhang, S. Wang, Y. Wang, J. Dai, Y. Zu, J. Sha, Densification and characterization of hot-pressed ZrC-based composite doped with Nb and CNT, Mater. Des. 104 (2016) 43–50.
[148] B.C. Ocak, B. Yavas, I. Akin, F. Sahin, G. Goller, Spark plasma sintered ZrC-TiC-GNP composites: Solid solution formation and mechanical properties, Ceram. Int. 44 (2018) 2336–2344.
[149] W. Zeng, X. Gan, Z. Li, K. Zhou, Effect of TiC addition on the microstructure and mechanical properties of TiN-based cermets, Ceram. Int. 43 (2017) 1092–1097.
[150] U.W. Bläß, T. Barsukova, M.R. Schwarz, A. Köhler, C. Schimpf, I.A. Petrusha, U. Mühle, D. Rafaja, E. Kroke, Bulk titanium nitride ceramics – significant enhancement of hardness by silicon nitride addition, nanostructuring and high pressure sintering, J. Eur. Ceram. Soc. 35 (2015) 2733–2744.
[151] M. Radajewski, S. Henschel, S. Grützner, L. Krüger, C. Schimpf, D. Chmelik, D. Rafaja, Microstructure and mechanical properties of bulk TiN–AlN composites processed by FAST/SPS, Ceram. Int. 42 (2016) 10220–10227.
[152] J. Song, L. Jiang, G. Liang, J. Gao, J. An, L. Cao, J. Xie, S. Wang, M. Lv, Strengthening and toughening of TiN-based and TiB_2-based ceramic tool materials with HfC additive, Ceram. Int. 43 (2017) 8202–8207.
[153] M. Sribalaji, A. Islam, B. Mukherjee, M.K. Pandey, A.K. Keshri, Tailoring the thermal shock resistance of titanium carbide by reinforcement with tungsten carbide and carbon nanotubes, Ceram. Int. 44 (2018) 2552–2562.
[154] X. Wang, M. Lu, L. Qiu, H. Huang, D. Li, H. Wang, Y.B. Cheng, Graphene/titanium carbide composites prepared by sol–gel infiltration and spark plasma sintering, Ceram. Int. 42 (2016) 122–131.
[155] L. Cheng, Z. Xie, G. Liu, Spark plasma sintering of TiC-based composites toughened by submicron SiC particles, Ceram. Int. 39 (2013) 5077–5082.
[156] J. Cabrero, F. Audubert, R. Pailler, Fabrication and characterization of sintered TiC–SiC composites, J. Eur. Ceram. Soc. 31 (2011) 313–320.
[157] S. Liu, W. Hu, J. Xiang, F. Wen, B. Xu, D. Yu, J. He, Y. Tian, Z. Liu, Mechanical properties of nanocrystalline TiC–ZrC solid

solutions fabricated by spark plasma sintering, Ceram. Int. 40 (2014) 10517–10522.
[158] L. Cheng, Z. Xie, G. Liu, Spark plasma sintering of TiC ceramic with tungsten carbide as a sintering additive, J. Eur. Ceram. Soc. 33 (2013) 2971–2977.
[159] A.S. Namini, Z. Ahmadi, A. Babapoor, M. Shokouhimehr, M.S. Asl, Microstructure and thermomechanical characteristics of spark plasma sintered TiC ceramics doped with nano-sized WC, Ceram. Int. 45 (2019) 2153–2160.
[160] T.P. Nguyen, Y. Pazhouhanfar, S.A. Delbari, Q.V. Le, S. Shaddel, A.S. Namini, Role of nano-diamond addition on the characteristics of spark plasma sintered TiC ceramics, Diamond Relat. Mater. (2020) 107828.
[161] Y. Pazhouhanfar, A.S. Namini, S.A. Delbari, T.P. Nguyen, Q.V. Le, S. Shaddel, M. Pazhouhanfar, M. Shokouhimehr, M.S. Asl, Microstructural and mechanical characterization of spark plasma sintered TiC ceramics with TiN additive, Ceram. Int. 46 (2020) 18924–18932.
[162] M. Fattahi, S.A. Delbari, A. Babapoor, A.S. Namini, M. Mohammadi, M.S. Asl, Triplet carbide composites of TiC, WC, and SiC, Ceram. Int. 46 (2020) 9070–9078.
[163] M. Fattahi, M.S. Asl, S.A. Delbari, A.S. Namini, Z. Ahmadi, M. Mohammadi, Role of nano-WC addition on microstructural, mechanical and thermal characteristics of TiC–SiC_w composites, Int. J. Refract. Met. Hard Mater. 90 (2020) 105248.
[164] V.H. Nguyen, S.A. Delbari, A.S. Namini, A. Babapoor, Q.V. Le, H.W. Jang, M. Shokouhimehr, M.S. Asl, M. Mohammadi, Microstructural, mechanical and friction properties of nano-graphite and h-BN added TiC-based composites, Ceram. Int. 46 (2020) 28969–28979.
[165] V.H. Nguyen, S.A. Delbari, M.S. Asl, Q.V. Le, M. Shokouhimehr, A.S. Namini, M. Mohammadi, Microstructure–property correlation in nano-diamond and TiN added TiC-based ceramics, Ceram. Int. 47 (2020) 449–460.
[166] V.H. Nguyen, S.A. Delbari, M.S. Asl, Q.V. Le, H.W. Jang, M. Shokouhimehr, M. Mohammadi, A.S. Namini, A novel TiC-based composite co-strengthened with AlN particulates and graphene nano-platelets, Int. J. Refract. Met. Hard Mater. 92 (2020) 105331.
[167] J. Sun, J. Zhao, Z. Huang, K. Yan, F. Chen, Y. Jian, H. Yang, B. Li, Preparation and properties of multilayer graphene reinforced binderless TiC nanocomposite cemented carbide through two-step sintering, Mater. Des. 188 (2020) 108495.
[168] J. Sun, Z. Cao, L. Zhao, X. Li, L. Meng, Q. Du, J. Zhao, Developing high performance in titanium carbide nanocomposites containing hybrid SiC nanowire and CNT, J. Eur. Ceram. Soc. 43 (2023) 5466–5473.
[169] F. Rezaei, M.G. Kakroudi, V. Shahedifar, N.P. Vafa, M. Golrokhsari, Densification, microstructure and mechanical properties of hot pressed tantalum carbide, Ceram. Int. 43 (2017) 3489–3494.
[170] C. Zhang, B. Boesl, L. Silvestroni, D. Sciti, A. Agarwal, Deformation mechanism in graphene nanoplatelet reinforced tantalum carbide using high load in situ indentation, Mater. Sci. Eng. A 674 (2016) 270–275.
[171] A. Nieto, D. Lahiri, A. Agarwal, Graphene NanoPlatelets reinforced tantalum carbide consolidated by spark plasma sintering, Mater. Sci. Eng. A 582 (2013) 338–346.
[172] D. Lahiri, E. Khaleghi, S.R. Bakshi, W. Li, E.A. Olevsky, A. Agarwal, Graphene-induced strengthening in spark plasma sintered tantalum carbide–nanotube composite, Scripta Mater. 68 (2013) 285–288.
[173] L. Pienti, L. Silvestroni, E. Landi, C. Melandri, D. Sciti, Microstructure, mechanical properties and oxidation behavior of TaC-and HfC-based materials containing short SiC fiber, Ceram. Int. 41 (2015) 1367–1377.
[174] S.R. Bakshi, V. Musaramthota, D. Lahiri, V. Singh, S. Seal, A. Agarwal, Spark plasma sintered tantalum carbide: Effect of pressure and nano-boron carbide addition on microstructure and mechanical properties, Mater. Sci. Eng. A 528 (2011) 1287–1295.
[175] D. Sciti, L. Silvestroni, S. Guicciardi, D. Dalle Fabbriche, A. Bellosi, Processing, mechanical properties and oxidation behavior of TaC and HfC composites containing 15 vol% TaSi2 or MoSi2, J. Mater. Res. 24 (2009) 2056–2065.
[176] A. Nisar, K. Balani, Role of interfaces on multi-length scale wear mechanics of TaC-based composites, Adv. Eng. Mater. 19 (2017) 1600713.
[177] A. Nisar, S. Ariharan, T. Venkateswaran, N. Sreenivas, K. Balani, Oxidation studies on TaC based ultra-high temperature ceramic composites under plasma arc jet exposure, Corros. Sci. 109 (2016) 50–61.
[178] D.S.H. Al-Habib, Z. Balak, M.S. Asl, R. Materials, Spark plasma sinterability of TaC-based composites co-doped with SiC, TiC and graphene, Diamond Relat. Mater. 130 (2022) 109496.
[179] W. Hao, N. Ni, F. Guo, F. Cao, J. Jiang, X. Zhao, P. Xiao, High fracture toughness of HfC through nano-scale templating and novel sintering aids, J. Am. Ceram. Soc. 102 (2019) 997–1009.
[180] B. Matovic, D. Bučevac, V. Maksimović, S. Nenadović, J. Pantić, D. Gautam, T. Yano, Synthesis and characterization of hafnium carbide based ceramics, Key Eng. Mater. 616 (2014) 1–7.
[181] L. Feng, S.H. Lee, H. Wang, H.S. Lee, Synthesis and densification of nano-crystalline hafnium carbide powder, J. Eur. Ceram. Soc. 35 (2015) 4073–4081.
[182] L. Silvestroni, A. Bellosi, C. Melandri, D. Sciti, J. Liu, G. Zhang, Microstructure and properties of HfC and TaC-based ceramics obtained by ultrafine powder, J. Eur. Ceram. Soc. 31 (2011) 619–627.
[183] C. Huang, B. Zou, Y. Liu, S. Zhang, C. Huang, S. Li, Study on friction characterization and wear-resistance properties of Si_3N_4 ceramic sliding against different high-temperature alloys, Ceram. Int. 42 (2016) 17210–17221.
[184] X. Tian, J. Zhao, N. Zhu, Y. Dong, J. Zhao, Preparation and characterization of Si_3N_4/(W, Ti) C nano-composite ceramic tool materials, Mater. Sci. Eng. A 596 (2014) 255–263.
[185] C. Tian, H. Jiang, N. Liu, Thermal shock behavior of Si_3N_4–TiN nano-composites, Int. J. Refract. Met. Hard Mater. 29 (2011) 14–20.
[186] W. Yang, F. Gao, C. Xu, G. Wei, L. An, Fabrication of Si_3N_4/SiC nanocomposites toughened by in-situ formed low-dimensional nanostructures, Solid State Sci. 12 (2010) 1692–1695.
[187] J. Tatami, T. Katashima, K. Komeya, T. Meguro, T. Wakihara, Electrically conductive CNT-dispersed silicon nitride ceramics, J. Am. Ceram. Soc. 88 (2005) 2889–2893.
[188] C. Tian, H. Jiang, Preparation and thermal shock properties of Si_3N_4-WC nanocomposites, in: 2011 Second International Conference on Mechanic Automation and Control Engineering, 2011, pp. 1482–1486, IEEE.
[189] L.S. Walker, V.R. Marotto, M.A. Rafiee, N. Koratkar, E.L. Corral, Toughening in graphene ceramic composites, ACS Nano 5 (2011) 3182–3190.
[190] C.Y. Tian, H. Jiang, Toughness enhancement in TiN/CNTs reinforced Si_3N_4 ceramic nanocomposites, in: The Proceeding of International Conference on Energy, Power, Electrical and Environmental Engineering (EPEEE 2018), 2018, pp. 1–6.
[191] V. Puchý, P. Hvizdoš, M. Ivor, D. Medveď, M. Hnatko, A. Kovalčíková, R. Sedlák, J. Dusza, Preparation, friction, wear, and fracture of the Si_3N_4-Ag-GNPs composites prepared by SPS, J. Eur. Ceram. Soc. 40 (2020) 4853–4859.

[192] J. Zhang, J. Zhang, G. Xiao, Z. Chen, M. Yi, Y. Zhang, C. Xu, Orentational effect of graphene on the friction and wear behavior of Si_3N_4/TiC based composite ceramic tool materials, Ceram. Int. 46 (2020) 3550–3557.
[193] F. Chen, K. Yan, Y. Zhu, J. Hong, Mechanical properties of hybrid multilayer graphene/whisker-reinforced ceramic composites: Simulation and experimental investigation, Ceram. Int. 48 (2022) 25673–25680.
[194] V.H. Nguyen, M.S. Asl, Z.H. Mahaseni, M.D. Germi, S.A. Delbari, Q. Van Le, Z. Ahmadi, M. Shokouhimehr, A.S. Namini, M. Mohammadi, Role of co-addition of BN and SiC on microstructure of TiB_2-based composites densified by SPS method, Ceram. Int. 46 (2020) 25341–25350.
[195] O. Popov, J. Vleugels, A. Huseynov, V. Vishnyakov, Reactive sintering of TiB_2-SiC-CNT ceramics, Ceram. Int. 45 (2019) 22769–22774.
[196] F.S. Moghanlou, S. Nekahi, M. Vajdi, Z. Ahmadi, A. Motallebzadeh, A. Shokouhimehr, M. Shokouhimehr, S. Jafargholinejad, M.S. Asl, Effects of graphite nano-flakes on thermal and microstructural properties of TiB_2–SiC composites, Ceram. Int. 46 (2020) 11622–11630.
[197] A. Kovalčíková, P. Tatarko, R. Sedlak, D. Medveď, Z. Chlup, E. Múdra, J. Dusza, Mechanical and tribological properties of TiB_2-SiC and TiB_2-SiC-GNPs ceramic composites, J. Eur. Ceram. Soc. 40 (2020) 4860–4871.
[198] G. Raju, B. Basu, Development of high temperature TiB_2-based ceramics, Key Eng. Mater. 395 (2009) 89–124.
[199] F. Ghafuri, M. Ahmadian, R. Emadi, M. Zakeri, Effects of SPS parameters on the densification and mechanical properties of TiB_2-SiC composite, Ceram. Int. 45 (2019) 10550–10557.
[200] Z. Ahmadi, B. Nayebi, M.S. Asl, I. Farahbakhsh, Z. Balak, Densification improvement of spark plasma sintered TiB_2-based composites with micron-, submicron-and nano-sized SiC particulates, Ceram. Int. 44 (2018) 11431–11437.
[201] T. Watanahe, K. Shoubu, Mechanical properties of hot-pressed TiB_2-ZrO_2 composites, J. Am. Ceram. Soc. 68 (1985), C-34-C-36.
[202] D. Demirskyi, H. Borodianska, Y. Sakka, O. Vasylkiv, Ultra-high elevated temperature strength of TiB_2-based ceramics consolidated by spark plasma sintering, J. Eur. Ceram. Soc. 37 (2017) 393–397.
[203] S. Nekahi, F.S. Moghanlou, M. Vajdi, Z. Ahmadi, Microstructural, thermal and mechanical characterization of TiB_2–SiC composites doped with short carbon fibers, Int. J. Refract. Met. Hard Mater. 82 (2019) 129–135.
[204] J. Lin, Y. Yang, H. Zhang, Q. Lin, B. Zhu, Synthesis and characterization of in-situ CNTs reinforced TiB_2-based composite by CVD using Ni catalysts, Ceram. Int. 44 (2018) 2042–2047.
[205] I. Akin, O. Kaya, Microstructures and properties of silicon carbide-and graphene nanoplatelet-reinforced titanium diboride composites, J. Alloys Compounds 729 (2017) 949–959.
[206] M.S. Asl, Z. Ahmadi, F.S. Moghanlou, M. Vajdi, M. Shokouhimehr, Nanocharacterization of spark plasma sintered TiB_2–SiC–graphene composites, Mater. Charact. 189 (2022) 111986.
[207] J. Sun, J. Zhao, Z. Huang, K. Yan, Y. Jian, H. Yang, Hybrid multilayer graphene and SiC whisker reinforced TiB_2 based nano-composites by two-step sintering, J. Alloys Compounds 856 (2021) 157283.
[208] M. Vajdi, F.S. Moghanlou, S. Nekahi, Z. Ahmadi, A. Motallebzadeh, H. Jafarzadeh, M.S. Asl, Role of graphene nano-platelets on thermal conductivity and microstructure of TiB_2–SiC ceramics, Ceram. Int. 46 (2020) 21775–21783.
[209] E. Cui, J. Zhao, X. Wang, Determination of microstructure and mechanical properties of graphene reinforced Al_2O_3-Ti (C, N) ceramic composites, Ceram. Int. 45 (2019) 20593–20599.
[210] T. Bai, T. Xie, Influence of TiO_2 contents and sintering temperature on the microstructure and mechanical properties of WC-Al_2O_3 cemented carbide reinforced by multi-wall carbon nanotubes, J. Alloys and Compounds 745 (2018) 562–568.
[211] X. Zhang, S. Zhu, W. Dong, Y. Luo, H. Ding, Y. Bai, P. Di, The effects of graphene platelets fillers on the sliding wear of WC-Al_2O_3 composites, Ceram. Int. 46 (2020) 27809–27821.
[212] X. Zhang, S. Zhu, T. Shi, H. Ding, Y. Bai, P. Di, Y. Luo, Preparation, mechanical and tribological properties of WC-Al_2O_3 composite doped with graphene platelets, Ceram. Int. (2020) 10457–10468.
[213] K. Chen, W. Xiao, Z. Li, J. Wu, K. Hong, X.J.M. Ruan, Effect of graphene and carbon nanotubes on the thermal conductivity of WC–Co cemented carbide, Metals 9 (2019) 377.
[214] N. Sun, Y. Cheng, T. Zhu, L. Pan, N. Liao, H. Wang, Y. Li, J. Dai, Z. Xie, S. Sang, Mechanical properties of binderless tungsten carbide enhanced via the addition of ZrO_2-20 wt% Al_2O_3 composite powder and graphene nanosheets, Ceram. Int. 49 (2023) 22853–22860.
[215] J. Sun, Y. Chen, P. Zhai, Y. Zhou, J. Zhao, Z. Huang, Tribological performance of binderless tungsten carbide reinforced by multilayer graphene and SiC whisker, J. Eur. Ceram. Soc. 42 (2022) 4817–4824.
[216] J. Sun, L. Zhao, X. Li, Q. Du, J. Zhao, Y. Zhou, L. Zhang, A. Li, Effect of graphene and SiC whisker on the mechanical properties of WC-TiC-TiN-Al_2O_3 nanocomposites, J. Alloys Compounds 938 (2023) 168612.
[217] T. Cao, X. Li, J. Li, Y. Huang, S. Qu, C. Yang, L. Liang, T. Song, Mechanical properties of WC-Si_3N_4 composites with ultrafine porous boron nitride nanofiber additive, Front. Mater. 8 (2021) 534407.
[218] X. Shen, N. Xu, H. Su, X. He, J. He, Preparation and characterization of high hard and high tough ultrafine WC ceramics containing hybrid graphene and SiC nanowire, J. Central South Univ. 31 (2024) 114–126.
[219] Y. Orooji, E. Ghasali, M. Moradi, M.R. Derakhshandeh, M. Alizadeh, M.S. Asl, T. Ebadzadeh, Preparation of mullite-TiB_2-CNTs hybrid composite through spark plasma sintering, Ceram. Int. 45 (2019) 16288–16296.
[220] Y. Orooji, M.R. Derakhshandeh, E. Ghasali, M. Alizadeh, M.S. Asl, T. Ebadzadeh, Effects of ZrB_2 reinforcement on microstructure and mechanical properties of a spark plasma sintered mullite-CNT composite, Ceram Int 45 (2019) 16015–16021.
[221] Y. Orooji, A. Alizadeh, E. Ghasali, M.R. Derakhshandeh, M. Alizadeh, M.S. Asl, T. Ebadzadeh, Co-reinforcing of mullite-TiN-CNT composites with ZrB_2 and TiB_2 compounds, Ceram. Int. 45 (2019) 20844–20854.
[222] A. Wang, L. Hu, W. Guo, X. Zhao, Y. Shi, Q. He, W. Wang, H. Wang, Z. Fu, Synergistic effects of TiB_2 and graphene nanoplatelets on the mechanical and electrical properties of B_4C ceramic, J. Eur. Ceram. Soc. 42 (2022) 869–876.
[223] M. Bahamirian, F. Alipour, R.B. Golenji, L. Nikzad, M.H. Barounian, M. Razavi, Role of carbon nanotubes on mechanical properties of SiC-B_4C-Ni hybrid composites fabricated by reactive spark plasma sintering, Ceram. Int. 47 (2021) 25221–25228.